BRAIN DELIVERY ENHANCEMENT OF CURCUMIN VIA NANOTECHNOLOGY

UMNART SUDYAJAI

A THESIS SUBMITTED IN PARTIAL FULFILLMENT
OF THE REQUIREMENTS
FOR THE DEGREE OF MASTER OF SCIENCE
(PHARMACEUTICAL CHEMISTRY AND PHYTOCHEMISTRY)
FACULTY OF GRADUATE STUDIES
MAHIDOL UNIVERSITY
2006

ISBN 974-04-6909-4

Thesis
Entitled

BRAIN DELIVERY ENHANCEMENT OF CURCUMIN VIA NANOTECHNOLOGY

Umnart Sudyajai

Mr. Umnart Sudyajai
Candidate

Opa Vajragupta

Assoc. Prof. Opa Vajragupta, Ph.D.
Major-Advisor

Pojawon Lawanprasert

Assoc.Prof. Pojawon Lawanprasert, Ph.D.
Co-Advisor

Salee Kiewkarnka

Asst. Prof. Salee Kiewkarnka, Ph.D
Acting Dean
Faculty of Graduate Studies

Weena

Assoc. Prof. Weena Jiratchariyakul,
Dr.rer.nat
Chair
Master of Science Programme
in Pharmaceutical Chemistry and
Phytochemistry Faculty of Pharmacy

Thesis
Entitled

BRAIN DELIVERY ENHANCEMENT OF CURCUMIN VIA NANOTECHNOLOGY

was submitted to the Faculty of Graduate Studies, Mahidol University
for the degree of Master of Science (Pharmaceutical Chemistry and Phytochemistry)

on

February 27, 2006

Umnart Sudyajai

Mr. Umnart Sudyajai
Candidate

Opa Vajragupta

Assoc. Prof. Opa Vajragupta, Ph.D.
Chair

Yuvadee Wongkrajang

Assoc.Prof. Yuvadee Wongkrajang, Ph.D.
Member

Pojawon Lawanprasert

Assoc.Prof. Pojawon Lawanprasert, Ph.D.
Member

Salee Kiewkarnka

Asst. Prof. Salee Kiewkarnka, Ph.D
Acting Dean
Faculty of Graduate Studies
Mahidol University

Ampol Mitrevej

Prof. Ampol Mitrevej, Ph.D.
Dean
Faculty of Pharmacy
Mahidol University

ACKNOWLEDGEMENTS

I would like to express my deep appreciation to the many people that have made this work possible. First of all, I would like to thank my advisor, Associate Professor Dr. Opa Vajragupta, for her encouragement and inspiration throughout my study. She always gives me invaluable advice.

My sincere thank are due to Assistant Professor Dr. Nongluck Ruangwises for her guidance, invaluable suggestion on HPLC techniques. I specially thank Associate Professor Dr. Pranee Jongwisut for her helpful discussion. I also would like to thank Assoc.Prof. Dr. Pojawon Lawanprasert and Assoc.Prof. Yuvadee Wongkrajang for her help in laboratory facilities.

A special acknowledgement is extended to Department of Pharmaceutical Chemistry, Faculty of Pharmacy, Mahidol University, for providing research facilities, the Royal Golden Jubilee (RGJ) Project, Thailand Research fund, for providing the opportunity to study in Ph.D. program and supporting the research fund in USA,

As well, my special appreciation to my fellow graduate students at the Faculty of Pharmacy, and other persons who have not been mentioned here for their helpful, friendship and encouragement.

Finally, I wish to express my deepest gratitude and infinite thankfulness to my family for their love, encouragement and support throughout my life.

Umnart Sudyajai

BRAIN DELIVERY ENHANCEMENT OF CURCUMIN VIA NANOTECHNOLOGY

UMNART SUDYAJAI 4536894 PYPP/M

M.Sc. (PHARMACEUTICAL CHEMISTRY AND PHYTOCHEMISTRY)

THESIS ADVISORS : OPA VAJRAGUPTA, Ph.D.,
POJAWON LAWANPRASERT, Ph.D.

ABSTRACT

Curcumin is well-known for having a potent antioxidant effect and various related effect on biological systems. Curcumin is penetrates poorly across the blood-brain barrier to the brain. One methodology to overcome this barrier is to prepare curcumin in the form of nanoparticles. Nanoparticles were prepared by free radical polymerization method and loaded with curcumin. The curcumin nanoparticles were coated with polysorbate 80 to yield polysorbate 80 coated curcumin loaded nanoparticles (P80-CLNP). The shape of the P80-CLNP is spherical, pebble like, with a mean size of 60-70 nm and zeta potential of -37 mV. Percentage entrapment of curcumin in nanoparticles was 80.00%. The content of curcumin in nanoparticles was 62.33%. Brain accessibility of curcumin from P80-CLNP was investigated in mice. Mice were injected subcutaneously with curcumin solution or P80-CLNP at the dose of 150 mg curcumin/kg, and the amounts of curcumin in the mice brain at 30 minutes, 1 hour, 2 hours, 3 hours, 4 hours, 6 hours, 8 hours, 10 hours, 12 hours and 15 hours after the injections were determined by HPLC. The amount of curcumin in the brain of mice treated with curcumin nanoparticles was significantly greater than in those treated with curcumin solution ($p < 0.001$). At two hours after injection, the amount of curcumin in the brains of the curcumin nanoparticles treated group was 6.5 times greater. The times to reach maximum level in the brain were 3 hours for P80-CLNP treated mice and 10 hours for curcumin solution treated mice. This result demonstrates the capability of nanoparticles in the enhancement of curcumin delivery to the brain.

KEY WORDS POLYMETHYLMETHACRYLATE / NANOPARTICLES / POLYSORBATE 80 / CURCUMIN / BLOOD-BRAIN BARRIER / BRAIN DELIVERY

124 P. ISBN 974-04-6909-4

การเพิ่มการนำส่งสู่สมองของเคอร์คูมินโดยใช้นาโนเทคโนโลยี (BRAIN DELIVERY ENHANCEMENT OF CURCUMIN VIA NANOTECHNOLOGY)

อำนาจ สุดยาใจ 4536894 PYPP/M

วท.ม. (เภสัชเคมีและพฤกษเคมี)

คณะกรรมการควบคุมวิทยานิพนธ์ : โอภา วัชระคุปต์, Ph.D., พจวรรณ ลาวัณย์ประเสริฐ, Ph.D.

บทคัดย่อ

เป็นที่ทราบกันโดยทั่วไปว่าเคอร์คูมินมีฤทธิ์เป็นสารต้านอนุมูลอิสระที่แรง และมีฤทธิ์ในกระบวนการทางชีววิทยาต่างๆ อันเนื่องจากฤทธิ์ต้านอนุมูลอิสระ เคอร์คูมินจากกระแสเลือดผ่านเข้าสมองได้ไม่ดีนัก วิธีการหนึ่งที่สามารถทำให้เคอร์คูมินผ่านไปสู่สมองได้มากขึ้นคือ การเตรียมเคอร์คูมินให้อยู่ในลักษณะที่เป็นอนุภาคระดับนาโนเมตร การเตรียมอนุภาคให้อยู่ในระดับนาโนเมตรทำโดยกระบวนการแรดิคัลโพลิเมอร์ไรเซชั่น หลังจากนั้นจึงนำอนุภาคนาโนมาบรรจุเคอร์คูมินและเคลือบด้วยโพลิซอร์เบต-80 อนุภาคระดับนาโนเมตรที่เตรียมด้วยวิธีดังกล่าวนี้มีลักษณะกลมคล้ายก้อนกรวด มีขนาดอนุภาคโดยเฉลี่ยอยู่ที่ 60-70 นาโนเมตร ค่าประจุที่ผิวอนุภาคมีค่าเท่ากับ –37.0 มิลลิโวลต์ อนุภาคนาโนสามารถผนวกจับเคอร์คูมินเข้าไว้ได้เท่ากับ 80.00% ของปริมาณเคอร์คูมินที่เติม และปริมาณเคอร์คูมินในอนุภาคนาโนที่เตรียมได้เท่ากับ 62.33% เมื่อนำเคอร์คูมินในรูปแบบอนุภาคระดับนาโนเมตร มาทดสอบหาการผ่านเข้าสมองเปรียบเทียบกับเคอร์คูมินในรูปสารละลาย โดยฉีดเคอร์คูมินทั้งสองรูปแบบเข้าใต้ผิวหนังหนูถีบจักรในขนาด 150 มก/กก. เมื่อวิเคราะห์หาปริมาณเคอร์คูมินในสมองด้วยเครื่อง HPLC ณ เวลา 30 นาที, 1 ชั่วโมง, 2 ชั่วโมง, 3 ชั่วโมง, 4 ชั่วโมง, 6 ชั่วโมง, 8 ชั่วโมง, 10 ชั่วโมง, 12 ชั่วโมง และ 15 ชั่วโมง ภายหลังการฉีด พบว่าปริมาณเคอร์คูมินในสมองหนูกลุ่มที่ถูกฉีดด้วยเคอร์คูมินในรูปอนุภาคระดับนาโนเมตรมีค่ามากกว่ากลุ่มที่ฉีดด้วยเคอร์คูมินในรูปสารละลายอย่างมีนัยสำคัญ ($p < 0.001$) และที่ 2 ชั่วโมง ภายหลังการฉีดพบว่าปริมาณเคอร์คูมินในสมองหนูของกลุ่มที่ถูกฉีดด้วยเคอร์คูมินในรูปอนุภาคนาโนมีค่าสูงกว่ากลุ่มที่ฉีดด้วยสารละลายเคอร์คูมิน 6.5 เท่า และณ เวลาที่พบว่าปริมาณเคอร์คูมินอยู่ในสมองมีมากที่สุด โดยฉีดเคอร์คูมินในรูปแบบอนุภาคระดับนาโนเมตรและเคอร์คูมินในรูปสารละลายจะอยู่ที่เวลา 3 ชั่วโมงและ 10 ชั่วโมง ตามลำดับ ผลการทดลองแสดงถึงความสามารถของอนุภาคนาโนสามารถเพิ่มการนำส่งเคอร์คูมินสู่สมอง

124 หน้า ISBN 974-04-6909-4

CONTENTS

CONTENTS (cont.)

CONTENTS (cont.)

LIST OF FIGURES

LIST OF FIGURES (Cont.)

LIST OF FIGURES (Cont.)

LIST OF FIGURES (Cont.)

LIST OF TABLES

LIST OF SCHEMES

LIST OF ABBREVIATIONS

S.D.	=	standard deviation
°C	=	degree celcius
mm	=	millimeter(s)
µm	=	micrometer(s)
nm	=	nanometer(s)
m	=	metre(s)
g	=	gram
µg	=	microgram
mg	=	milligram
HPLC	=	high-performance liquid chromatography
i.e.	=	id est (that is)
l	=	litre(s)
ml	=	milliliter(s)
min	=	minute(s)
m.p.	=	melting point
MW.	=	molecular weight
No.	=	number
%RSD	=	percentage of relative standard deviation
w/w	=	weight by weight
mV	=	millivoltage
TEM	=	transmission electron microscope
PCS	=	photon correlation spectroscopy

CHAPTER I
INTRODUCTION

The blood-brain barrier is considered to be an insurmountable obstacle for a large number of drugs, such as antibiotics, antioxidants, and a variety of central nervous system-active drugs. For many years attempts have been made to overcome this problem by various procedures, including enhancement of brain blood vessel membrane fluidity with liposomes (1-3), chemical modification (4-6), or opening of the blood-brain barrier by osmotic methods (7). One of the possibilities to overcome this barrier is a drug delivery to the brain using nanoparticles. Drugs that have successfully been transported into the brain using this carrier include the hexapeptide dalargin (8), the dipeptide kytorphin (9), loperamide (10), tubocurarine (11), the NMDA receptor antagonist MRZ 2/576 (12-13), and doxorubicin (14-15).

Nanoparticle is a general word used to designate small-sized polymer particles with a diameter ranging from several tens to several hundred nanometers. Thus, this term is somewhat general since it dose not take into account the morphological and structural organization of the polymer. Method based on emulsion polymerization micelle-confined reaction is very popular approach used to form nanosphere consisting of an active polymer core shell surrounded by a stabilizer. In these systems, the polymerization is initiated by the radical ions of initiator, and elongation of the polymer chains occurs according to a radical polymerization mechanism. The size of nanospheres produced can vary from 50 to 300 nm (16-17). The nanoparticle has two components in form of micelle (Figure 1.). The inner component is polymer acting as skeleton, such as poly(alkyl cyanoacrylate) (18), poly(D,L-lactide)-block-poly(ethylene oxide) (19) and others (20-23). The outer component is surfactant for stabilization, such as poloxamer 407, dextran 70, pluronic F68 and others. The advantage of using nanoparticles for drug delivery results from their two basic properties. Firstly, due to their small size, nanoparticles penetrate into even capillaries and are taken up within cells, allowing an efficient drug accumulation at the targeted sites in the body. Secondly, the use of biodegradable materials for

nanoparticle preparation, allows sustained drug release at the targeted site over a period of days or even weeks after injection. Poly(methyl methacrylate) nanoparticles were so far successfully used for the *in vivo* delivery of drugs to the brain. This polymer has the advantage that it is very rapidly biodegradable (24-27). Poly(methyl methacrylate) nanoparticles coating with surfactant, especially with polysorbate 80 (28), led to significantly higher total brain concentration after intravenous injection to mice.

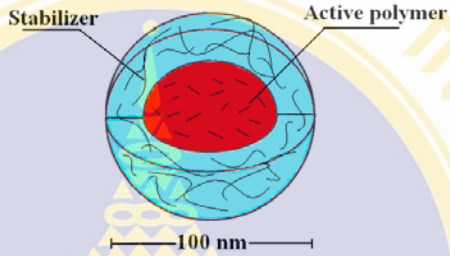

Figure 1. Schematic representation of the PMMA nanosphere (29)

The mechanism of nanoparticle-mediated transport of drugs across the blood-brain barrier has not fully elucidated. The most likely mechanism is endocytosis by the endothelial cells that line inside the blood capillaries of the brain. Nanoparticle-mediated transport to the brain depends on the overcoating of the particles with polysorbates, especially polysorbate 80 (8, 18, 28). Overcoating with these materials leads to the adsorption of apolipoprotein E from blood plasma onto the nanoparticle surface. The particles then mimic low density lipoprotein (LDL) particles and could interact with the LDL receptor leading to their uptake by the endothelial cells. After endocytosis, the drug will be released in these cells and diffuse into the brain interior (Figure 2.) (9).

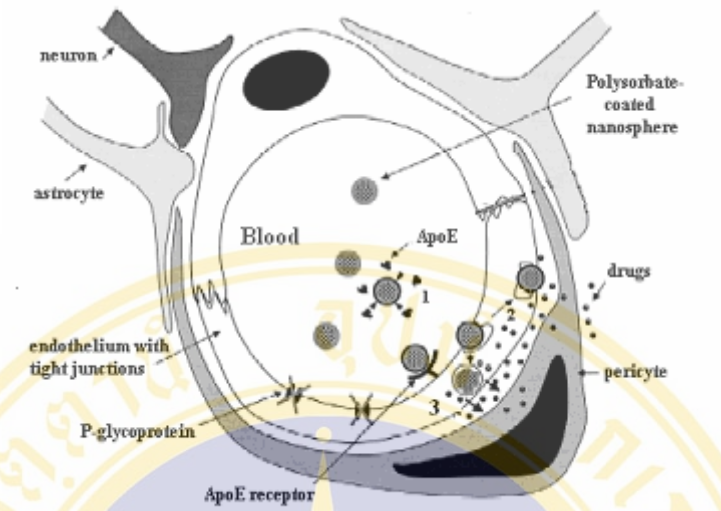

Figure 2. Hypothetical mechanism of drug delivery to the brain by means of polysorbate 80-coated PMMA nanospheres. (1) Adsorption of apolipoprotein E (ApoE) onto the nanosphere; (2) transcytosis of the nanospheres; (3) endocytosis followed by intracellular degradation of the nanospheres, resulting in release of the drug and diffusion towards the interior of the brain (18).

Curcuma longa Linn. or tumeric (Zingiberaceae) is a medicinal plant widely cultivated in tropical region of Asia. Turmeric extract from the rhizomes commonly called curcumin is composed of curcumin or curcumin-I [**1**], curcumin-II (demethoxycurcumin) [**2**] and curcumin-III (bisdemethoxycurcumin) [**3**]. Curcumin is well-known for having a potent antioxidant activity and various related activities in biological systems (30-32). Curcumin has been shown to exhibit anti-inflammatory action (33), anticarcinogenic activities (34), neuroprotection with the improvement of learning and memory impairment (35) and anti HIV-1 integrase activity (36). It has been reported that curcumin rapidly react with many reactive oxidants such as NO_2 (37), peroxyl radicals ($ROO^{\bullet}$) (38), alkoxyl radical ($RO^{\bullet}$) (39-40), $^{\bullet}CH_3$ (40), haloperoxyl radicals ($CCl_3O^{\bullet}$), azide radicals ($N_3^{\bullet}$), $Br_2^{-\bullet}$ and glutathione radicals ($RS^{\bullet}$) (41). However, recent studies have demonstrated that curcumin is not an effective superoxide radical scavenger (42-43).

Structurally, curcumin consists of two *ortho* methoxylated phenols and a *β*-diketone moiety, and they are all conjugated providing as electron-rich donor structure.

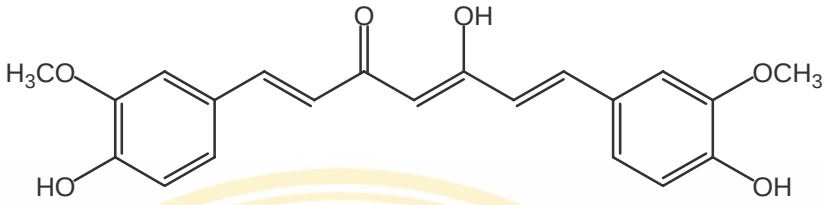

Curcumin-I [**1**]

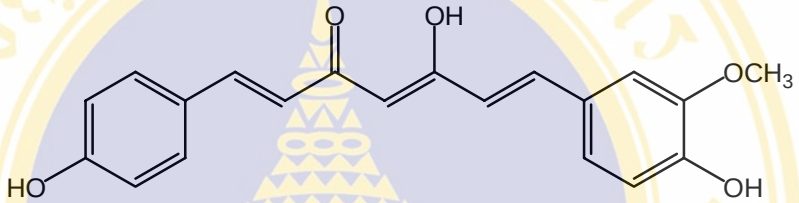

Curcumin-II (demethoxycurcumin) [**2**]

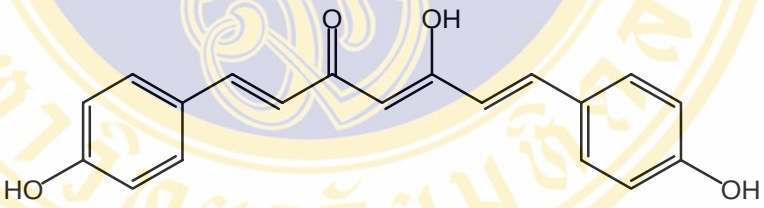

Curcumin-III (bisdemethoxycurcumin) [**3**]

So the goal of this research is to improve the free radical scavenging ability by incorporation of curcumin in the nanoparticles, this would enhance the brain accessibility and will consequently result in good neuroprotective actions. Poly(methyl methacrylate) nanoparticles of curcumin coating with surfactant, i.e. polysorbate 80 (28), was prepared in this study. The physicochemical properties of the prepared polysorbate 80 coating curcumin nanoparticles were investigated by transmission electron micrographs (TEM) and photon correlation spectroscopy (PCS). Since the preparation aims at significantly higher total brain concentration, the transport of from curcumin from curcumin loaded nanoparticles through the blood-brain barrier was also determined.

CHAPTER II
LITERATURE REVIEW

A. The Blood Brain Barrier

The blood brain barrier (BBB) is the homeostatic defense mechanism of the brain against pathogens and toxins. Complex and highly regulated, the BBB screens the biochemical, physicochemical and structural features of solutes at it periphery, thus affording barrier selectivity in the passage of desired molecules into the brain parenchyma. Early revelations of the BBB illustrated its biological character in the murine model, and provided insights into contemporary understandings of its physiology. Electron microscopic analyses of isolated cerebral cortices, post intraveneous injection of the enzymatic tracer horse radish peroxidase (HRP), exposed the presence of exogeneous HRP in the vascular space and in endothelial cell pinocytotic vacuoles (44). The pinocytic vacuoles were not found to transport the enzyme, and furthermore, no peroxidase was found beyond the vasculature endothelium, suggesting a “barrier” between the blood and the brain.

1. Biology of the BBB

Cerebral capillaries are created by the process of angiogenesis, which is the development of blood vessels from those existing in previously formed complexes. Figure 3 shows a depiction of the cerebral capillaries, while the features of the BBB are exhibited in Figure 4. During angiogenesis, endothelial cells (EC) traverse the extracellular matrix (ECM) and degrade the basement membrane to create a microvascular network (45, 46) thus subsequent proliferation. Proliferation of endothelial cells is influenced by neural determinants. These confer the characteristic physiological properties upon the BBB, and consequently, cerebral EC are distinguished from the periphery. For instance, the brain EC have fewer endocytotic vessels than peripheral EC, which limits the transcellular flux at the BBB. The occluded tight junctions (TJ), whose great electrical resistance imposes barriers to paracellular flux, join endothelial cells of the brain.

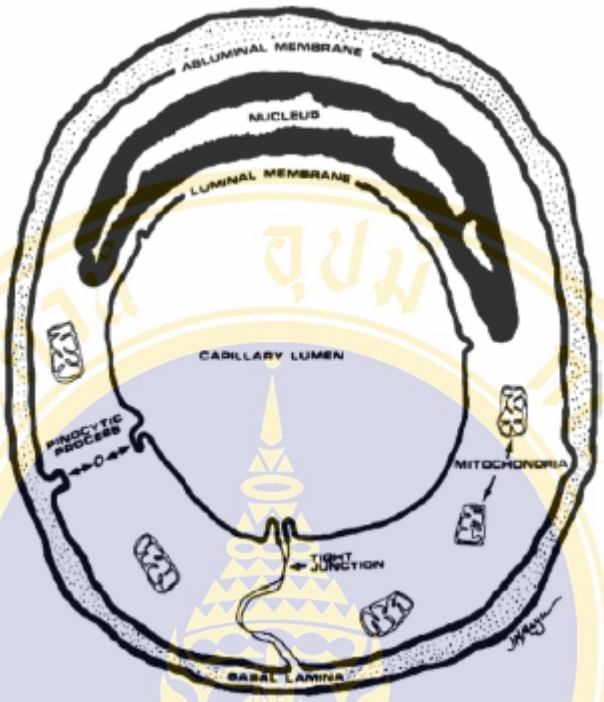

Figure 3. Characteristic features of BBB are represented in this schematicpinocytic diagram of a cerebral capillary viz., tight junctions and scarcity of vacuoles. Note the presence of mitochondria, which are denser in cerebral EC as compared to peripheral EC. This may be attributed to extra metabolic workload required to maintain ionic gradients at BBB

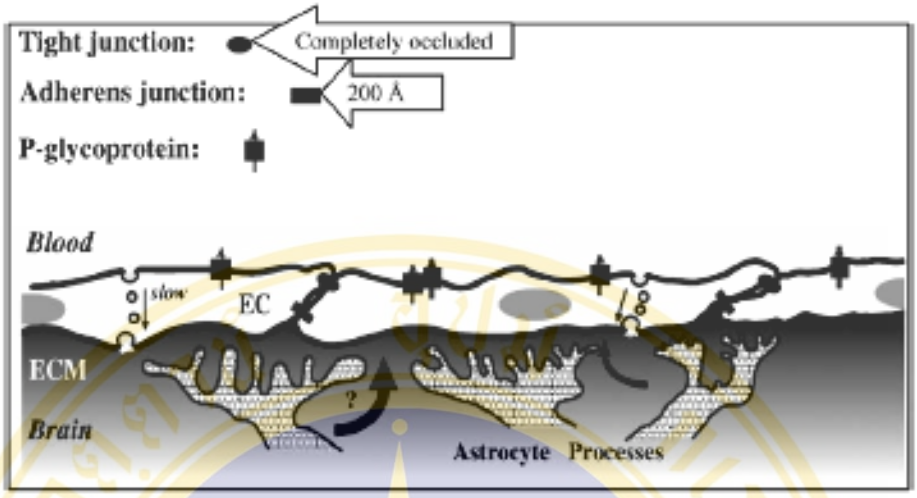

Figure 4. Features of BBB. The endothelial cells (EC) of BBB are coupled by tight junctions (TJ) that are completely occluded and adherens junctions (200 Å). The increased electrical resistance at the TJ strains paracellular movement of substances into the brain. Proteins of the adherens junction work in accordance with TJ proteins for cellular adherence. Astrocytic processes (glial cells) in the extracellular matrix (ECM) envelope the capillaries and influence transport across the EC. Questions once arose as to whether or not astrocytes actually participated in BBB. It is now accepted that 20 nm gap between adjacent astrocytes supports that they do not. P-glycoproteins (P-gp) on apical EC membrane efflux substances from brain into bloodstream

The structural properties of cerebral EC, mentioned above, help to define the selectiveness at the BBB. Furthermore, cerebral EC have more mitochondria (47) than peripheral EC, which drives the increased metabolic workload necessary to maintain ionic gradients across the BBB.

The electron-dense layers of the basement membrane fuse EC and astrocytes, while dividing EC and pericytes from the surrounding extracellular space. Pericytes lie along the outer axes of cerebral capillaries and perform in contractility. This close association (and function) helps to monitor blood flow, and thus, the adhesion of pericytes with the microvasculature indirectly regulates EC activity and BBB transport. Pericytes could also manage endothelial growth and development by inhibiting cell proliferation (48), and in a contrasted dual role, by contributing to angiogenesis (49).

Astrocytes envelop more than 99% of the basal capillary membrane (50), and they also play a role in the BBB induction of high paracellular electrical resistance. A gap of only 20 nm separates the astocytes from the EC and the pericytes. Likewise, the significant interplay amongst the three cells contributes to the solute transportation. Namely, molecular route into the brain (from the blood) is first accomplished by moving through the immediate perivascular spaces, and onto the pericytes bordering the capillaries. Consequentially, transporters, receptors and enzymes located on the plasma membranes of astrocytes and pericytes govern the fates of solutes before they reach the EC (50-51).

2. Molecular physiology of the BBB

The BBB restricts solute entry into the brain, by the transcellular route, due to an increased electrical resistance between the endothelial cells at the tight junction (TJ). The intact BBB exhibits estimated electrical resistances up to 8000 Ω/cm^2, whereas leaky endothelial demonstrates the resistances between 100 and 200 Ω/cm^2 (52-54). Key indispensable proteins, including claudin 1-, 3-, and 5-, occluding and the junctional adhesion molecule (JAM), compose the tight junction (55-59). The claudins form the seal of the TJ by homotypically binding to each other on adjacent EC cells. In an interesting review of the pathophysiology of tight junctions, Mitic *et al*. provide convincing evidence for the role of claudins in fibrilizing and forming the TJ seal (60). However, the claudins are not the sole components of the fibrils; this role being shared with occluding. In addition, the occluding protein directs the BBB to decrease paracellular permeability by localizing into intramembrane strands of the TJ (61); the number of localized protein parallels the impedance to solute flux (62). Meanwhile, the JAM regulates leukocyte transmigration at the BBB compromise (47). As well, a host of other transmembrane proteins lie in accessory to the three integral proteins (60). According to Reichel *et al*., the expression of complex tight junctions between the ECs is one of the most critical features because of their consequences on the function of the BBB (63): (i) nearly complete restriction of the paracellular pathway, (ii) enforcement of transendothelial passage and hence, control over the CNS penetration, (iii) association with expression of specific carrier systems for hydrophilic solutes essential for the brain (e.g. nutrients), and (iv) differential (i.e.

polarized) expression of receptors, transporters, and enzymes at either the luminal or abluminal cell surface allowing the BBB to act as a truly dynamic interface between the body periphery (blood) and the central compartment (brain).

3. BBB breakdown and mechanisms of disease

Decomposition of the BBB occurs in response to initiators such as infection (e.g. bacterial, viral), inflammation, cerebrovascular disease, and neoplasia. Motivators of BBB breakdown augment permeability, and underlie a myriad of neuropathologies. In pneumonia, the pneumococcus bacterium joins the BBB via platelet activating factor receptors (64). The outcome of bacterial adhesion is an increased vesicular transport across the endothelial cells, thus permitting separation of the tight junctions, and creating an entry for inflammatory peptides. Likewise, inflection of the brain space ensues. The consistency of the BBB is also influenced by the actions causing bacterial meningitis. The meningococcus bacterium (65) enters the body through the nose, and thereafter infiltrates the endothelial (via the pili) of the cerebrum to cause infection of the CNS (65). Viral invasions of the CNS pronounce less impairment to the BBB than do bacterial interferences, and therefore, the integrity of the BBB is upheld to a greater extent following the viral attack (66). Inflammatory stimuli such as pain induce the extravasation of lymphoid cells through the BBB (67), opening the barrier to cytokines and chemokines, and resulting in autoimmune inflammatory disorders like multiple sclerosis (MS) and CNS lupus. In addition, the BBB can be compromised in cerebrovascular disease, for example stroke, by hypertension and ischemia. Ischemia complicates the disease progession by activating cytokines and proteases (66).

As previously mentioned, degradation of the BBB occurs in states of pathology, such as hypertension, ischemia, and hydrocephalus or in cases of trauma. The various factors involved in the BBB breakdown and homeostasis are compiled in Table 1. Degradation leads to leakiness and the consequential unrestrained migration of malicious agents into the cerebrum. In addition to existing pathological conditions, and even in the intact BBB, crucial parameters must be regarded when ascertaining the capabilities of molecules to cross the BBB, especially for the intended purpose of drug design. The implication is that targeted, controlled drug delivery through the

BBB, would promote a greater understanding at the molecular level of many unfathomable neurological disorders, as well as aid in their early diagnoses, and their therapeutic advancements.

Table 1. BBB degradation and homeostatic organs

Causes of BBB degradation	BBB homeostatic organs	Focus of homeostatic regulation
Hypertension	Pineal gland	Circadian rhythm
Abnormal development	Neurohypophysis	Posterior pituitary hormones
Microwaves	Area postrema	Vomiting reflex
Radiation	Subfornical organ	Bodily fluids
Infection	Lamina terminalis	Chemosensory
Trauma	Median eminance	Anterior pituitary hormones

4. Drug transport to the barrier and targeting mechanisms

The BBB is circumferential, formed by the polarized luminar (apical) and abluminal (basal) endothelial membranes (and other tissue (67) interfaces not mentioned in this review), which lie in series. Thus, solutes have to pass a set of membranes to gain brain entry, making the BBB dynamic in its regulation. The barrier uptakes essential nutrients, hormones and vitamins, while enzymatically degrading many peptides and neurotransmitters through enzymatic BBB. Additionally, the energy-requiring toxin efflux mechanisms help to maintain cerebral vitality by disavowing injurious substances. Kinetic flux analyses reveal a unidirectional, concentration-dependent movement of the solutes (68). Furthermore, the direction of flow is from the plasma to the brain, or visa versa, with these two parameters defining influx and efflux (see Figure 5).

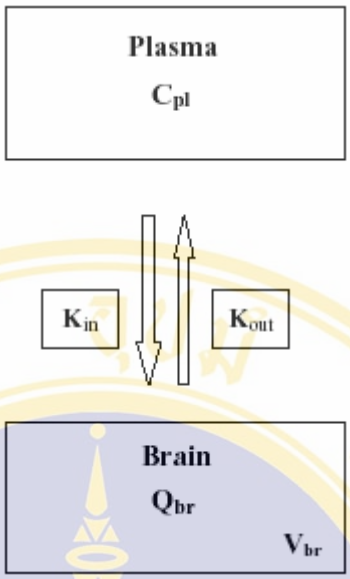

Figure 5. Schematic representation of unidirectional, concentration-dependant solute flux. The transfer coefficient, K, quantifies the rates of influx (Kin) and efflux (Kout) at the BBB, which rely on solute concentrations in blood plsma (Cpl) in the brain. The concentration of the solute in the brain is represented as Qbr, which describes the quantity (Q) of the solute/gram wt of the brain tissue. The concentration of solute in the brain is determined by the brain volume distribution (Vbr) as: Cbr = Qbr/Vbr, Even though these specific quantitative variables are not explicitly stated in the text, the importance of BBB flux to drug delivery is important

Thus, net flux is the difference between the two unidirectional rates, and is greatly influenced by the nature of the BBB. Importantly, BBB flux is a determinant in drugs reaching therapeutic concentrations within the CNS (69). Numerous transport mechanisms define the BBB (see Figure 6). Small lipophilic molecules that are charge bearing, large or hydrophilic, require gated channels, ATP, proteins and/or receptors, to facilitate passage through the BBB. One exceptional regulatory aspect of the BBB is that it is not fully present throughout the brain. The circumventricular organs, which border the ventricles of the brain, do not possess a BBB. These organs are concerned with chemosensation, hormonal adjustment (from the autonomic nervous system), circadian rhythm, vomiting and the regulation of bodily fluids. The absence of a BBB at these checkpoint organs encourages the maintenance of a constant cerebral internal atmosphere by monitoring the blood make-up and activating feedback controls as necessary.

Transport mechanisms at the BBB can be manipulated for cerebral drug targeting. Naturally, ideal drug candidates should be small, lipophilic (as measured by the octanol: water partition coefficient), hydrophobic, and compact (a parameter measured by the polar surface area). Physicochemical factors notwithstanding, though, the nature of the drug candidate within the biological system is paramount to the drug design. In the peripheral circulation, systemic enzymatic attack and plasma protein opsonization can lead to the metabolism of the drug before it reaches the brain. The factors influencing drug transport into the brain are given in Table 2. Moreover, the probability of cellular sequestration and the clearance rate of the drug in the bloodstream are additional issues to consider in drug targeting. Finally, an understanding of the clearance rate of the candidate drug in the brain is imperative, and as such, focus should be given to the concentration of the drug in the brain, with respect to the concentration of the drug in the blood, called the log BBB. While designing the drug, it is extremely important to consider several parameters such as drug concentration, lipophilicity, and polar surface area. Efflux proteins and other obstacles at the BBB must be surmounted before the drug reaches the interior of the brain.

At the endothelial cell membrane, the drug can proceed through a variety of routes. In a hypothetical situation, considering all drug molecules as the same (which are being defined as Drug A, Drug B, and Drug C), Drug A attaches to the basal EC membrane (see Figure 7). If Drug A has an affinity for efflux proteins at the BBB, it is shuttled back into the bloodstream without reaching its goal. If there is no affinity for efflux proteins, Drug A settles into the internal compartment of the EC cell where it faces the chances of encountering metabolic cellular enzymes, again jeopardizing its likelihood of reaching the target site. Assuming that Drug A hurdles all obstacles imposed by efflux proteins and cellular enzymes, it then proceeds through the cell, to the apical EC membrane, and into the brain towards its target. Drug A in the extracellular space (ECS) may proceed by different paths to reach its objective.

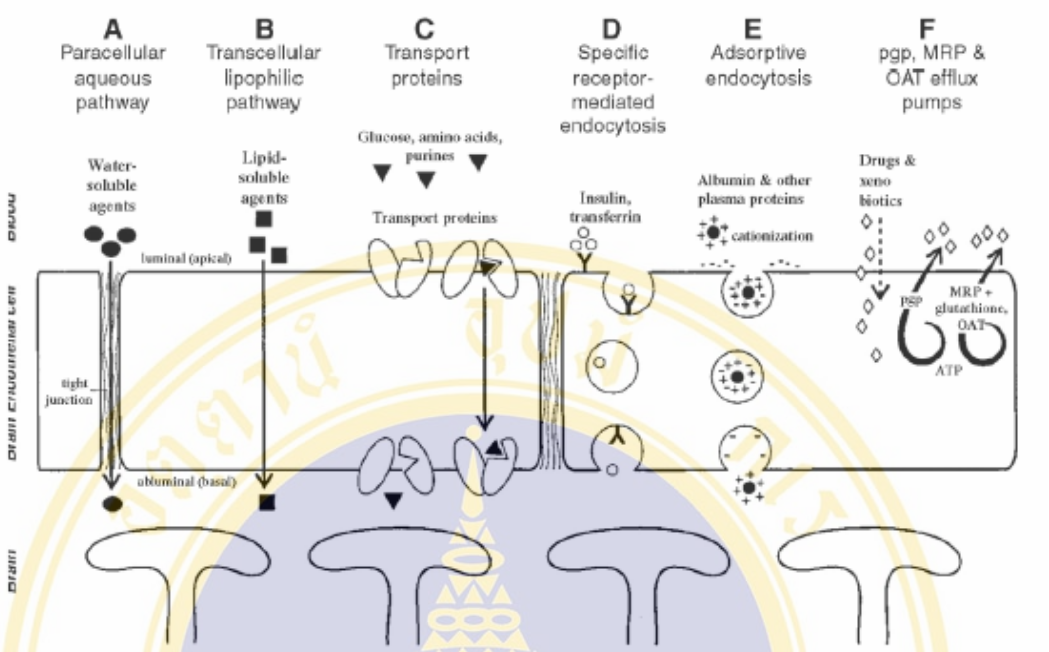

Figure 6. Transport mechanisms at the BBB

Table 2. Considerations for drug transport into the brain

Factors at the BBB	Peripheral factors
Concentration gradients of drug/ polymer	Systemic enzymatic stability
Molecular weight (of drug)	Affinity for plasma proteins
Flexibility, conformation of drug/ polymer	Cerebral blood flow
Amino acid composition	Metabolism by other tissues
Lipophilicity	Clearance rate of drug/ polymer
Sequestration by other cells	Effect of existing pathological conditions
Affinity for efflux proteins (e.g. P-gp) Cellular enzymatic stability Existing pathological conditions Molecular charge (of drug/ polymer) Affinity for receptors or carriers	

It can leave the ECS before reaching its destination, travel directly to its target, or it may act like Drug B, traveling to its target via the cerebrospinal fluid (CSF). If Drug A leaves the ECS, its fate becomes that of the peripheral circulation and the actions of serum enzymes. Additionally, Drugs A and B may be in equilibrium between the CSF and the ECS, between the CSF and the target cell, and between the target cell and the ECS. In the peripheral circulation, Drug C equilibrates with red

blood cells (RBC) and plasma proteins. Plasma proteins can attach to the surface of Drug C, making it more amenable for macrophage uptake by the liver and spleen, and therefore, less likely to reach the brain. As previously mentioned, Drug C can also be metabolized by serum enzymes or it can be taken up by systemic tissues and metabolized, never to reach the targeted cells of the brain.

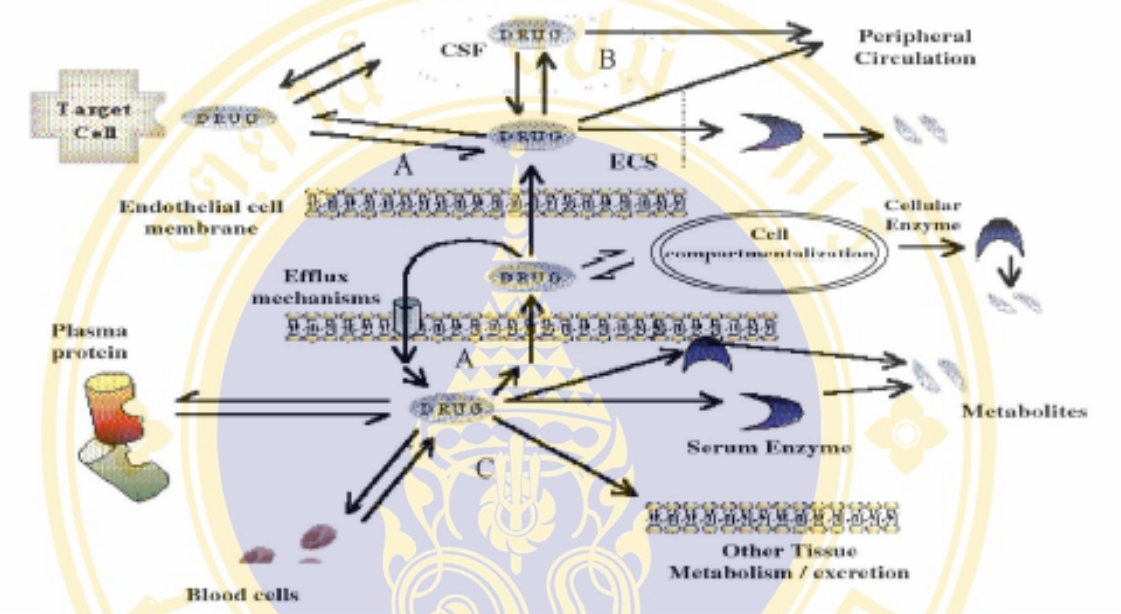

Figure 7. Mechanism of drug transport and delivery. Hypothetical Drug A, B and C

Two basic paradigms in cerebral drug targeting are found for the molecular approach and the polymeric carrier approach. By the molecular approach, two further schemes can be probed. First, drugs can be targeted to the brain cells (based upon the vital determinants such as lipophilicity, size and polar surface area) and then activated once inside the target cell by the specific enzymatic machinery. The disadvantage to this tactic, though, is the limited availability of such drugs and metabolic pathways for potential exploitation. Also, by the molecular approach, candidate drugs can be targeted to the BBB via receptor-mediation. However, receptor targeted moieties face additional challenges. In particular, many receptors are not specific to only one cell type. Thus, candidate drugs may have an affinity for cells other than their intended targets. The second major paradigm in cerebral drug targeting is by using particulate carriers. Examples of particulate carriers are liposomes, oil-in-water (O/W) emulsions, and polymeric nanoparticles.

Polymeric nanoparticles are advantageous in a number of ways. For one, they possess the high drug-loading capacities, thereby increasing intracellular delivery of the drug. Secondly, the solid matrix of particulate carriers protects the incorporated drugs against degradation, thus increasing the chances of the drug reaching the brain. Furthermore, carriers can target delivery of drugs, and this targeted delivery can be controlled. One additional benefit of particulate carriers is that their surface properties can be manipulated in such a way as to evade recognition by the macrophages of the reticuloendothelial system (RES), hence improving the likelihood of nanoparticles reaching the brain. Kabanov and Batrakova (70) gave an interesting review of maximizing drug transport through the BBB by inhibiting efflux transporters by block copolymers, by using artificial hydrophobitization of peptides and proteins by fatty acids, and by using receptor-mediated drug encapsulated nanoparticles (70).

B. Polymeric Nanoparticle

One potential in delivering drugs to the brain is the employment of nanoparticles. Nanoparticles are polymericparticles made of natural or artificial polymers ranging in size between 10 and 1000 nm (1 mm) (71). Compared with other colloidal carriers, polymeric nanoparticles present a higher stability when in contact with the biological fluids. Also, their polymeric nature permits the attainment of desired properties such as controlled and sustained drug release. Different approaches in the fabrication of nanoparticles consisting of biodegradable polymers have been described. Likewise, methods for the preparation of surface-modified sterically stabilized particles are reviewed in the literature (72-86).

Nanoparticles can be synthesized from preformed polymers or from a monomer during its polymerization, as in the case of methylmethacrylates. As such, nanospheres or nanocapsules can be synthesized, with their resultant structures that are dependent upon the technology employed in the manufacture. Nanospheres are the dense polymeric matrices in which drug is dispersed, whereas nanocapsules present a liquid core surrounded by a polymeric shell. Most techniques involving the polymerization of monomers include the addition of the monomer into the dispersed

phase of an emulsion, an inverse microemulsion or dissolved into a non-solvent of the polymer (72-86). Starting from the preformed polymers, nanoparticles are formed by the precipitation of synthetic polymers or by denaturation or gelification of natural macromolecules (71, 74-76, 78, 79, 81-84, 86). Finally, two main approaches have been proposed for the preparation of nanoparticles by synthetic polymers. The theory of the first figure follows the emulsification of a water-immiscible organic solution of the polymer, in a surfactant-containing aqueous phase, and followed by solvent evaporation. The second approach follows the precipitation of a polymer after the addition of a non-solvent of the polymer.

Thus far, the only successfully used nanoparticles for the *in vivo* administration of drugs targeted to the brain, is the rapidly biodegradable polymethylmethacrylate (PMMA) (87). The mechanism of emulsion polymerization of polymethylmethacrylate (PMMA) is represented in Figure 8. Kreuter *et al*. have suggested that the passage of PMMA nanoparticles through the BBB probably occurs by phagocytosis or endocytosis by the endothelial cells (88).

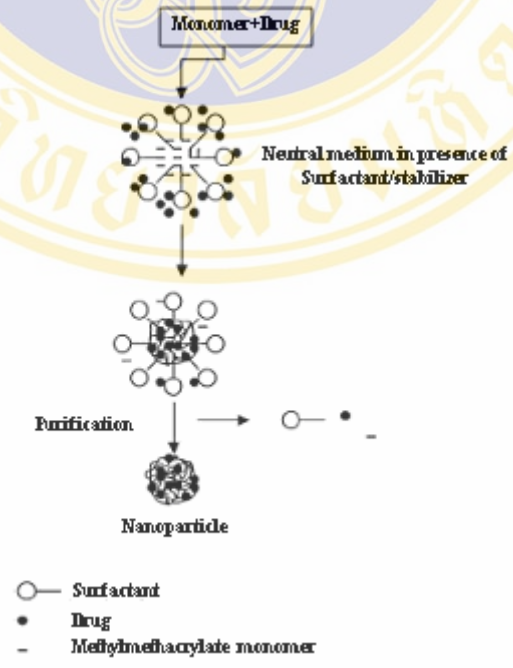

Figure 8. Emulsion polymerization of alkylcyanoacrylates

Schroeder *et al*. (89) replicated the work of Kreuter *et al*. (88) and pointed to a model of diffusion of the poly(methylmethacrylate) nanoparticles at the BBB (90). Vauthier *et al*. refutes endocytosis as the mechanism for EC uptake of PMMA, and suggests NP adherence to the cell membrane with subsequent escape by the P-gp efflux proteins (91).

1. Production of nanoparticles by different techniques

1.1 Emulsion polymerization

The radical polymerization of methylmethacrylate monomers into polymeric NPs follows the emulsion polymerization technique. By this method, the monomer is dispersed in aqueous solution as a uniform emulsion and stabilized by the surfactants. The polymerization is initiated by the radical ions of initiator, and elongation of the polymer chains occurs according to a radical polymerization mechanism. The surfactants facilitate emulsification of the monomer into the aqueous phase by decreasing surface tension at the monomer–water interface. Dispersion of the surfactant persists until the critical micellar concentration (CMC) is realized. The CMC is the concentration beyond which the surfactant no longer exists as a soluble dispersion, but rather as molecular aggregates called micelles (92). Henceforth, equilibrium is maintained between the dispersed surfactant molecules and the micelles. Beyond the CMC, only micellar formation is possible.

Micelles contain both polar and non-polar ends. They aggregate with the polar heads lying outwards, allowing the nonpolar hydrocarbons to form the interior, where the monomer is solubilized. Upon addition of the monomer, and with agitation, emulsification commences. Typically, water-soluble initiators are used in emulsions. The system contains monomer droplets in the aqueous phase, and the solubilized monomer in the interior of the micelle. With water-soluble initiators, chain growth starts at the surface of the micelle, it being hydrophilic. Once the monomer inside the micelle is expended, more droplets enter from the aqueous phase. Thus, polymerization proceeds inwards and continues until prohibited by free-radical termination. Many polymer chains grow within the system and eventually aggregate into fine particles. The emulsifier layer of the micelle stabilizes these particles until

the micelle bursts, releasing the particles. Nanoparticles are uniformly dispersed in the aqueous phase, and stabilized by the emulsion molecules, which originally formed the micelle (92).

1.2 Dispersion polymerization

Gubha and Mandal have prepared the NPs of poly(acrylamide) (PAM) by the dispersion polymerization of acrylamide monomer at 40 °C (76). They used the partial isopropyl ester derivative of poly(vinyl methyl ether-alt-maleicanhydride) (PVME-alt-MA), called PVME-co-MA-co-*i*PrMA, as the stabilizer, and ammonium persulfate (APS) as the initiator. In *t*-butyl alcohol (TBA)–water media, they achieved successful polymerization at an alcohol concentration of 90%. However, it was found that if the maleic anhydride groups are not converted to monoisopropyl ester in PVME-alt-MA (i.e. using PVME-alt-MA as opposed to PVME-co-MA-co-*i*PrMA), then the NPs coagulate in acetone upon isolation, suggesting that the stabilizer detaches from the surface of the particles upon centrifugation. The stabilizer, PVME-co-MAco-*i*PrMA, yielded stable dispersions of the particles (even after isolation), even though polydisperse in size. A schematic representation of the dispersion polymerization of acrylamide in TBA is given in Figure 9. Note that emulsion and/or dispersion techniques have been employed depending upon the nature of the polymers employed.

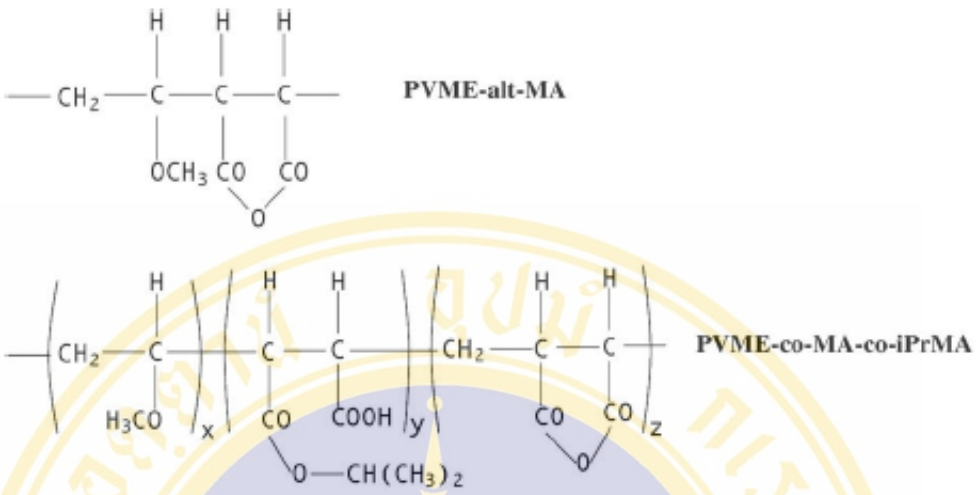

Figure 9. Dispersion polymerization of acrylamide

1.3 Interfacial polymerization/denaturation and desolvation

Nanoparticles can also be polymerized by interfacial polymerization and denaturation/desolvation for drug delivery to the CNS. Like emulsion polymerization, in interfacial polymerization, the monomers are used to create the solution. High-torque mechanical stirring brings the aqueous and organic phases together by emulsification or homogenization. Polymethylmethacrylate NPs have been polymerized by this method. In addition, denaturation and desolvation have been used to produce the polymeric NPs. Lockman *et al*. gives a more detailed review of these procedures (93).

2. Nanoparticles and the BBB permeability

Koziara *et al*. have prepared the novel NPs, by warm microemulsion precursors, for transport across the BBB (94). Two types of nanoparticles (emulsifying wax NPs/Brij 78 surfactant, and Brij 72 NPs/ Tween-80 surfactant) were fabricated and radiolabelled by entrapment of [^{3}H]cetyl alcohol. The entrapment efficiency and release of the radiolabel were evaluated by an *in situ* rat brain perfusion method to determine the transport of NPs across the BBB. In the perfusion method, the animal's circulating blood is substituted with vascular perfusion fluid. Meanwhile, the *in vivo* constitution of the BBB and brain tissue is exploited. Briefly, buffered perfusion fluid

(containing NaCl, Na_2PO_3 $NaHCO_3$, KCl, $CaCl_2$, $MgCl_2$, and d-glucose), with [^{3}H] NP and [^{14}C] sucrose (to determine the vascular volume), was infused into the left common carotid artery at a rate of 10 ml/min for periods of 15–60 s; the pressure in the carotid artery was maintained at ~120 mm Hg. Kinetics analyses were performed on the labeled NPs at the end of perfusion. The brain uptake of Brij 72 coated NPs was found higher than that observed for Brij 78 NPs, a fact attributed to the use of Tween-80 in the former polymerization. Moreover, [^{14}C] sucrose labeling verified the integrity of the BBB when it was found that the vascular space did not increase in the presence of nanoparticles. Lastly, the authors suggested endocytosis or transcytosis as possible mechanisms for transport; however, they have not elucidated these figures.

Nanoparticles have also been used in the *in vivo* investigation of BBB permeability following cerebral ischemia and reperfusion. Fluorescent polystyrene NPs were injected intravenously into rats under ischemic attack. A microdialysis probe was implanted directly into the brains of the rats by stereotaxic injection. The nanoparticles were collected in the extracellular interstitial fluid by *in vivo* microdialysis; the presumption being that these particles were extravasated from the capillaries, and so therefore, represent permeability of the BBB (see Figure 10). The cerebral oxygenation level was determined by oxygen-dependent quenching of phosphorescence of the nanoparticles. This was done to correlate the BBB permeability to extravasated NPs with oxygen concentration, following the cerebral ischemia and reperfusion. The induced ischemia was by the occlusion of the middle cerebral artery (MCA), and was followed by fluorescence intensity. Yang *et al*. found that this technique could be used to measure extracellular NPs *in situ* in the brain (95). Under normal oxygen conditions, the NPs remained in the vasculature. However, MCA occlusion yielded an immediate increase in the extracellular concentration of the NPs. Subsequent fluorescent intensity in the microdialysate was resultant from the induced states of ischemia and reperfusion. This model represents the BBB permeability and so can be further probed as a system for drug delivery to the brain.

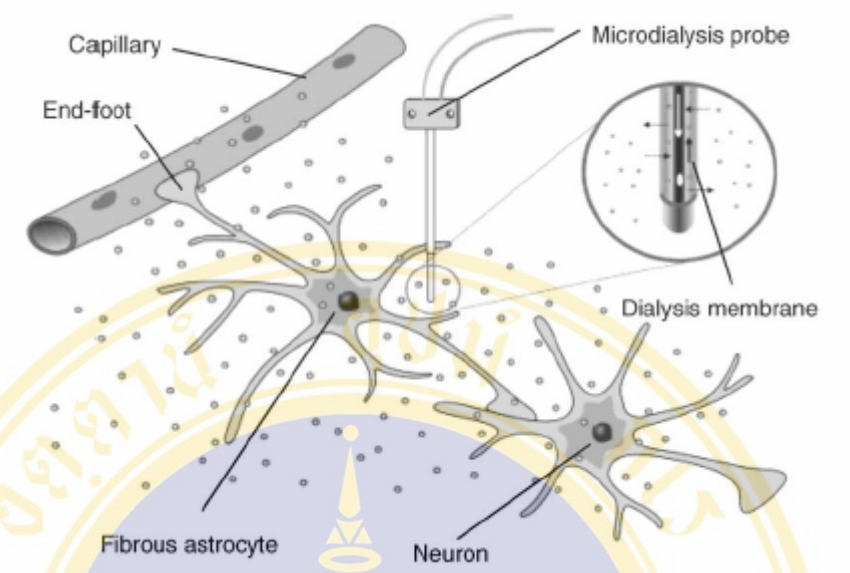

Figure 10. Schematics of nanoparticles used to investigate BBB permeability by *in vivo* microdialysis following cerebral ischemia and reperfusion

Oligonucleotides (ODN) are the negatively charged macromolecules that exhibit poor cellular uptake (96). Their charge and size characteristics alone make them unsuitable for facile passage through the BBB. In addition, ODN have high renal clearances and are prone to enzymatic degradation, both in the systemic circulation (97) and by intracellular nucleases (94). Examples of cationic carriers to improve the cellular uptake of ODN are reviewed in the literature (98-101). Vinogradov *et al*. have encapsulated ODN within stable dispersions of cross-linked poly(ethylene glycol) (PEG) and polyethyleneimine (nanogelQ) for the delivery of the macromolecule across the BBB (78,102). The theory behind nanogels is that they are fabricated without the drug using the emulsification solvent evaporation method (73,103). Afterwards, the nanogels are swollen in water to load the drug. Cationic cross-linked covalent chains of PEG and PEI spontaneously encapsulate the negatively charged ODN. After drug loading, the solvent volume decreases and the gel collapses to form nanoparticles.

Nanogel was conjugated with biotin, and the biotinylated nanogel was subsequently labeled with rhodamine isothiocyanate (RITC). The ODN was labeled with fluorescein isothiocyanate (FITC) and with tritium for fluorescent and radiographic analysis. Nanogels were tritium labeled to aid in radiographic analysis

upon *in vivo* biodistribution. To the solution of rhodamine labeled biotinylated ODN encapsulated nanogels, avidin and biotinylated bovine transferrin or biotinylated bovine insulin was added, to prepare the complex as vectors for drug delivery (see Figure 11). Bovine brain microvessel endothelial cells (BBMEC) were isolated and grown as a polarized monolayer to mimic the BBB; transepithelial electrical resistance (TEER) values were recorded as a standard measure of the integrity of the monolayer.

Figure 11. Schematic representation of a vectorized nanogel, manipulated for *in vivo* brain delivery of oligonucleotides (ODN)

Transport studies were conducted by placing the BBMEC monolayers in side-by-side diffusion chambers. The donor chamber contained the nanogel–ODN dispersions with the paracellular diffusion marker ^{3}H-mannitol. Cellular accumulations of FITC–ODN and RITC–nanogel were accessed by confocal laser fluorescent microscopy of BBMEC cells grown on chamber slides. Finally, *in vivo* biodistribution studies were preformed by intravenous administration to wild type mice, using the ^{3}H-labeled compounds in the nanogel–ODN complex. After injection, organs were homogenized and the amounts of ^{3}H-nanogel or ^{3}H-ODN in the homogenate were measured by liquid scintillation.

Vinogradov *et al.* found an 80% uptake of the ^{3}H-nanogel by the BBMEC (102). The rate of transport of the drug-loaded nanogels was a function of the BBMEC complexes; positively charged complexes more efficiently transported the

drug-loaded nanogels than did the negatively charged complexes. It was also found that the ODN transported with the nanogel to the BBMEC monolayer remained at least 2/3 bound in the receiver unit of the diffusion chamber. In addition, the layer was 6-fold more permeable to the nanogel–ODN as compared to the free ODN. The BBB permeability further increased by vectorizing the nanogels with the insulin and transferrin ligands (11- to 12-fold increases compared to the free ODN). Furthermore, the paracellular marker ^{3}H-mannitol was transported along with the nanogel–ODN complex in the diffusion chamber, suggesting a mechanism of transport at the BBB and verifying the integrity of the tight junctions of the monolayer.

Cytotoxicity of the nanogels was assessed, and conclusions were drawn that the complexes and complex compounds were nontoxic to the BBMEC monolayer, thus suggesting the potential of this carrier in the biological system. Uptake of the FITC–ODN and RITC–nanogels by the BBMEC was found mainly in the cytoplasm, although some FITC–ODN was localized in the nucleus. This suggested that a small portion of ODN released and transported to the nucleus since nanogels cannot penetrate the nuclear membrane due to size exclusion of the pores. The *in vivo* biodistribution studies exhibited high levels of free ODN in the liver and spleen, with increasingly smaller amounts in the brain. The nanogel–ODN complex, however, greatly increased the BBMEC permeability to ODN, with decreases in the liver and the spleen. Therefore, nanogels increased the brain uptake of the ODN and protected the macromolecule from rapid clearance by peripheral organs.

Lin *et al*. have prepared novel NPs by ionic gelation of poly-g-glutamic acid (g-PGA) into a hydrophilic, low-molecular weight (MW) chitosan (CS) solution; the application of the NPs to paracellular transport was investigated in an *in vitro* design by measuring the transepithelial electrical resistance (TEER) of Caco-2 cell monolayers (104). TEER values are informative of the tightness of the junctions between the cells. Hence, decreased TEER values are expected when TJs open. The NPs were physicochemically characterized by Fourier transformed infrared (FTIR) spectroscopy, dynamic light scattering (DLS), transmission electron microscopy (TEM) and atomic force microscopy (AFM). Paracellular transport was visualized by confocal laser scanning microscopy (CLSM). The CS was depolymerized by enzymatic hydrolysis to produce the low-MW CS, which was characterized by gel

permeation chromatography (GPC). Colonies of *Bacillus licheniformis* were cultured and grown to produce the g-PGA, which was purified by centrifugation and dialysis, and confirmed by proton NMR ([^{1}H] NMR) and FTIR analyses. The NPs were obtained instantaneously, by mixing (by magnetic stirring) varying concentrations of aqueous solutions of the g-PGA (pH 7.4) and the low-MW CS (pH 6.0), and were isolated by ultracentrifugation (38,000 rpm, 1 h). Morphology of the NPs was examined by TEM and AFM. The Caco-2 cells were cultured for use in the transport experiments. The cells were equilibrated with transport media, in which they were incubated along with the NPs, which were fluorescently labeled (with fluorescein isothiocyanate, FITC) (fCS-g-PGA NP) for visualization by CLSM. This suspension was introduced into the donor compartment of the transport chamber, whereby the TEER values were monitored.

The authors found that the particle size and zeta potential of CS-g-PGA NP could be controlled by their constituent components, thus ensuring stabilization of the NPs upon manipulation of the component concentrations (104). In addition, stability studies of the positively (0.10% g-PGA: 0.20% CS) and negatively (0.10% g-PGA: 0.01% CS) surface charged NPs were performed, and no aggregation or precipitation of either (for up to 6 weeks) was reported. Figure 12 shows the TEM and AFM results of the CS-g-PGA NPs. A significant reduction in the TEER values of the Caco-2 cells was found upon incubation with the positively charged (CS dominated on the surface) NPs. In fact, the NPs with the positive surface charge reduced the TEER values of the Caco-2 cells by 50%, indicating that the TJs between the cells had been opened, presumably by chitosan.

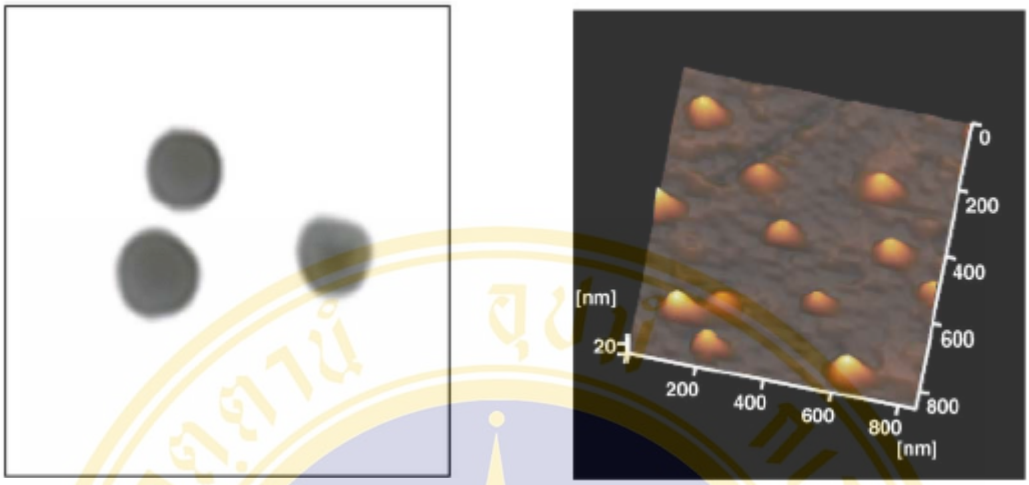

Figure 12. TEM (0.10% g-PGA: 0.20% CS) and AFM (0.01% g-PGA: 0.01% CS) micrographs of CS-g-PGA NPs (107)

Moreover, when the incubated NPs were removed from the transport chamber, the TEER values of the Caco-2 cells increased (see Figure 13), indicating recovery of the TJ. However, the NPs with a negative surface charge (g-PGA dominated on the surface) did not significantly change the TEER values of the Caco-2 cells, as compared to the control (no NP incubation) group. These results indicate that the CS, and not the g-PGA, opens the intercellular TJ, a phenomenon visualized by CLSM (see Figure 14). By CLSM, fCS-g-PGA NP transport through the Caco-2 cells was visualized at both incubation time and monolayer depth variables; fluorescence intensity was measured at 20 and 60 min of incubation with the NPs, and at depths of 0–15 μm from the apical surface of the monolayer. The authors, therefore, successfully verified the passive diffusion of NPs through the paracellular pathway (104).

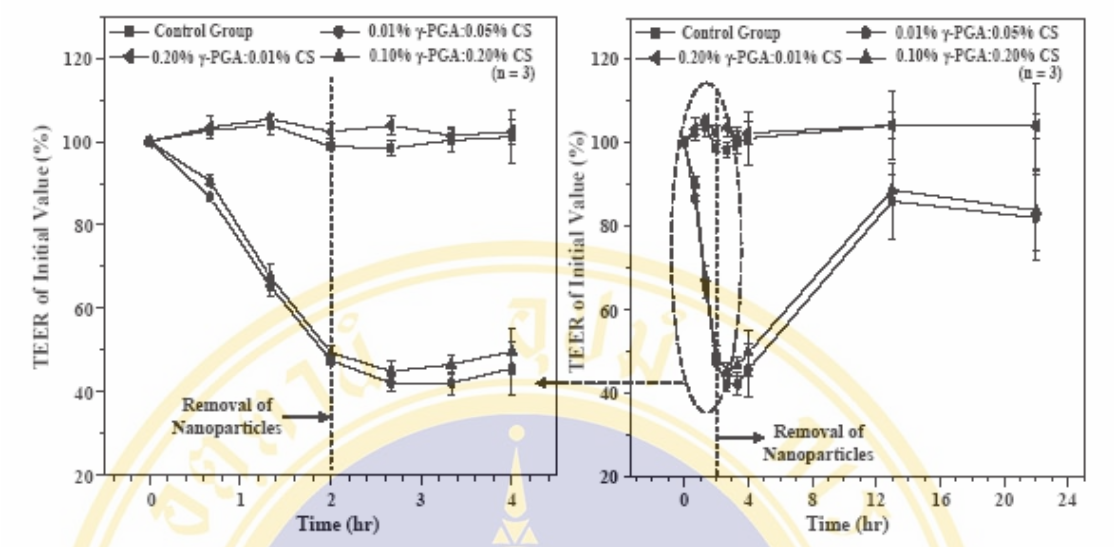

Figure 13. Effect of CS-g-PGA NPs on TEER values of Caco-2 cells. NPs with a positive surface charge have reduced the values of TEER. This suggests that CS-g-PGA NPs can open intercellular tight junctions, thereby enhancing paracellular transport of ions, macromolecules and hydrophilic drugs (107)

It should be noted that Caco-2 is a human epithelial colorectal adenocarinoma cell line, and does not represent the endothelial cells required to study the properties of the BBB. However, integral and accessory proteins of the TJ are not unique between epithelial and endothelial cells, particularly the zona occludens protein, the protein implicated by Lin *et al*. (104), and its role on paracellular transport (47,55,58,60,61,63,105,106). The line of work undertaken by Lin *et al*. is applicable to the field of targeted drug delivery through the BBB (107). Particularly, NPs can be chemically designed with the appropriate surface characteristics to cross the brain microvascular endothelial cells, and the physics of this occurrence verified by TEER (see Figure 13). Biologically, the live cells can be visualized by CLSM (see Figure 14), and at last, the NPs introduced into the murine model for the *in vivo* assessment of neurological disorders such as AD; these surveys are currently in progress.

Advances in the merging fields of BBB/CNS disorders and nanoparticle technology, such as vectorization, drug loading/release, etc., are widely reported. For example, Garcia-Garcia *et al*. give an interesting review on using polymers as implantable intracerebral controlled-release devices to deliver drugs directly to brain interstitium in a sustained way (108). By this method, the rates of drug transport,

metabolism and elimination can be carefully upheld. Furthermore, Lockman *et al.* (109) have employed nanoparticles, surface-coated with a radiolabelled thiamine ligand, as a vector to the BBB in order to understand the *in situ* brain perfusion of a rat (109).

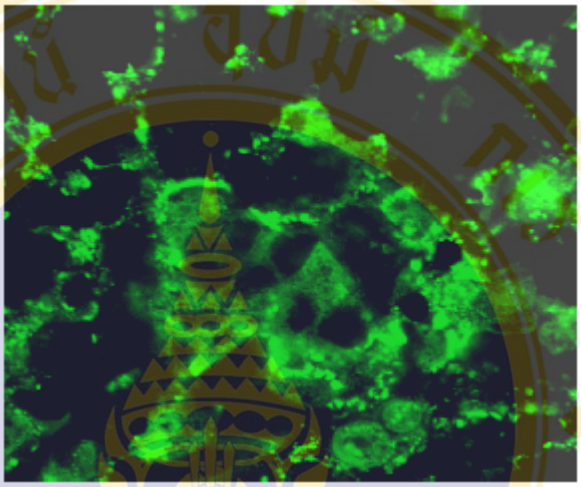

Figure 14. Fluorescence image (taken by an inversed confocal laser scanning microscope) of an optical section (0 Am) of a Caco-2 cell monolayer that had been incubated with fCS-g-PGA nanoparticles with a positive surface charge (0.10% g-PGA: 0.20% CS) for 20 min (107)

Successful brain entry of the thiamine-coated nanoparticles was shown (109). Moreover, the thiamine associates with BBB transporters, thereby providing a possible explanation for the facilitation of NP-assisted drug delivery. In addition, solid lipid nanoparticles (SLN) have been investigated as drug vectors to the brain. For example, Wang *et al*. have found enhanced targeting, and subsequent increased brain uptake, of the drug 3, 5-dioctanoyl-5-2deoxyuridine (DO-FUdR) once it is incorporated into SLNs (110). A nearly 30% drug loading efficiency was achieved, and the targeting efficiency to the brain was significantly increased from 11.77% to 29.81%, and with a prolonged half-life. SLNs improve the lipophilicity of the drug complex, thereby increasing the chances of the delivery of the incorporated drug across the BBB. Finally, NPs have been found to increase the BBB permeability of brain capillary endothelial cells (by transcytosis) when vectorized with cationic

bovine serum albumin (CBSA) and poly(ethyleneglycol)–poly(lactide) (PEG–PLA) (111).

C. A Free Radical

A Free Radical is any chemical species that has an odd number of electrons, because it contains one more unpaired electron(s), which is an electron that occupies an atomic or molecular orbital by itself (112-114). A radical will thus be indicated, as recommended, by a superscripted dot at the right side of the formula in parenthesis so as to show that no judgment as to the location of the unpaired electron is made. The symbol R will be used throughout to represent an unspecified radical which may be positively charged (cation radical, $R^{\bullet+}$), negatively charged (anion radical, $R^{\bullet-}$) or neutral (neutral radical, Rn). Radical can be formed by the loss of a single electron from a non-radical, or by the gain of a single electron by the non-radical. They can easily be formed when a covalent bond is broken if one electron from each of the pair shared remains with each atom, a process known as homolytic fission.

$$A{:}B \longrightarrow A^{\bullet} + B^{\bullet}$$

1. Properties of radicals

Because of its unopposed electron a radical is slightly attracted to a magnetic field; it is paramagnetic. This unique physical property allows for its detection and spectroscopy in aqueous solution at room temperature (117). Fast flow techniques are used to detect short-lived radicals (118). The most popular methodology is spin trapping, in which a diamagnetic organic molecule, called the spin trap, reacts with the radical, to produce a secondary more stable radical called a spin adduct. The spin adduct is more readily detectable by ESR. Methylnitrosopropane (MNP) and 5,5 dimethyl-1-pyrroline-N-oxide (DMPO) are two common spin traps as shown in Figure 15 (118).

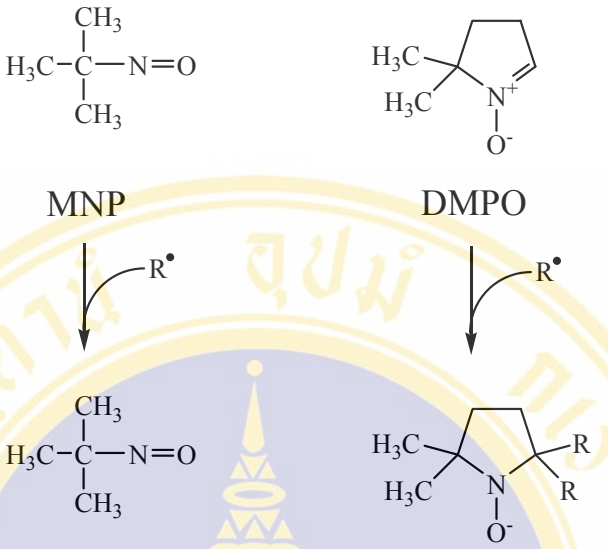

Figure 15. Spin trapping of radicals

The chemical reactivity of radicals is usually high, although differences are great. Like that of any other chemical species, the reactivity of radicals is influenced by the nature of the solvent, by pH and by other properties. At temperatures near 37 °C, most radicals are so reactive and normally exist only at a very low concentration.

2. Biological radicals

Radical reactions are generally chain reactions. The radicals are generated in a step or steps called "initiation". They participate in a sequence of "propagation" reactions in which their number is conserved; finally they are destroyed in a "termination" process or processes (119).

Initiation of radical chain reactions: Oxygen (O_2), hydrogen peroxide (H_2O_2), water (H_2O) and polyunsaturated fatty acids appear to play an essential role as major substrate for these events. O_2 does so because it serves as addition are the major substrate for these events. O_2 does so because it serves as an acceptor for single electrons arising in cells either via the one-electron enzymatic (or radiolytic) O_2 does so because it serves as reduction of endogenous and exogenous organic molecules or as a side product of incomplete electrons transport in mitochondria, endoplasmic reticulum or nuclear membranes. Monoelectronic reduction of O_2 produces superoxide anion ($O_2^{\bullet -}$). H_2O_2, the end product of peroxidases catalyzed reactions or

the product of $O_2^{\bullet-}$ dismutation, plays a role mainly because it is the substrate of metal in catalyzed decomposition to yield the hydroxyl radical ($HO^{\bullet}$). Polyunsaturated fatty acids occupy a key position in radical chain reaction, not because they are direct substrates of major initiation processes, but they can easily be transformed in alkyl hydroperoxides (ROOH). The alkyl hydroperoxides are transformed to either alkoxyl and alkylperoxyl radicals ($RO^{\bullet}$, $ROO^{\bullet}$) as a result of a molecule assisted homolysis (Figure 16).

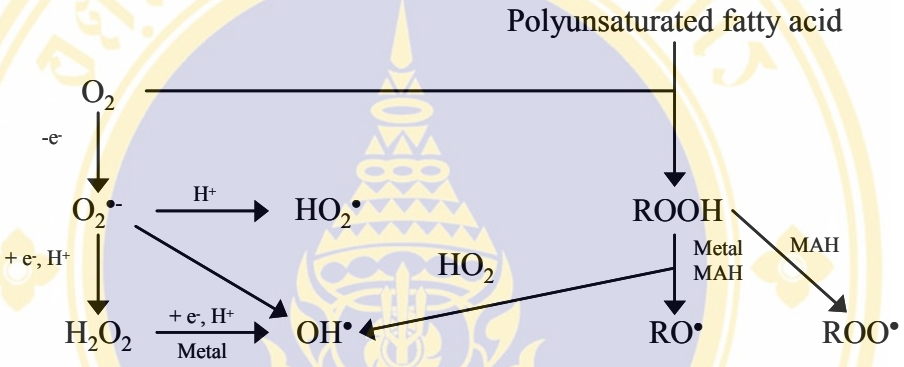

Figure 16. Biological initiation of the radical chain reaction, MAH = molecule assisted homolysis

Propagation of radical chain reactions: The hydroxyl radical ($HO^{\bullet}$) plays a major role, but hydroperoxide (ROOH) as well as alkoxyl or alkylperoxyl radicals ($RO^{\bullet}$, $ROO^{\bullet}$) of polyunsaturated fatty acids are still key targets and/or key intermediate. H atom transfers (or H atom abstraction), electron transfer, as well as addition (Figure 17) are the major events in biologically relevant radical propagation. β-Scission is a rather rare event that may concern only alkoxyl radicals that arise from the molecule assisted homolysis of hydroperoxide of polyunsaturated fatty acid in lipids.

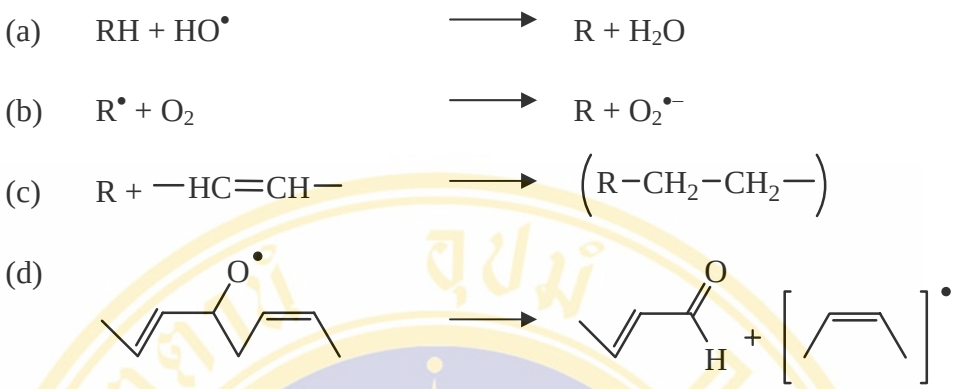

Figure 17. Biological relevant propagation reaction, (a) = atom transfer, (b) = electron transfer, (c) = addition, (d) = β-Scission

Termination of radical chain reaction: Figure 18 summarizes the major termination processes of radical chain reaction that are likely to occur in cells. Both dismutation and reduction involve electron transfer, either by electron exchange between identical molecular entities or by electron capture in a classic oxidoreduction propagate the radical but, rather, is likely to homolink. The most important homolinking reaction in biological system is that involving 2 glutathione radical ($GS^{\bullet}$) to form the oxidized glutathione (GSSG).

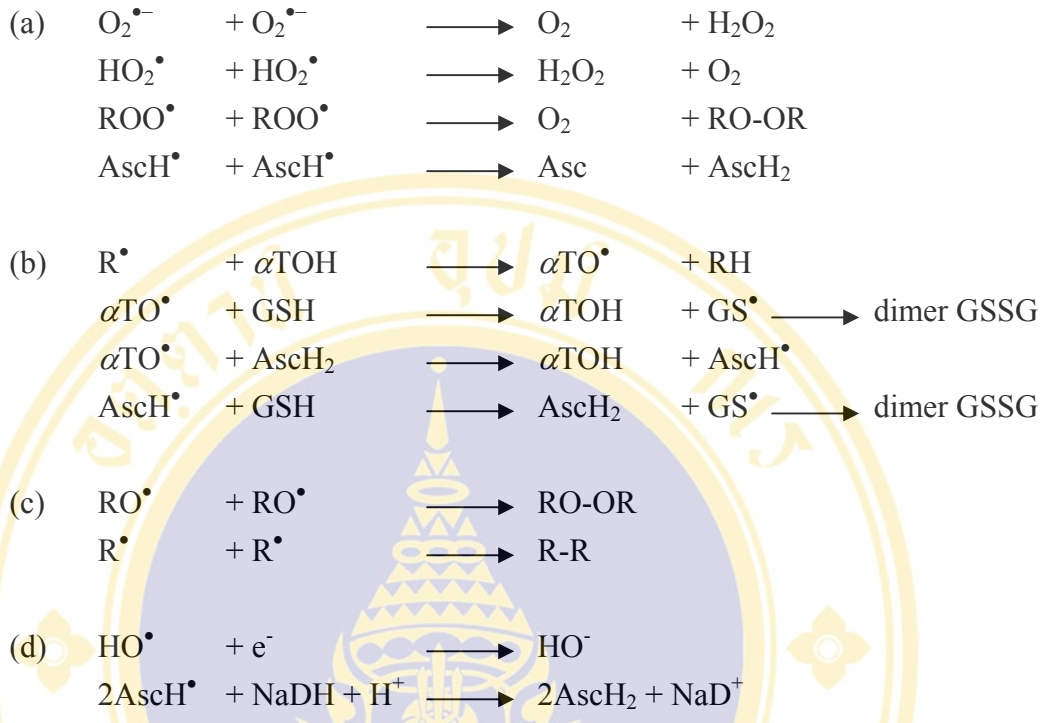

Figure 18. Termination processes in radical chain reaction. GSH = reduced glutathione, GSSG = oxidized glutathione; $AscH_2$ = ascorbate; AscH = semidehydro-ascorbyl radical, Asc = dehydroascorbate, αTOH = α-tocopherol, $\alpha TO^{\bullet}$ = α-tocopherol radical

3. Lipid peroxidation

Oxygen-derived radicals ($O_2^{\bullet-}$, $HO^{\bullet}$) as well as their organic counterparts, $ROO^{\bullet}$ and $RO^{\bullet}$ are the most frequent molecular entities likely to be formed in biological radical reaction chains. Because of their high chemical reactivity, these radicals react readily with many of the biomolecules: substrates, metabolites or products of biochemical pathways, vitamins, small peptides and lipids and also macromolecules (proteins and nucleic acids). Such reactions may participate in the propagation step in the radical reaction chain that leads to radical mediated damages or terminate the chain of reaction (119-120).

Unsaturated fatty acids are essential biomolecules which play an important role in cellular metabolism and cellular structure. They exist as free acids (e.g., arachidonic acid, leukotrienes, and prostacyclins), as thioesters (acylScoA) but mainly

as esters e.g. triglycerides, phospholipids, sphingolipids and cholesteryl-lipid. The main pools of unsaturated fatty acyl esters inside the organism are the biomembranes and the circulating lipoproteins. In the biomembranes, unsaturated fatty acid moieties play a major role to the fluidity (that increases with increasing number of double bonds) of the lipid bilayer within which proteins diffuse laterally. Because of their peculiar chemical structure (cis-double bonds separated by an allylic CH_2), unsaturated fatty acids are sensitive targets for radicals that easily abstract an H-atom from an allylic CH_2 to give a C-centered radical to which O_2 readily attaches to form a $ROO^{\bullet}$ and finally an ROOH. The oxidizability of unsaturated fatty acids by radicals depends linearity on the number of bis-allylic methylene it contains. Moreover, the reactive oxygen can attach to a C=C double bond to produce a similar ROOH. In the presence of Fe^{2+} or Fe^{3+} (including iron ions in proteins or hemeproteins) (121-122), ROOH decomposes to yield $ROO^{\bullet}$ and $RO^{\bullet}$, respectively.

Even though in a pure lipid containing polyunsaturated fatty acyl moieties H abstraction to give $C^{\bullet}$ is the initiating event, as soon as ROOH is formed it also becomes between ROOH-independent and ROOH-dependent lipid peroxidation (Figure 19). In that context the exact role of the iron ion in initiating or supporting a radical reaction chain is difficult to define unequivocally. But it seems to be rather well established today that its major role is to catalyze the oxidation or reduction of ROOH rather than to participate in H-abstraction. β-Scission of ($RO^{\bullet}$) and dismutation of 2($ROO^{\bullet}$) give hydrocarbons plus various aldehydes, hydroxyunsaturated fatty acid (ROH), and O_2, respectively (123-124). The most important aldehydes are 4-hydroxyalkenals and malondiadehyde (Figure 20).

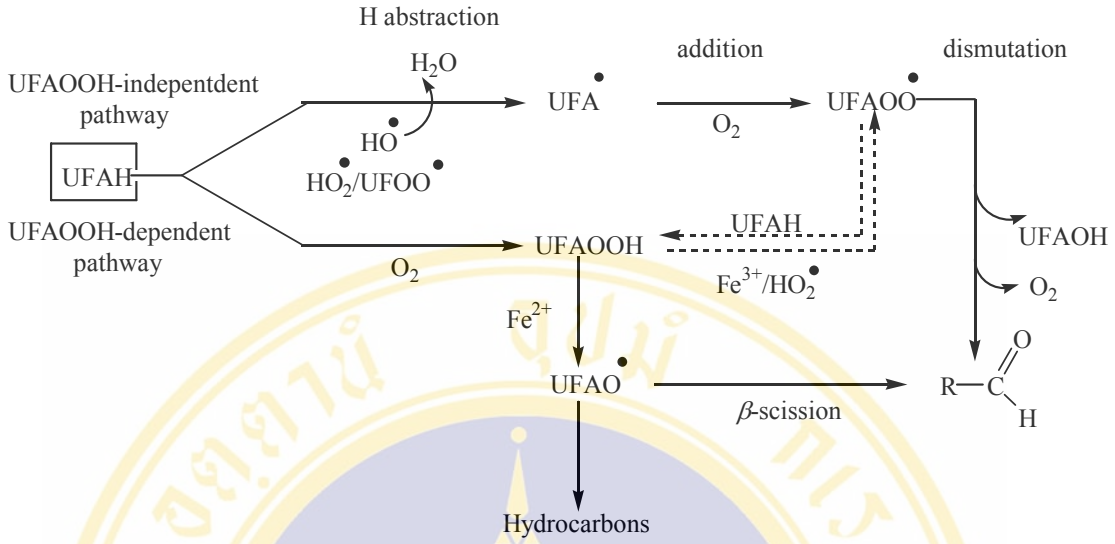

Figure 19. Radical- and O^{2-} mediated oxidative destruction of unsaturated fatty acyl moiety in lipids. Major potentially damaging molecular species are UFA, UFA$^{\bullet}$, UFAOO$^{\bullet}$, UFAO$^{\bullet}$: UFA = unsaturated fatty acid moiety in a lipid, UFA$^{\bullet}$ = bis-allylic methylenic C-centered radical, UFAOO$^{\bullet}$ = peroxyl radical, UFAO$^{\bullet}$ = alkoxy radical, UFAOH = hydroxyl UFA

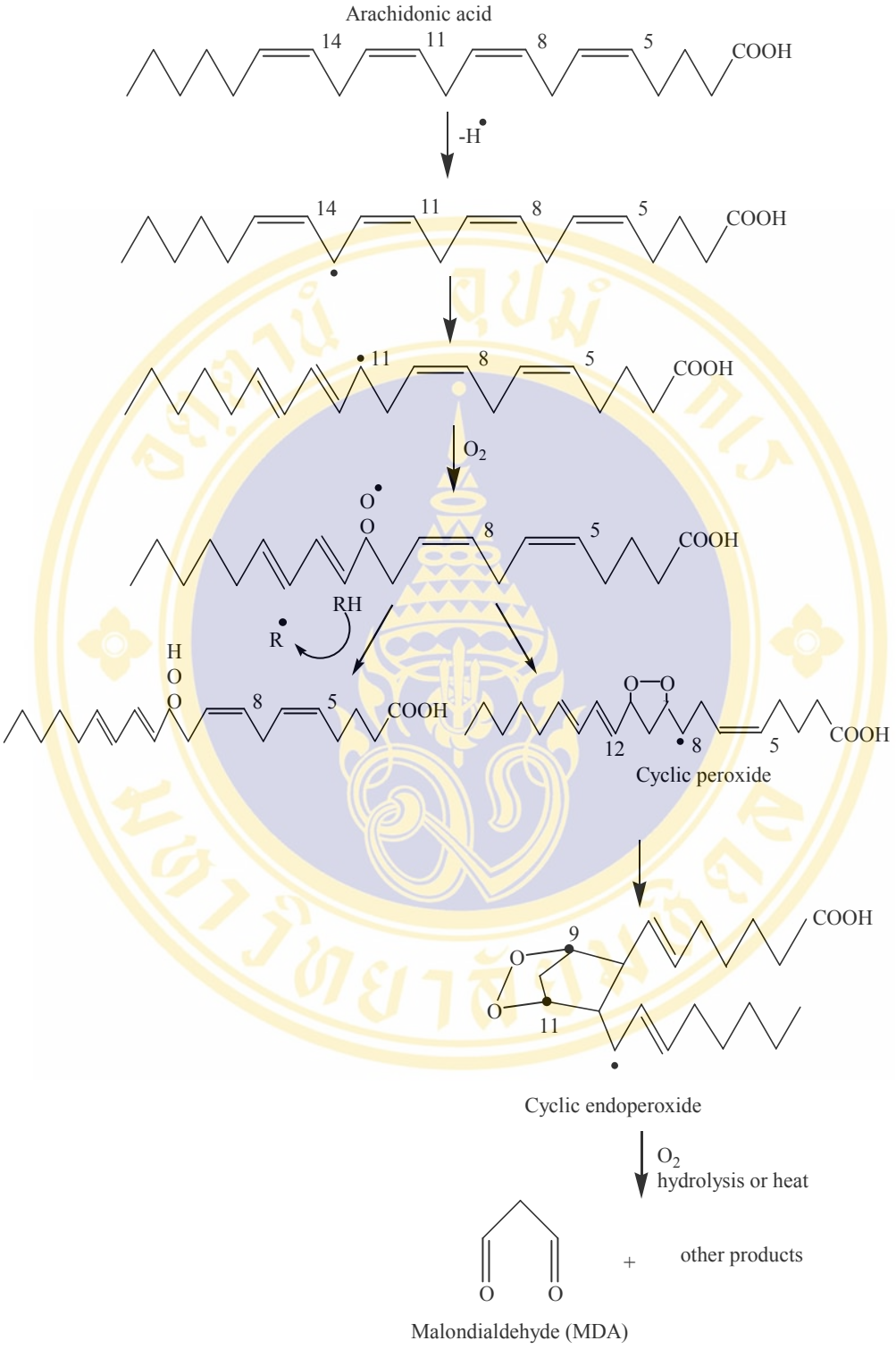

Figure 20. The peroxidation of arachidonic acid

4. Source of free radical

Free radicals are normal products of cellular aerobic metabolism. Superoxide and hydroxyl ($HO^{\bullet}$) species are predominant cellular free radicals. Hydrogen peroxide (H_2O_2) and peroxynitrite ($ONOO^-$), although not themselves radical containing molecules are referred to as reactive oxygen species (ROS). The major source of ROS is mitochondrial oxidative metabolism, enzymatic reactions involving mixed-function oxidation and autoxidation of small molecules. Mixed function oxidation reactions occur in the cytoplasm, plasma and nuclear membrane, endoplasmic reticulum and peroxisomes is formed by leakage of high-energy electrons along the mitochondrial electron transport chain and by a variety of cytosolic and membrane-bound enzymes, including xanthine oxidase, the cytochrome P450 complex and phospholipase A2 (PLA2). H_2O_2 also is produced along the electron transport chain as well as through (SOD). Though not itself reactive, H_2O_2, in the presence of reduced metal via the Fenton reaction, forms the highly reactive $^{\bullet}OH$. Peroxynitrite ($ONOO^-$), formed by the reaction of nitric oxide ($NO^{\bullet}$) with, is a highly reactive molecule that also breaks down to form $^{\bullet}OH$ (125).

D. Curcumin and Related Compounds

Curcuma longa Linn. or turmeric (Zingiberaceae) is a medicinal plant widely cultivated in tropical regions of Asia and it has been found to be a rich source of phenolic compounds, namely curcuminoids. Turmeric extract from the rhizomes are mainly composed of three different of diarylheptanoids, curcumin (diferuloylmethane), demethoxycurcumin (feruloylmethane), and bisdemethoxy curcumin (di-p-hydroxycinnamoylmethane) (126-127). Commercially available curcumin consists of a mixture of three naturally occurring curcuminoids with curcumin as the main (~77%) constituent (128). Curcuminoids are recognized for their broad spectrum of biological activities and safety in foods or pharmaceuticals. Curcumin, the principal natural yellow pigment, is widely used for the coloring of foods. Curcumin [1,7-bis(4-hydroxy-3-methoxyphenyl)-1,6-heptadiene-3,5-dione] is known for its antioxidant, anti-inflammatory, anticancer, antimutagenic, anitmicrobial, and antiparasitic properties (126-127). A large number of publications

and several reviews have appeared. However, turmeric and its components are still attracting attention and many new properties are being discovered.

1. Chemistry of curcumin

Curcumin is in the most important fraction of *C. longa* L. and its chemical structure, was determined by Roughley *et al* (129). It melts at 176-177 °C and forms red-brown salts with alkalis. Curcumin is soluble in ethanol, alkalis, ketone, acetic acid and chloroform; and is insoluble in water. In the molecule of curcumin, the main chain is aliphatic, unsaturated and the aryl group can be substituted or not. Structurally, curcumin consists of two ortho methoxylated phenols and a *β*-diketoned moiety, and they are all conjugated providing as electron-rich donor structure. Curcumin is unique in structure, which has two isomers, *β*-diketone and enol form. From the calculated results, it can be found that the structure of *β*-diketone form is not completely planar and two methoxy phenol rings show a dihedral angle of –124.9°. However, each methoxyphenol ring is completely planar owing to the conjugation and the intramolecular H-bond. The structure of enol form is different from that of *β*-diketone form. The two methoxyphenol rings in the enol form are well conjugated and coplanar. It is also interesting to note that the two forms are different in energy. The energy of enol is lower than that of *β*-diketone form, suggesting that the enol form of curcumin predominates in solution (130).

2. Biological activities of curcumin

2.1 Antioxidant activity

Unnikrishnan *et al* (131) studied the antioxidative properties of curcumin and its three derivatives (demethoxycurcumin, bisdemethoxycurcumin and diacethylcurcumin). The authors demonstrated that these substances provide a protection of hemoglobin from oxidation at a concentration as low as 0.08 mM, except the diacetylcurcumin which has little effect in the inhibition of nitrite induced oxidation of hemoglobin. The effect of curcumin on lipid peroxidation, a main role in the inflammation, in heart diseases, and in cancer, has also been studied in various models by several authors (132-136). Curcumin is a good antioxidant and inhibits lipid peroxidation in rat liver

microsomes, erythrocyte membranes and brain homogenates (132). Turmeric can lower lipid peroxidation by maintaining the activities of antioxidant enzymes like superoxide dismutase, catalase and glutathione peroxidase at higher levels (133). These enzymes play an important role in the regulation of lipid peroxidation. Another article about curcuminoids as potent inhibitors of lipid peroxidation was described by Sreejayan *et al* (134-135), in which the authors showed that three curcuminoids were inhibitors of lipid peroxidation in rat brain homogenates and rat liver microsomes. All of these compounds were more active than α -Tocopherol (drug reference) and curcumin showed the better results. In the case of curcumin, the methoxy group seems to play a major role. The phenolic and the methoxy group on the phenyl ring and the 1,3-diketone system seems to be important structural features that can contribute to these effects. The diketone system is a potent ligand for metals such as iron, used in these experiments. Another fact proposed in the literature is that the antioxidant activity increases when the phenolic group with a methoxy in at the ortho position (134-136).

Its antioixidant effects were confirmed in various systems. Curcumin was found to suppress the generation of ROS including $O^{2-\bullet}$ and H_2O_2 in peritoneal macrophage, an important role in the initiation of inflammation (137). Ghoneim *et al* reported the potential protective effects of curcumin against ischemia/reperfusion (I/R) insult in rat forebrain performed by means of bilateral common carotid artery occlusion. It was found that curcumin at 200 mg/kg decreased the IR-induced elevated xanthine oxidase (XO) activity, $O^{2-\bullet}$ production, malondehyde level and GPX, SOD, and lactate dehydrogenase (LDH) activities. These antioxidant properties seem to have a role in inhibiting $O^{2-\bullet}$ generation directly or indirectly (via inhibiting of XD/XO conversion) (138).

In modification of antioxidant properties, Oyama *et al* (139) have synthesized the curcumin derivatives, 5'-alkylated curcumins. It was found that the inhibitory actions of 5'-alkylated curcumins on lipid peroxidation in cell-free conditions and on living cells suffering from oxidative stress induced by H_2O_2 increased as the length of 5'-n-alkyl chain increased. Of the 5'-n-alkyl curcumins, 5'-n-C_3H_7-curcumin and 5'-n-C_5H_{11}-curcumin have a protective action much more potent than that of curcumin.

The authors concluded that the 5'-n-alkylation of curcumin not only increased the antioxidant activities, but also increased the permeation across the cell membranes and into the cells.

A number of study demonstrated that curcumin is capable of scavenging oxygen free radicals such as $HO^{\bullet}$ and $O^{2-\bullet}$ (132, 140-142). However, recent studies showed that curcumin is not an effective $O^{2-\bullet}$ radical scavenger. It was able to inhibit only 24% in the reduction of ferricytochrome c (in xanthine/xanthine oxidase system) at the high concentration of 80 mM (143) and a 39% inhibition of a reduction of nitroblue tetrazolium (NBT) was observed by 54 mM curcumin (144). However, by EPR technique, it was demonstrated that curcumin is a potent singlet oxygen ($^1O_2$) quencher; curcumin at low concentration inhibited the 2,2,6,6-tetramethyl piperidine (TEMP)-$^1O_2$ adduct in dose dependent manner (143). Moreover, it has been reported that curcumin rapidly react with many reactive oxidants such as NO_2 (145), peroxyl radicals ($ROO^{\bullet}$) (146), alkoxyl radical ($RO^{\bullet}$) (147-148), $^{\bullet}CH_3$ (148), haloperoxyl radicals ($CCl_3O^{\bullet}$), azide radicals ($N_3^{\bullet}$), $Br^{2-\bullet}$, glutathione radicals ($RS^{\bullet}$) (149), etc., by electron transfer and the most possible site of attack by the oxidant is the phenolic OH group.

The antioxidant mechanism of curcumin has attracted much attention, and several physiochemicals studies were recently reported. Pulse radiolysis study in aqueous and laser flash photolysis study in the acetonitrile solution indicated the curcumin radical was an oxygen-centered radical rather than a carbon-centered radical. However, the presence of both β-diketone and phenol is necessary for optimal antoxidant function of curcumin (147-148). By density function theory (DFT) method, Sun *et al* (150) demonstrated that the antioxidant mechanism of curcumin was a H-atom abstraction from the phenolic group, not from the central CH_2 group in the heptadienone link. The O-H bond dissociation enthalpy (BDE) is much lower than the C-H BDE of the central CH_2 group in the heptadienone link for the curcumin and curcumin-related compounds, suggesting that the antioxidant mechanism of curcumin is a H-atom abstraction mainly from the phenolic group. Masuda *et al* (151-153) indicated that curcumin shows potent antioxidant activity

against the oxidation of ethyl linoleate, as one of the polyunsaturated lipids, by its radical chain-breaking ability, dividing into two stages:

(i) radical trapping stage

$$S{-}OO^{\bullet} + AH \rightleftharpoons SOOH + A^{\bullet}$$

(ii) radical termination stage

$$A^{\bullet} \longrightarrow \text{nonradical materials such as A-A, AOOS, and Aox}$$

Where S is the oxidation substrate, AH is the phenolic antioxidant, $A^{\bullet}$ is the antioxidant radical, A-A is the dimer of A, AOOS is the substrate antioxidant peroxide and Aox is the oxidized A. Although the first stage is a reversible, the second stage is irreversible and must produce stable radical terminated compounds. In this study the structural elucidation of such terminated compounds was carried out. Masuda *et al* suggested that curcumin is first converted to the curcumin radical at the phenolic position. The radical can move to appropriate position as represented in Figure 21. There are two types of radical terminations, which include the dimer formation (A-A termination) and the formation of the coupling product between curcumin and the lipid hydroperoxides (AOOS termination). From the quantitative data for the production of these termination products, the formation rate of the AOOS termination products was almost constant regardless of the curcumin concentration, while the rate of the dimer production depended on the concentration (153).

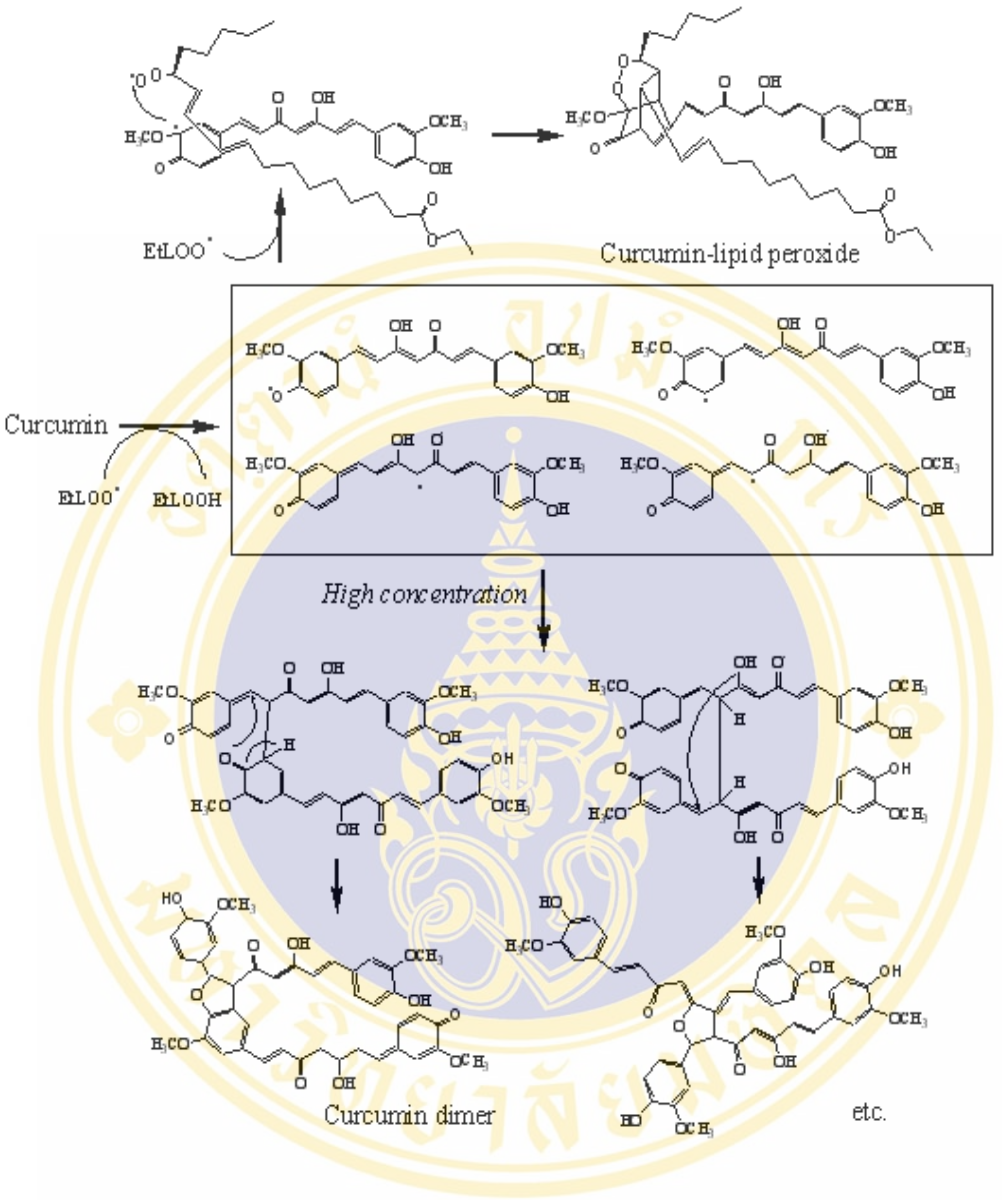

Figure 21. Proposed chain-breaking antioxidant mechanism of curcumin against the oxidation of ethyl linoleate (153)

2.2 Anti-inflammatory activity

Curcumin showed anti-inflammatory effect in acute, subacute and chronic models of inflammation in mice and rats. Mukophadhyay *et al* (154) demonstrated the activity of curcumin and other semi-synthetic analogues (sodium curcuminate, diacetyl curcumin and triethyl curcumin) in carrageenin-induced rat paw edema and cotton pellet granuloma models of inflammation in rats. In these experiments the authors used ferulic acid and phenylbutazone as reference drugs. Curcumin and its

analogues showed similar action in carrageenin-induced paw edema in rats; however the sodium curcuminate was the most potent analogue and was more water-soluble than curcumin. Among the curcumin analogues, triethylcurcumin was the most potent anti-inflammatory in the chronic model of inflammation, when compared with the others and with the drug reference. In the acute inflammation condition, all the substances were more effective. The authors concluded that the activity of the compounds used in these experiments, would depend on the model of inflammation. Arora *et al* (155) investigated the anti-inflammatory activity in different fractions of the petroleum ether extract of the rhizomes of turmeric (two constituents) in animals. They found that the extracts reduced the granuloma growth and no toxic effects were observed. Ghatak *et al* (156) showed the action of sodium curcuminate as an anti-inflammatory agent, being better than curcumin and hydrocortisone acetate, in experimental inflammation induced by carrageenin and formalin in albino rats (ED_{50} = 144 μg/kg), its more soluble in water than curcumin and no side effects were observed. Srimal *et al* (157) reported that the compound was effective in acute as well as chronic models of inflammation. The potency of this drug is approximately equal to phenylbutazone in the carrageenin-induced edema test, but it is only half as active in the chronic experiments. It was observed that curcumin was less toxic than the reference drug (no mortality up to a dose of 2 g kg^{-1}). Huang *et al* (158) examined the inhibitory effects of curcumin on the proliferation of blood mononuclear cells and vascular smooth muscle cells. In blood mononuclear cells, curcumin was capable to impair the response of cells to mitogen, PHA and the response to alloantigen, MLR. The investigators suggested that curcumin could be used clinically in transplant atherosclerosis. Ammon *et al* (159) demonstrated curcumin as an inhibitor of leucotriene formation in rat peritoneal polymorphonuclear neutrophils (PMNL), with an EC_{50} of 2.7 mM, in contrast, the hydrocortisone did not show any effect. Abe *et al* (160) reported the effect of curcumin on inflammatory cytokine production by human peripheral blood monocytes and alveolar macrophages. The results showed that curcumin exhibits an inhibitory effect on the production of IL-8, MIP-1α, MCP-1, IL-1β, and TNF-α, by 4β-phorbor 12α-myristate-13α-acetate (PMA)- or lipopolysaccharide (LPS)-stimulated monocytes and alveolar macrophages. Moreover, Chuang *et al* (161) showed that curcumin at concentrations of 200 mg/kg

or 600 mg/kg could effectively suppressed diethylnitrosamine-induced liver inflammation and hyperplasia in rats, by inhibiting the increased expression of cellular gene products such as oncogenic p21 (ras) and p53 proteins, and reducing the expression of cell-cycle-related proteins such as proliferating cell nuclear antigen (PCNA), cyclin E and p34 (cdc2).

Clinically, curcumin did not produce any side effect up to 1600 mg/kg/day for 4 weeks in phase-I trials in male volunteers. Phase-II trials have been conducted in patients with rheumatoid arthritis and osteoarthritis (162-163). The first results of a controlled clinical in 18 patients showed satisfactory improvement, treated with 120 mg/kg/day orally. Although curcumin was found weaker than phenylbutazone, no side effect was reported. Satoskar *et al* (164) published the results of a double blind trial with curcumin in case of acute inflammation comparing it with oxyphenbutazone and placebo. Curcumin produced significant effect. Subsequently, the number of patients in each category has gone up with satisfactory. No side effects have been reported in any patient.

2.3 Antitumor and anticancer activities

Curcumin showed a potent anticarcinogenic activity against a broad range of tumor types. Curcumin inhibits mutagenicity of certain chemical carcinogenesis and also hampers their covalent DNA binding *in vivo* as well as *in vitro* (127-128, 165). Curcumin protected against chemically induced liver damage in experimental animals (166). Its anticarcinogenic activity was evaluated in many animal tumor models. One of the most prominent effects of curcumin exerted on experimental carcinogenesis was its capability to inhibit tumor promotion (167-169). Thus, curcumin was reported to alleviate 12-O-tetradecanoyl-13-acetate (TPA)-induced skin tumor promotion (168) and epidermal ornithine decarboxylase (ODC) mRNA expression (169). Curcumin was also evaluated for its photochemopreventive effects. Ultraviolet A (UVA) irradiation significantly enhanced ODC induction after topical application of TPA in the epidermis of CD-1 mice and aggravated TPA-mediated dermatitis. A pretreatment of skin with curcumin was found to significantly inhibit these UVA-enhancing effects (170). Topical application of curcumin onto dorsal skins of mice significantly inhibited epidermal cyclooxygenase (COX) and lipoxygenase (171).

Colonic mucosal COX and lipoxygenase activities were suppressed by curcumin, which appeared to account for its chemopreventive effects on colon carcinogenesis. Likewise, F344 rats fed curcumin in the diet exhibited reduced catalytic activities of phospholipse A2 and phospholipase Cg1 that are involved arachidonic acid release from cellular phospholipid (172). It also attenuates oxidative DNA damage in mouse epidermis (169) and in cultured mouse fibroblast cells (173). TPA-induced protein kinase C activation and c-jun expression were markedly suppressed by curcumin in mouse fibroblast cells (174). When applied topically on the dosal side of mouse skin, curcumin significantly inhibited expression of such proto-oncogenes as c-fos, c-jun, and c-myc (175). Curcumin also exhibited inhibitory effects on epidermal growth factor (EGF) receptor kinase activity in cultured human epidermoid carcinoma a431 (176) or NIH3T3 cells (177). Other types of protein kinases were also found to be inhibited by this compound in a non-competitive manner (178). According to a recent study by Huang *et al* (179), curcumin suppresses TPA-responsive element-binding activity of c-jun/AP-1, the transcription factor related to cell growth signaling in the final stage of cell proliferation, which may account for the ant-tumor promoting effect of this chemopreventive agent. Curcumin has been reported to inhibit TNF-α-induced binding of AP-1 to DNA in bovine aortic endothelial cells (180). Besides interfering with AP-1 activation, curcumin has been shown to suppress the activation of nuclear factor-kB (NF-kB) that is another important eukaryotic transcription factor (181). The suppression of protein kinases, ODC, and nuclear transcription factors by curcumin suggests that it can act as a cytostatic agent by interfering with certain signal transduction pathways that are critical for cell growth and proliferation activity and the capability of inducing programmed death or apoptosis in cancer cells.

In another study, Iersel *et al* (182) demonstrated that curcumin was the most potent inhibitor of glutathione S-transferase, the major pi-class GST subunit P1 activity, towards 1-chloro-2, 4-dinitrobenzene in intact human IGR-39 melanoma cells. Curcumin have been showed to induce apoptosis in human basal carcinoma cells and human breast cancer cells in a dose- and time-dependent manner where p53-associated signaling pathway was critically involved in curcumin-mediated apoptotic cell death (183-184). Ozaki *et al* (185) demonstrated that curcumin drastically inhibits osteoclastic bone resorption supporting its stimulation of apoptosis in the

cells. Recently, curcumin has been entered into the phase-I clinical trials for chemoprevention by National Cancer Institute (186). Cheng *et al* (187) reported the chemoprevention in patients with high-risk or pre-malignant lesions. The results suggested a biologic effect of curcumin in the chemoprevention of cancer and demonstrated that curcumin is not toxic to humans up to 8,000 mg/day when taken orally for 3 months.

Analogues of curcumin have also been prepared in an effort to increase the activity. Devasena *et al* (188) investigated the protective effect of curcumin and its analogs, bisdemethoxycurcumin and synthesized BDMC-A (bis-1.7-(2-hydroxyphenyl)-hepta-1,6-diene-3,5-dione), on hepatic lipid peroxidation and antioxidant status during 1,2-dimethylhydrazine (DMH)-induced colon carcinogenesis in male Wistar rats. The effect of both analogs were compared with that of curcumin. As both curcumin and BDMC-A are equally effective in ameliorating the DMH-induced colon tumorigenesis and hepatic oxidative stress, the authors concluded that methoxy group is not essential for their antioxidant and/or anticarcinogenic properties.

Shim *et al* (189) synthesized new curcumin analogs, named hydrazinocurcumin and hydrazinobenzoylcurcumin. The inhibitory potency of both hydrazinocurcumin and hydrazinobenzoylcurcumin against the proliferation of ovine aortic endothelial cells (BAECs) was over 30 and 26-fold higher than that of curcumin, respectively. Hydrazinocurcumin also effectively inhibited the *in vivo* neovasuclarization of chick embry (73%) without without affecting endothelial cell viability.

Adams *et al* (190) developed the novel synthetic curcumin analog, EF24, which could induced cell cycle arrest and apotosis by means of a redox-dependent mechanism in MDA-MB-231 human breast cancer cells and DU-145 human prostate cancer cells. Cell cycle analysis demonstrated that EF24 cause a G2/M arrest in both cell lines, and that this cell cycle arrest is followed by the induction of apotosis as evidenced by caspase-3-activation, phosphatidylserine externalization and an increased number of cells with a sub-G1-DNA fraction. In addition, EF24 induced a depolarization of the mitochondrial membrane potential, suggesting that the compound may also induce apotosis by altering mitochondrial function. EF24, like

curcumin, serves as a Michael acceptor reacting with glutathione (GSH) and thioredoxin 1. Reaction of EF24 with GSH and thioredoxin 1 *in vivo* significantly reduced intracellular GSH as well as oxidized GSH in both the wild-type and Bcl-xL overexpressing HT29 human colon cancer cells. This studied demonstrated that fluorine atom at the ortho position of the terminal aromatic rings of EF24 confers the most potent anticancer activity. The free OH groups at the ortho position of the terminal aromatic rings of a substituted cyclopentanone proved to exhibit the best induction of quinone reductase, enhancing the nucleophilic reactivity of the SH groups of mediator compounds, such as GSH. These suggest that EF24, at least with respect to proteins and mediators bearing the SH group, has potential to modulate the action of multiple targets.

2.4 Anti-human immunodeficiency virus (HIV)

Mazumber *et al* (191) have demonstrated the inhibitory activity of curcumin against HIV-1 integrase (IC_{50} = 40 μM), which is essential for integration of a double stranded DNA copy of viral RNA genome into a host chromosome and for HIV replication. This finding suggested that curcumin analogs may be developed as anti-AID drugs. Data showed that curcumin inhibited the replication of HIV-1 integrase protein. Mazumber *et al* (192) also reported two curcumin analogs, dicaffeoylmethane, and rosmarinic acid, which showed potent activity against HIV-1 integrase in both a dual 3'-processing and strand transfer tests with IC_{50} values below 10 mM. The data showed that these analogs inhibited the catalytic activity of integrase by binding of the enzyme to the viral DNA but this inhibition is independent of divalent metal ion (Mg^{2+}, Mn^{2+}). The authors suggested the importance of both the hydroxyls and unsaturated linker present in curcumin, while the methoxy groups do not play a key role in potency. Curcumin and related compounds were claimed for anti-HIV-1 and HIV-2 activities in a recent patent application (193).

2.5 Antibacterial activity

Curcuma oil was tested against cultures of *Bacillus coagulans*, *Bacillus subtilis*, *Staphylococcus aureus*, *Escherichia coli*, and *Pseudomonas aeruginosa*. (194). The results show that the turmeric oil and its column fractions exhibited an antibacterial effect against all the bacteria tested. In the case of Gram-positive bacteria, curcumin

oil brought about complete inhibition of growth at the 50 ppm level, while for Gram-negative bacteria a higher concentration (200 ppm) was required to inhibit complete growth. Bhavani *et al* (195) investigated the activity of turmeric fractions against some intestinal bacteria *in vitro*. In this work, total inhibition of growth of Lactobacilli in the presence of whole turmeric was observed (4.5-90 µl/100 ml). The other fraction, the alcoholic extract, was effective too (10-200 mg/ml), but the inhibition was not equal as the whole turmeric. Curcumin (2.5-50 mg/ml) only inhibited *S. aureus*.

2.6 Hepatoprotective activity

Curcumin and turmeric have been shown to protect liver against a variety of toxicants *in vitro* as well as *in vivo*. These include carbon tetrachloride (196), aflatoxin B-1 (197), paracetamol (198-199), iron (200) and cyclophosphamide (201) in mouse, rat and ducking. Soni *et al* (198) reported more than 80% inhibition of mutagenesis induced by aflatoxin B-1 in *Salmonella thyphimurium* tester strains TA98 and TA100 by turmeric and curcumin at a concentration of 2 mg/plate. Singh *et al* (202) studied the effect of turmeric (4 g/kg/day) and curcumin (0.4 g/kg/day) on the hepatic levels of glutathione-S-transferase, acid soluble sulfhydryl (-SH), cytochrome b5 and cytochrome P-450 enzymes after 14 or 21 days of administration in lactating dams and transtactationally exposed F-1 pups. All the enzymes examined were significantly elevated in lactating dams as well as in pups. Curcumin has been reported to inhibit cytochrome P450 in the liver, an isozyme involved in the bioactivation of several toxins including benzo[a]pyrene (203-204). Other interesting action was demonstrated by Park *et al* (196), when acute hepatotoxicity was induced by intraperitoneal injection of carbon tetrachloride in rats. After these animals had been treated with curcumin, the liver injury was inhibited.

2.7 Antiprotozoal activity

The first work to relate the activity of curcumin and some semi-synthetic derivatives in the literature against tripanosomatids was studied in promastigotes (extracellular) and amastigotes (intracellular) forms of Leishmania amazonensis. The authors showed that curcumin in experiments *in vitro* has an excellent activity (LD_{50} = 24 µM or 9 mg/ml) and the semi-synthetic derivative, methylcurcumin (a non-

phenolic curcuminoid), has the best action with a LD_{50} < 5 μg/ml and LD_{90} = 35 μM against promastigotes forms. This derivative was tested *in vivo* in mice and showed a good activity with 65.5% of inhibition of the lesion size of the footpad of the animals, when compared with the group inoculated with the parasites alone (205-206). Rasmussen *et al* reported that curcumin, demethoxycurcumin and bisdemethoxy curcumin showed moderated efficacy against *Plasmodium falciparum* (IC_{50}: 3.5, 4.2 and 3.0 mg/ml) and *Leishmania* major (IC_{50}: 7.8, 14.1 and 21.5 mg/ml) respectively (207).

2.8 Other activities

Vaenkatesan and Chandrakasan have reported the protective effect of curcumin on rat lung against the toxicity induced by cyclophosphamide (208) and bleomycin (209). Several reports suggest that curcumin as well as turmeric increase bile flow and increase the excretion of bile salts and decrease the amount of solids in the bile in low doses, but increased the excretion of bile salts, bilirubin and cholesterol in high doses (210-211). Curcumin has been reported to inhibit lipopolysaccharide (LPS)- and interferon-g-induced production of nitric oxide in macrophage or nitrite in mouse peritoneal cells, possibly by suppression of nitric oxide synthase (212-213). Chan *et al*. have reported the inhibition by curcumin of inducible nitric oxide synthase gene expression in isolated BALB/c mouse peritoneal macrophages and also in the livers of lipopolysaccharide-injected mice (214). More recently, Onoda *et al*. have shown that curcumin (100 mM) obviously suppressed the iNOS expression in rat mammary gland cultured with LPS, and a recovery in the eNOS expression was observed (215).

3. Pharmacokinetics

Pharmacokinetic studies in rats indicated that the absorption of pure curcumin from the gastrointestinal tract is about 60-65% after administration of a single oral dose of 400 mg/kg. About 40% of the administered dose was recovered unchanged in the faces over a period of 5 days with a peak after 3 days. Free curcumin was not detected in urine but excretion of glucuronic acid and sulfate conjugates was observed, supporting an enterohepatic circulation (215-217). This result was confirmed by *in vitro* experiments using intestine of rat and [^{3}H]-curcumin. About

30-80% of the labeled compound disappeared from the mucosal side but could not be detected on the serosal side, indicating that it undergoes transformation during absorption. Studies with [^{3}H]-curcumin *in vivo* confirmed that absorption from gastrointestinal tract remained between 60-66% irrespective of the dose, but the duration of retention of label was dose-dependent (218).

CHAPTER III
MATERIALS AND METHODS

A. Preparation of Nanoparticles

1. Materials

Equipment

Analytical balance	Satorius 2842, USA
Magnetic stirrer	Heidolph MR 3001K, Germany
Sub-micron particle analyzer	Coulter model N4, USA
UV spectrophotometer	Shimadzu, Japan
Centrifuge	Sorvall RC 5C plus, USA
Lyophilizer	Model Alpha 1-4, Germany

Apparatus

Rotary evaporator	Eyela, Japan
TEM	JSM 6400, Japan
Lazer zee meter	Zeta H7, USA
Rotary vacuum evaporator	Eyela, Japan

Chemicals

Methylmethacrylate	Fluka, Switzerland
Ammonium peroxodisulfate	Fluka, Switzerland
Poloxamer 407	Garguar lab, Thailand
Polysorbate 80	Fluka, Switzerland
4-Fluoro-4′-hydroxy-benzophenone	Aldrich, USA
Disodium hydrogen phophate	M&B, England
Sodium chloride	M&B, England
Potassium dihydrogen phosphate	UNILAB, Australia
Sodium sulfate anhydrous	M&B, England
Sodium hydroxide pellets	BDH, England
Citric acid	M&B, England
Curcumin	TCFF, Thailand
Chloroform	Labscan, Iceland
Acetone	Labscan, Iceland
Ethanol	Labscan, Iceland
Methanol	Labscan, Iceland
Acetonitrile	Labscan, Iceland
Seasand	Ferak, Germany
Silica gel 60 No. 1.07734	Merck, Germany
Dry ice	TIC AC, Thailand
Sodium sulfate, anhydrous	Aldrich, U.S.A.

2. Methods

Nanoparticles were formed by a technique derived from radical polymerization. The mean particle size of nanoparticles was determined by photon correlation spectroscopy using a Coulter sub-micron particle analyzer (Coulter model N4MD). Transmission electron microscopes (TEM) analysis was performed to visualize the shape and to measure the size of nanoparticles. The zeta potential was measured in demineralized water using a Delsa 440SX. The brains were assayed for the amount of curcumin by HPLC.

2.1 Separation of curcumin from commercial curcuminoids

Commercial curcuminoids or tumeric extract (1 g) was mixed with silica gel (0.5 g) and separated using silica gel column chromatography (eluent: chloroform/methanol/acetic acid, 98:5:2). Curcumin was eluted first and then eluent was dried as yellow powder and recrystallied with ethanol to give the yellow crystals of curcumin (0.600 g, 60%), m.p. 185-187 °C. IR (KBr) (cm^{-1}): 3414 (O-H), 3010 (aromatic C-H), 2973 (alkene C-H), 2940 (alkane C-H), 1631 (C=O ketone), 1604-1435 (C=C), 1288-1032 (C-O). ^{1}H NMR (d-DMSO): δ 3.82 (s, 6H, O-C<u>H</u>$_3$), 6.05 (s, 1H, -CO-C<u>H</u>=COH-), 6.75 (d, J 15.87 Hz, 2H, Ph-CH=C<u>H</u>-CO-, Ph-CH=C<u>H</u>-COH-), 6.81 (dd, J 1.53 and 8.24 Hz, 2H, Ph-<u>H</u>5, Ph-<u>H</u>5$^{/}$), 7.14 (d, J 7.93 Hz, 2H, Ph-<u>H</u>6, Ph-<u>H</u>6$^{/}$), 7.31 (d, J 1.53 Hz, 2H, Ph-<u>H</u>2, Ph-<u>H</u>2$^{/}$), 7.53 (d, J15.87 Hz, 2H, Ph-C<u>H</u>=CH-), 9.67 (br, 1H, exchangeable with D_2O, Ph-CO<u>H</u>=CH). TLC: stationary phase-silica gel GF 254, mobile phase-chloroform/ ethanol/acetic acid (98:5:2): R_f of curcumin = 0.7, R_f of demethoxycurcumin = 0.63 and R_f of bisdemethoxycurcumin = 0.52. MS (m/z) (% relative intensity): M^{+}368(19.56).

2.2 Preparation of polymethylmethacrylate nanoparticles

Poly(methylmethacrylate) (PMMA) nanoparticles were prepared at 78 °C using free radical polymerization medium containing poloxamer 407 (2% poloxamer 407 in water) as a stabilizer and ammonium peroxodisulfate (APS) as an initiator (0.02% APS in water). One percent of methylmethacrylate was added under constant magnetic stirring at 600 rpm. After 4 h of polymerization, a milky white nanoparticle suspension was obtained. The suspension was filtered through a sintered glass filter (10 μm pore size) and the filtrate was ultracentrifuged. The obtained residue from the centrifugation was lyophilized.

2.3 Preparation of polysorbate 80 coated curcumin nanoparticles

A 500 mg amount of the freezed-dried nanoparticles was re-suspended in 10 ml of 10 mM phosphate-buffered saline (PBS) under constant stirring by magnetic stirrer. Curcumin solution (2 g in 10 ml of 10 mM phosphate-buffered saline containing 0.2 ml of ethanol) was added dropwise to the nanoparticle suspension. The curcumin was allowed to adsorb onto the nanoparticles surface under conditions of constant stirring (300 rpm) for 4 h. The obtained curcumin nanoparticles suspension was filtered through a nylon membrane filter (0.025 μm pore size), the curcumin loaded nanoparticles were stored at 4 °C until use. Before administration, curcumin loaded nanoparticles were coated with polysorbate 80. Polysorbate 80 at 0.01% relative to the total suspension volume was added to the curcumin loaded nanoparticles and incubated with shaking for 30 min.

B. Characterization of Nanoparticles

1. Materials

Apparatus

Centrifuge apparatus	Hettich Universal, Germany
HPLC	Shimadzu, Japan
Communication Bus	Module CBM-10A
UV-Visible Detector	SPD-10A
Data processing	(class-LC10)
Column : Hypersil ODS C18 (5 μm, 4.6 mm I.D. × 150 mm L)	Shandon,U.K.
Nylon membrane filter (13 mm dia., 0.45 μm)	German Science, USA
Nylon membrane filter (47 mm, 0.025 μm)	Millipore, USA
Filter paper No.1	Whatman, England
Filter apparatus	Sartorius, Germany
pH meter	Schott gerate, Germany
Ultrasonic bath	J.P. Selecta, Japan
Centrifuge apparatus	Sorvall RC 5C plus, USA

Chemicals

Potassium dihydrogen phosphate	Merck, Germany
Potassium chloride	Mayer & Baker, U.K.
4-Fluoro-4′-hydroxy-benzophenone	Aldrich, USA
Sodium hydroxide pellets	BDH, England
Water for Injection	General Hospital Products Public Co., Ltd.
Methanol (HPLC)	Labscan Asia, Thailand
Acetonitrile (HPLC)	Labscan Asia, Thailand

Water (HPLC) Labscan Asia, Thailand

2. Methods

2.1 Size and shape of nanoparticles

The mean particle size of nanoparticles was determined by photon correlation spectroscopy using a Coulter sub-micron particle analyzer (Coulter model N4MD). Nanoparticles were diluted with water to give a particle count rate between 5×10^4 and 1×10^6 counts per second. Mean particle diameter was calculated in size distribution processor mode (SDP) using the following conditions: fluid refractive index 1.33; temperature 20 °C; viscosity 0.93 centipoise; angle of measurement 90.0°; sample time 10.5 μs, and sample run time 90s. Transmission electron microscope (TEM) analysis was performed to visualize the shape and to measure the size of nanoparticles.

2.2 Zeta potential of nanoparticles

The zeta potential was measured in demineralized water using a Delsa 440SX. The zeta potential of nanopaticle samples were determined using the following conditions: current 0.7 mA; frequency range 500 Hz; temperature 25 °C; fluid refractive index 1.33; viscosity 0.8872 centipoise; dielectric constant 78.55; conductivity 0.1121 ms/cm; on time 2.5 s, off time 0.5 s, and sample run time 60 s. Each sample was analyzed in triplicate.

2.3 Curcumin assay

HPLC was used for the determination of curcumin in nanoparticles and in mice brain. The mobile phase was a mixture of acetonitrile (eluent A) /citric acid pH 3 (eluent B) (80:20, v/v). 4-Fluoro-4′-hydroxy-benzophenone was used as internal standard in the concentration of 2.0 μg/ml. The method for the determination of curcumin in brain and curcumin in nanoparticles were developed and validated. The parameters used to validate the developed assay method in this study were linearity (r^2), accuracy (% recovery), precision (% RSD), limit of detection and limit of quantitation.

2.3.1 Instrumentation

The essential parts of HPLC consisted of pumps, column oven, UV detector set at 423 nm and a 150×4.6 mm i.d. column. The stationary phase in column was Hypersil ODS C18, 5-μm particle size, 150×4.6 mm i.d. (Shandon, U.K). Manual injections were carried out using a Rheodyne model 7725 injector with a 20-μl sample loop.

The mobile phase was a mixture of acetonitrile (eluent A) /citric acid pH 3 (eluent B) (80:20, v/v). The mobile phase was filtered through a nylon membrane (47 mm, 0.45 μm) and degassed by sonication. Isocratic flow rate of 0.3 ml/min was maintained. The eluent was monitored with a UV/VIS detector (SPD-10A, Shimadzu, Japan) at 423 nm.

2.3.2 Stock and working standard solutions

A 1 mg/ml stock solution of curcumin was prepared. One ml of the prepared stock solution was accurately transferred to a 100 ml volumetric flask, diluted to volume with methanol, and mixed to obtain diluted stock solution. Standard solutions (1.0, 2.0, 4.0, 6.0, 8.0 and 10.0 μg/ml) were prepared by diluting the diluted stock solution with methanol in 10 ml volumetric flask and added 2 ml of internal standard solution (10 μg/ml) to give 2 μg of internal standard per ml of standard solutions. All of the solutions were kept in a refrigerator at 4-8 °C and filtered through 0.2 μm membrane filter before injection to HPLC.

2.3.3 Linearity

The linearity of the method was determines by injecting the standard solutions to the HPLC system described in section 2.3.2. The calibration curve data of the mixture of curcumin standard covering the range of 1.0-10.0 μg/ml and 4-fluoro-4′-hydroxy-benzophenone (2.0 μg/ml) were carried out. The calibration curve was accomplished by plotting peak-area ratios between curcumin and internal standard versus the concentrations of curcumin. Each solution was injected in triplicate. A calibration curve was described by the equation below:

$$y = ax + b$$

where

y = the response (peak area ratio between curcumin and internal standard)

x = the concentration of an analyte,

a = the slope, and

b = the intercept of a line fit to the data.

The correlation coefficient (r^2) of the calibration curve was determined.

2.3.4 Accuracy

The accuracy of an analytical method is the closeness of test results obtained by that method to the true value, expressed by percent recoveries. Percent recoveries were calculated by using standard addition method. The determination of the accuracy of the method was performed by injecting the homogenized brain spiked with standard solutions to the HPLC system. Standard solutions were concentration in the range of 3.2-4.8 μg/ml and added 4-fluoro-4′-hydroxy-benzophenone (2.0 μg/ml) was spiked into the mice brains. The brains were homogenized in 10 ml of iced-cold phosphate buffer saline pH 7.4. The homogenate was centrifuged at 3300 g for 10 min at 4 °C. The supernatant was filtered through a nylon membrane filter (0.2 μm pore size), the filtrate was adjusted to 10 ml with methanol and 20 μl of the filtrate was then injected into the HPLC column. Each sample was injected in six replicated (n = 6). Percent recoveries were calculated by the following equation:

$$\% \text{ Recovery} = \frac{X_{found}}{X_{added}} \times 100$$

where

X_{found} = the concentration of standard found the spiked sample,

X_{added} = the concentration of standard added

2.3.5 Precision

The injection precision and the intra-day precision of the method were assessed by the following methods:

(a) Injection precision

The injection precision was determined by repetitive injection (n = 6) of the standard solution (4.0 μg/ml).

(b) Intra-day precision

The standard solutions at concentration of 2.0, 3.0 and 4.0 μg/ml were injected for six replicated (n = 6), at same time within day, the retention time and the peak area were recorded for the determination of the intra-day precision.

(c) Inter-day precision

The standard solutions at concentration of 2.0 μg/ml was injected for six replicated (n = 6), at differential day, the retention time and the peak area were recorded for the determination of the inter-day precision.

Precision was assessed from the percent relative standard deviations (% RSDs), which was determined from the following formula:

$$\text{RSD (\%)} = \frac{100\,SD}{\overline{X}}$$

where

S.D. = The standard deviation from average value,

$\overline{X}$ = The average value of the retention time or peak area

2.3.6 Limit of detection and limit of quantitation

The limit of detection (LOD) and limit of quantitative (LOQ) of the method was studied by injecting homogenized brain solution (blank solution) to the developed HPLC system. The brains were homogenized in 10 ml of iced-cold phosphate buffer saline pH 7.4. The homogenate was centrifuged at 3300 g for 10 min at 4 °C. The supernatant was filtered through a nylon membrane filter (0.2 μm pore size), the filtrate was adjusted to 10 ml with methanol and 20 μl of the filtrate was then injected into the HPLC column. The noise from the blank at 7.21 minutes (the retention times of curcumin) and 4.98 minutes (retention time of 4-fluoro-4′-hydroxy-benzophenone, an internal standard) were measured and calculated for the area ratio (An). The peak area ratios of the measured noises were multiplied with 3 and 10, respectively equations (1) and (2). The LOD and LOQ were the concentrations of curcumin at the noise area ratios (An) multiplied by 3 and 10, respectively calculated from the regression equation of the standard curve.

$$A_n = \frac{\text{noise at t}_{7.21\ \text{min}}}{}$$

$$A_n = \frac{\text{noise at t}_{4.98\ \text{min}}}{}$$

where A_n is the peak area ratio from noise of the blank

2.4 Determination of curcumin content and entrapment efficiency

2.4.1 Determination of curcumin content

The quantitative determination of curcumin in nanoparticles was carried out using a reversed phase isocratic HPLC (Shimadzu HPLC) with UV–Vis detector SPD-10A VP and C-18 column (150 mm × 4.6 mm, particle size 5 mm, UK). A mixture of acetonitrile/ citric acid pH 3.0 (80:20) was used as the mobile phase. The filtered mobile phase was pumped at a flow rate of 0.3 ml/min and the eluent was monitored at 423 nm. 4-Fluoro-4′-hydroxy-benzophenone was used as internal standard in the concentration of 2.0 μg/ml. The peak areas of curcumin and the internal standard were measured for the calculation of peak area ratios. The concentration of curcumin were determined in triplicate from the regression equation of the standard curve was used to analyse. The curcumin content (%) was calculated according to the following equation:

Curcumin content (% w/w)

$$= \frac{\text{Weight of added curcumin- Weight of curcumin in filtrate}}{\text{Weight of curcumin loaded nanoparticles}} \times 100 \quad (1)$$

2.4.2 Determination of curcumin entrapment

The curcumin was analysed as described in section 2.4.1 and curcumin entrapment (%) was calculated according to the following equation:

Curcumin entrapment (% w/w)

$$= \frac{\text{Weight of added curcumin- Weight of curcumin in filtrate}}{\text{Weight of added curcumin}} \times 100 \quad (2)$$

C. Brain Accessibility

1. Materials

Apparatus

Analytical balance	Mettler AE 160, Switzerland
Centrifuge apparatus	Hettich Universal, Germany
HPLC	Shimadzu, Japan
Communication Bus	Module CBM-10A
UV-Visible Detector	SPD-10A
Data processing	(class-LC10)
Column : Hypersil ODS C18 (5 μm, 4.6 mm I.D. × 150 mm L)	Shandon,U.K.
Nylon membrane filter (13 mm dia., 0.45 μm)	German Science, USA
Nylon membrane filter (47 mm, 0.025 μm)	Millipore, USA
Filter paper No.1	Whatman, England
Filter apparatus	Sartorius, Germany
pH meter	Schott gerate, Germany

Ultrasonic bath	J.P. Selecta, Japan
Centrifuge	Sorvall RC 5C plus, USA

Chemicals

Potassium dihydrogen phosphate	Merck, Germany
Potassium chloride	Mayer & Baker, U.K.
4-Fluoro-4′-hydroxy-benzophenone	Aldrich, USA
Sodium hydroxide pellets	BDH, England
Water for Injection	General Hospital Products Public Co., Ltd.
Methanol (HPLC)	Labscan Asia, Thailand
Acetonitrile (HPLC)	Labscan Asia, Thailand
Water (HPLC)	Labscan Asia, Thailand

Animals

ICR mice	National Laboratory Animal Center, Mahidol University

2. Methods

ICR mice weighing 20-25 g were kept in a temperature-controlled room on a 12/12-h cycle. The mice were divided into 18 groups with 3-4 animals per group. Mice in group 1-8 were treated with a curcumin solution (CS) (150 mg of cucumin /kg, sc.). Mice in group 9-18 was treated with polysorbate 80-coating curcumin-loaded nanoparticles (P80-CLNP) (equivalent to curcumin 150 mg/kg, sc). Each mouse was subcutaneously injected with 0.1-0.15 ml of CS or P80-CLNP preparations according to its weight. Groups 1-8 were killed at 2, 3, 4, 6, 8, 10, 12 and 15 hours after the injections, respectively. Groups 9-18 were killed at 0.5, 1, 2, 3, 4, 6, 8, 10, 12 and 15 hours after the injections, respectively. The brains were taken and assayed for the amount of curcumin by HPLC.

2.1 Determination of curcumin in mice brain

For the determination of curcumin content in the brain of treated mice, the removed brains were homogenized in 10 ml of iced-cold phosphate buffer saline pH 7.4. The homogenate was centrifuged at 3300 g for 10 min at 4 °C. The supernatant was filtered through a nylon membrane filter (0.2 μm pore size), the filtrate was adjusted to 10 ml with methanol and 20 μl of the filtrate was then injected into the HPLC column. The mobile phase was a mixture of acetonitrile (eluent A) /citric acid pH 3 (eluent B) (80:20, v/v). The mobile phase was filtered through a nylon membrane (47 mm, 0.45 μm) and degassed by sonication. Isocratic flow rate of 0.3 ml/min was maintained. The eluent was monitored with a UV/VIS detector (SPD-10A, Shimadzu, Japan) at 423 nm. 4-Fluoro-4′-hydroxy-benzophenone was used as internal standard in the concentration of 2.0 μg/ml and the retention times were 4.98 and 7.21 min for 4-fluoro-4′-hydroxy-benzophenone and curcumin, respectively. The amount of curcumin in samples was determined in by triplicate injections of the test concentration. Samples were analyzed in triplicate using the HPLC condition and were calculated from area ratio by the equation derived from the standard curve mentioned above.

CHAPTER IV
RESULTS

A. Preparation of Nanoparticles

Curcumin in the nanoparticles was proposed and prepared to enhance the brain accessibility and consequently improve the neuroprotective efficacy. Free radical polymerization was performed to obtain the desired nanoparticles using ammonium peroxodisulfate (APS) as an initiator agent. The obtained preparations were unloaded nanoparticles (ULNP), curcumin loaded nanoparticles (CLNP) and polysorbate80-coated CLNP (P80-CLNP). The mean particle size of nanoparticles was determined by photon correlation spectroscopy (PCS). Transmission electron microscope (TEM) analysis was performed to visualize the shape and to measure the size of nanoparticles. The zeta potential was determined by electroacoutic measurement. All nanoparticles were characterized for physicochemical properties as described in experimental section B.

B. Physicochemical Characterization

1. Size and surface charge

The size and shape of the prepared nanoparticles, unloaded nanoparticles ULNP, curcumin loaded nanoparticles CLNP and polysorbate80-coated CLNP (P80-CLNP), were determined by photon correlation spectroscopy and transmission electron microscopy, the results were shown in Tables 3-4 and Figures 22-24. The zeta potentials of all nanoparticles determined by electroacoutic measurement were tabulated in Tables 5-6.

Table 3. Particle sizes data of P80-CLNP, CLNP and ULNP from photon correlation spectroscopy

PMMA nanoparticles	Means diameter (nm)	95% limit (nm)	S.D. (nm)
P80-CLNP	92.2	88.20-97.20	9
	93.5	89.50-97.50	8
	94.2	90.20-98.20	8
	93.1	89.10-97.10	8
	94.2	90.20-98.20	8
	96.8	92.80-100.80	8
CLNP	79.0	75.00-84.00	9
	79.5	75.50-84.50	9
	77.8	73.80-82.80	9
	78.6	74.60-83.60	9
	79.1	75.10-84.10	9
	80.0	76.00-84.00	8
ULNP	61.4	57.40-65.40	8
	60.8	56.80-64.80	8
	62.3	58.30-66.30	8
	62.0	58.00-67.00	9
	61.8	57.80-65.80	8
	63.7	59.70-68.70	9

P80-CLNP = polysorbate 80-coated CLNP, CLNP = curcumin loaded-nanoparticles and ULNP = unloaded nanoparticles

Table 4. Particle sizes of P80-CLNP, CLNP and ULNP*

PMMA nanoparticles	Particle size (nm)		
	Average	S.D.	% R.S.D.
P80-CLNP	94.0	1.56	1.66
CLNP	79.0	0.76	0.96
ULNP	62.0	0.98	1.58

*measured by photon correlation spectroscopy, P80-CLNP = polysorbate 80 coated CLNP, CLNP = curcumin loaded nanoparticles and ULNP = unloaded nanoparticles

Table 5. Surface charge data of P80-CLNP, CLNP and ULNP at 25 °C

PMMA nanoparticles	Zeta potential (mV)	Mobility (mcm/Vs)	Conductivity (mS/cm)
P80-CLNP	-31.62	-2.479	0.0326
	-31.50	-2.469	0.0279
	-31.10	-2.438	0.0303
CLNP	-20.72	-1.624	0.0159
	-20.43	-1.602	0.0154
	-19.25	-1.509	0.0177
ULNP	-37.33	-2.927	0.1099
	-36.95	-2.897	0.1141
	-37.66	-2.952	0.1121

P80-CLNP = polysorbate 80 coated CLNP, CLNP = curcumin loaded nanoparticles and ULNP = unloaded nanoparticles

Table 6. Average of surface charges of P80-CLNP, CLNP and ULNP

PMMA nanoparticles	Zeta potential (mV)			Mobility (mcm/Vs)			Conductivity (mS/cm)		
	Average	S.D.	% R.S.D.	Average	S.D.	% R.S.D.	Average	S.D.	% R.S.D.
P80-CLNP	-31.41	0.270	0.870	-2.462	0.020	0.870	0.030	0.002	7.679
CLNP	-20.13	0.779	3.867	-1.578	0.061	3.867	0.016	0.001	7.274
ULNP	-37.31	0.355	0.952	-2.925	0.028	0.941	0.112	0.002	1.875

P80-CLNP = polysorbate 80 coated CLNP, CLNP = curcumin loaded nanoparticles and ULNP = unloaded nanoparticles

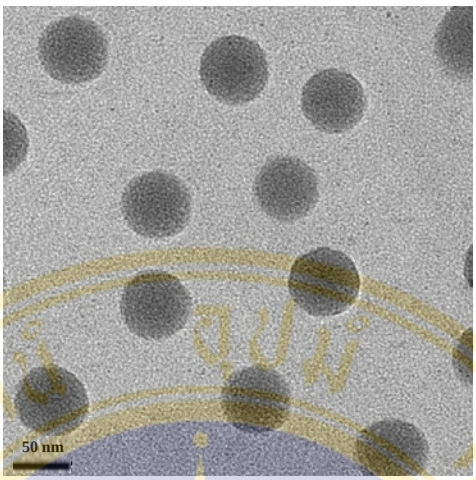

Figure 22. Transmission electron microscopy of ULNP. Bar represents 50 nm

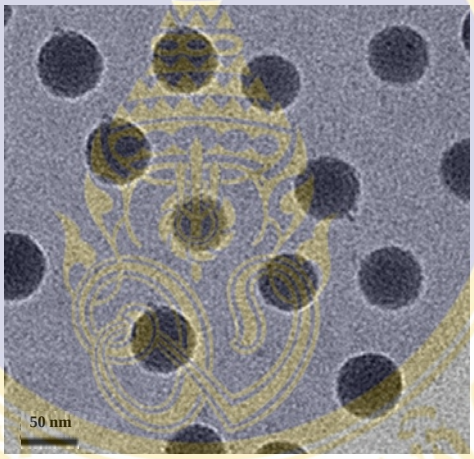

Figure 23. Transmission electron microscopy of CLNP. Bar represents 50 nm

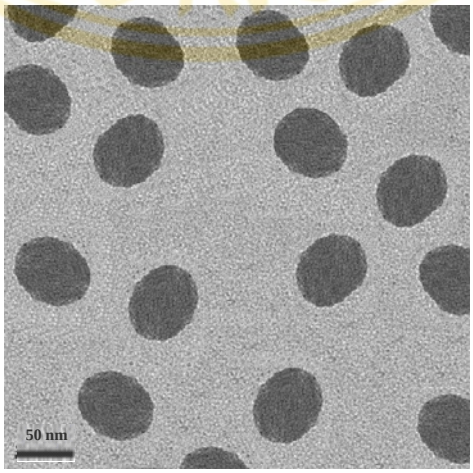

Figure 24. Transmission electron microscopy of P80-CLNP. Bar represents 50 nm

2. Curcumin assay

The prepared nanoparticles were determined for entrapment efficiency of curcumin loading, the HPLC method to assay curcumin was developed. The curcumin was assayed as the following conditions. The analytical column was Hypersil ODS C18 (5 µm, 150 mm L × 4.6 mm I.D.) column, the mobile phase was a mixture of acetonitrile /citric acid pH 3 (80:20, v/v); flow rate of 0.3 ml/min and injection volume was 20 µl. The eluent was detected by UV absorbance at 423 nm; The retention times were found to be 7.21 minutes for curcumin and 4.98 minutes for 4-fluoro-4′-hydroxy-benzophenone, an internal standard. Chromatogram of the curcumin and internal standard was shown in Figure 25. The analytical method was validated by the following parameters. The developed method was validated by the below parameters.

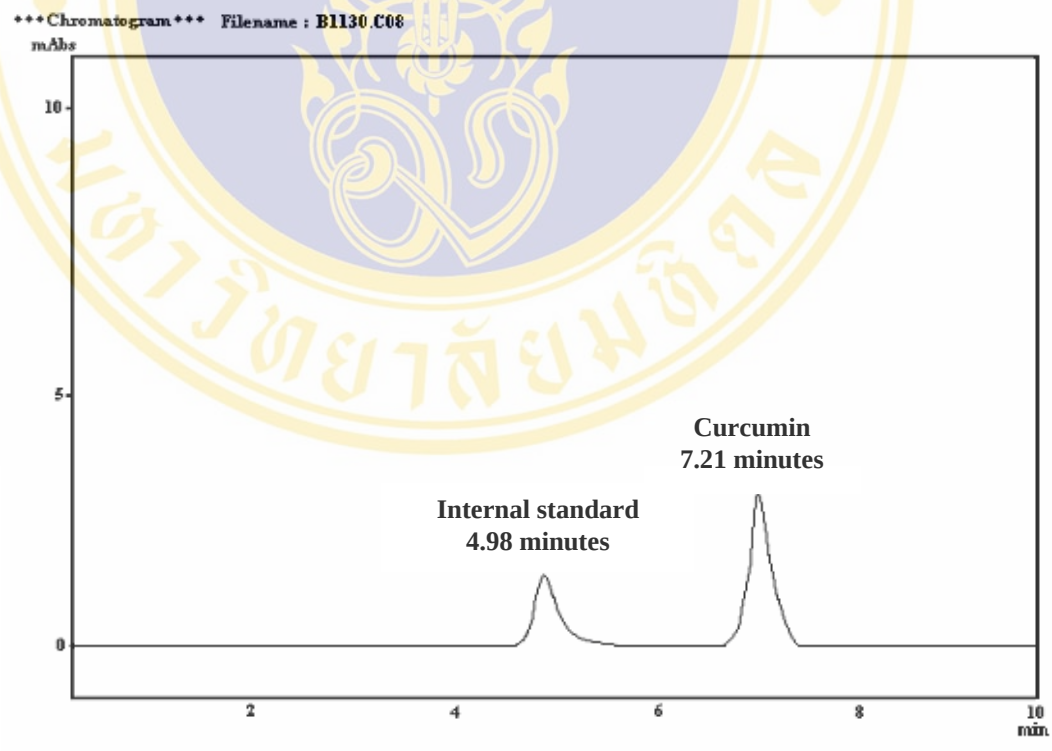

Figure 25. HPLC chromatograms of curcumin and 4-fluoro-4′-hydroxy-benzophenone. Condition: analytical column was Hypersil ODS C18 (5 µm, 150 mm L × 4.6 mm I.D.) column; mobile phase was a mixture of acetonitrile /citric acid pH 3 (80:20, v/v); detection by UV absorbance at 423 nm; flow rate 0.3 ml/min; injection volume was 20 µl.

2.1 Linearity

The calibration curve data of curcumin standard covering the range of 1.0-10.0 µg/ml were carried out. The 20 µl curcumin standard solutions containing the internal standard were injected in triplicated to HPLC (n =3). The HPLC chromatograms of curcumin standard covering the range of 1.0-10.0 µg/ml were shown in Figure 26. The peak areas were shown in Table 7 and the peak area ratios of curcumin and internal standard were tabulated in Table 8. The peak area ratio was selected for establishing the calibration curve as the peak area ratios provided better correlation than the peak heights. Calibration curve plotted between peak area ratios of curcumin standard and internal standard versus concentrations was shown in Figure 27. The calibration curve of standard curcumin was found to be linear with r^2 of 0.9992 and the regression equation was y = 1.1315x + 0.5724; where y is peak area ratio between curcumin and internal standard and x is the concentration of curcumin standard solutions in µg/ml.

Table 7. Calibration curve data[a] of curcumin standard solutions

Concentration (µg/ml)	Peak area	
	internal standard[b]	curcumin standard
1	17118 ± 0.09	26704 ± 0.12
2	17549 ±0.07	51769 ± 0.17
4	17256 ± 0.11	89904 ± 0.16
6	17441 ± 0.09	128017 ± 0.11
8	17342 ± 0.10	165096 ± 0.13
10	17581 ± 0.08	209741 ± 0.10

[a] Average ± S.D. (n = 3), [b] 4-fluoro-4′-hydroxy-benzophenone

Table 8. Peak area ratios[a] of curcumin standard solutions

Concentration (µg/ml)	Peak area ratio ± S.D. *	% R.S.D.
1	1.56 ± 0.13	8.33
2	2.95 ± 0.07	2.37
4	5.21 ± 0.09	1.28
6	7.34 ± 0.05	0.68
8	9.52 ± 0.10	1.05
10	11.93 ± 0.07	0.59

[a]Average ± S.D. (n = 3)

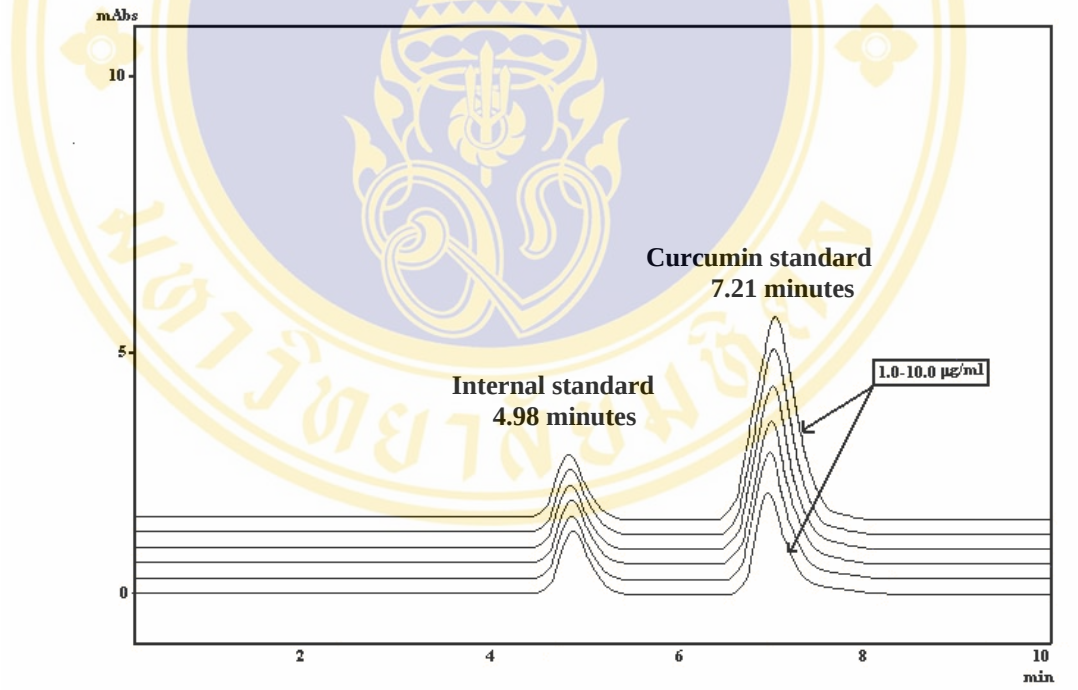

Figure 26. HPLC chromatogram of curcumin standard in the range of 1.0-10.0 µg/ml and 4-fluoro-4′-hydroxy-benzophenone, the internal standard at 2 µg/ml. Condition: analytical column was Hypersil ODS C18 (5 µm, 150 mm L × 4.6 mm I.D.) column; mobile phase was a mixture of acetonitrile /citric acid pH 3 (80:20, v/v); detection by UV absorbance at 423 nm; flow rate 0.3 ml/min; injection volume was 20 µl.

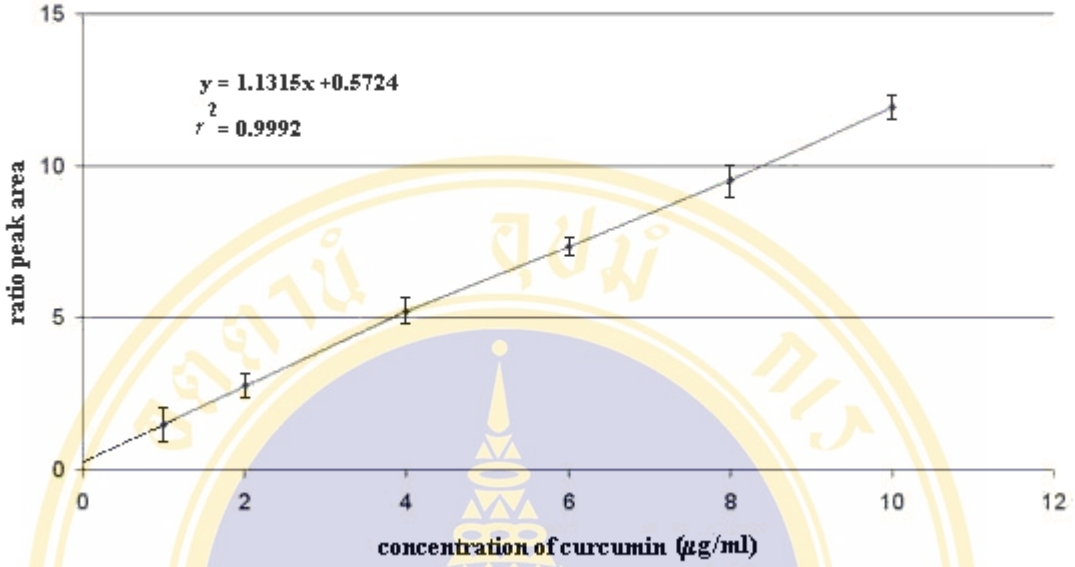

Figure 27. Calibration curve of curcumin standard covering the range of 1.0-10.0 µg/ml. Condition: analytical column was Hypersil ODS C18 (5 µm, 150 mm L × 4.6 mm I.D.) column; mobile phase was a mixture of acetonitrile /citric acid pH 3 (80:20, v/v); detection by UV absorbance at 423 nm; flow rate 0.3 ml/min; injection volume was 20 µl. The internal standard was 4-fluoro-4′-hydroxy-benzophenone, the internal standard at 2 µg/ml.

2.2 Precision

Method reproducibility or precision was determined by measuring repeatability of injections and intermediate precision (intra-day precision) of the peak area and retention time.

2.2.1 Injection precision

Injection precision was performed by replicated injections (n = 6) of the mixture of curcumin standard (4.0 µg/ml) and 4-fluoro-4′-hydroxy-benzophenone (internal standard, 2.0 µg/ml). The precision expressed as % R.S.D. of retention times and peak area ratios were calculated and shown in Table 9-10.

Table 9. Analytical data of injection precision

No. of injection (n = 6)	Retention time		Peak area	
	Curcumin[a]	Internal standard[b]	Curcumin[a]	Internal standard[b]
1	7.261	4.912	90125	17118
2	7.242	4.962	89826	17311
3	7.251	4.958	89582	17200
4	7.268	4.992	89874	17469
5	7.259	4.986	89763	17258
6	7.235	4.945	90254	17180

[a] 4.0 µg/ml
[b] Internal standard was 4-fluoro-4′-hydroxy-benzophenone at 2.0 µg/ml

Table 10. Precisions of retention times and peak areas in curcumin assay

	Type	Average ± S.D. (n = 6)	% RSD
Retention time	Internal standard*(2.0 µg/ml)	4.959 ± 0.03	0.59
	Curcumin (4.0 µg/ml)	7.253 ± 0.01	0.17
Peak area	Internal standard*(2.0 µg/ml)	17256 ± 123.58	0.27
	Curcumin(4.0 µg/ml)	89904 ± 245.72	0.72

* Internal standard was 4-fluoro-4′-hydroxy-benzophenone

2.2.2 Intra-day precision

Intra-day precision was performed by injections of the mixture of curcumin standard and 4-fluoro-4′-hydroxy-benzophenone (internal standard) at three concentrations: 2.0, 4.0 and 6.0 µg/ml (n = 6). The determinations were performed in 3 different times within day. The % R.S.D.s of retention times and peak area ratios were shown in Tables 11-12.

Table 11. Analytical data of intra-day precision of curcumin assay[a]

injection	Retention time (min)						Peak area					
	Curcumin			Internal standard[b]			Curcumin			Internal standard[b]		
	2.0 µg/ml	4.0 µg/ml	6.0 µg/ml	2.0 µg/ml	4.0 µg/ml	6.0 µg/ml	2.0 µg/ml	4.0 µg/ml	6.0 µg/ml	2.0 µg/ml	4.0 µg/ml	6.0 µg/ml
1	7.229	7.261	7.242	4.925	4.935	4.9161	51777	90125	129476	17526	17118	17321
2	7.270	7.242	7.251	4.965	4.977	4.981	51852	89826	129512	17422	17311	17566
3	7.235	7.251	7.236	4.913	4.918	4.953	51623	89582	129622	17489	17200	17484
4	7.259	7.268	7.224	4.928	4.926	4.937	51524	89874	129852	17621	17469	17477
5	7.247	7.259	7.259	4.933	4.919	4.961	51712	89763	129488	17588	17258	17225
6	7.239	7.235	7.224	4.942	4.954	4.922	52126	90254	129530	17648	17180	17573

[a] 6 determination in 3 different times within day, [b] 4-fluoro-4′-hydroxy-benzophenone.

Table 12. Average of intra-day precision of curcumin assay

Concentration (µg/ml)	Peak area ratio ± S.D (n = 6)	% R.S.D.
2.0	2.95 ± 0.02	0.59
4.0	5.21 ± 0.09	0.84
6.0	7.38 ± 0.03	0.41

2.2.3 Inter-day precision

Inter-day precision was performed by injections of the mixture of curcumin standard and 4-fluoro-4′-hydroxy-benzophenone (internal standard) at 2.0 (n = 6). The determinations were performed in 3 different days. The % R.S.D.s of retention times and peak area ratios were shown in Tables 13-14.

Table 13. Analytical data of inter-day precision of curcumin assay[a]

injection	Retention time (min)						Peak area					
	Curcumin			Internal standard[b]			Curcumin			Internal standard[b]		
	day 1	day 2	day 3	day 1	day 2	day 3	day 1	day 2	day 3	day 1	day 2	day 3
1	7.229	7.251	7.256	4.925	4.912	4.939	51777	51584	51477	17526	17234	17254
2	7.270	7.223	7.249	4.965	4.935	4.928	51852	51623	51689	17422	17123	17489
3	7.235	7.235	7.267	4.913	4.967	4.941	51623	51881	51587	17489	17258	17412
4	7.259	7.261	7.235	4.928	4.919	4.946	51524	51665	51698	17621	17564	17578
5	7.247	7.243	7.221	4.933	4.915	4.935	51712	51756	51775	17588	17582	17677
6	7.239	7.238	7.215	4.942	4.924	4.923	52126	51723	51821	17648	17801	17452

[a] 6 determination in 3 different days, [b] 4-fluoro-4′-hydroxy-benzophenone.

Table 14. Average of inter-day precision of curcumin assay

Day	Peak area ratio ± S.D (n = 6)	% R.S.D.
1	2.95 ± 0.02	0.59
2	2.97 ± 0.03	0.86
3	2.95 ± 0.02	0.66

2.3 Accuracy

The mixture of standard curcumin in the range of 80-120% (3.2-4.8 μg/ml) and 4-fluoro-4′-hydroxy-benzophenone (2.0 μg/ml) were spiked into the mice brains. The brains were homogenized and centrifuged. The supernatant was filtered, the filtrate was adjusted to volume. The filtrated was assayed for curcumin by the HPLC condition described in experimental section 2.3.4. The obtained chromatograms for accuracy determinations were shown in Figure 28. The measured peak areas of curcumin and the internal standard were calculated for the area ratios. The results of curcumin found obtained from regression equation were shown in Tables 15-16.

Table 15. Recovery data of curcumin assay*

Sample No.	Amount of standard curcumin								
	80% of curcumin standard			100% of curcumin standard			120% of curcumin standard		
	Added (%)	Found (%)	Recovery (%)	Added (%)	Found (%)	Recovery (%)	Added (%)	Found (%)	Recovery (%)
1	80	79.96	99.95	100	100.10	100.10	120	120.23	100.19
2	80	79.83	99.79	100	100.21	100.21	120	119.87	99.89
3	80	79.48	99.35	100	99.08	99.08	120	120.13	100.11
4	80	80.14	100.18	100	100.06	100.06	120	120.15	100.13
5	80	80.22	100.28	100	99.67	99.67	120	119.90	99.92
6	80	80.39	100.49	100	100.14	100.14	120	120.08	100.10

* from standard addition in mice brains at 80% (3.2 µg/ml), 100% (4.0 µg/ml) and 120% (4.8 µg/ml) of curcumin standard. The concentration at 4.0 µg/ml (100%) obtained from calibration curve, which provided the small % R.S.D.

Table 16. Recovery data of the analysis of curcumin in mice brain

Amount of standard curcumin	% Recovery ± S.D.	% R.S.D.
3.2 µg/ml	100.00 ± 0.40	0.40
4.0 µg/ml	99.88 ± 0.43	0.43
4.8 µg/ml	100.05 ± 0.12	0.12
3.2-4.8 µg/ml	99.97 ± 0.09	0.09

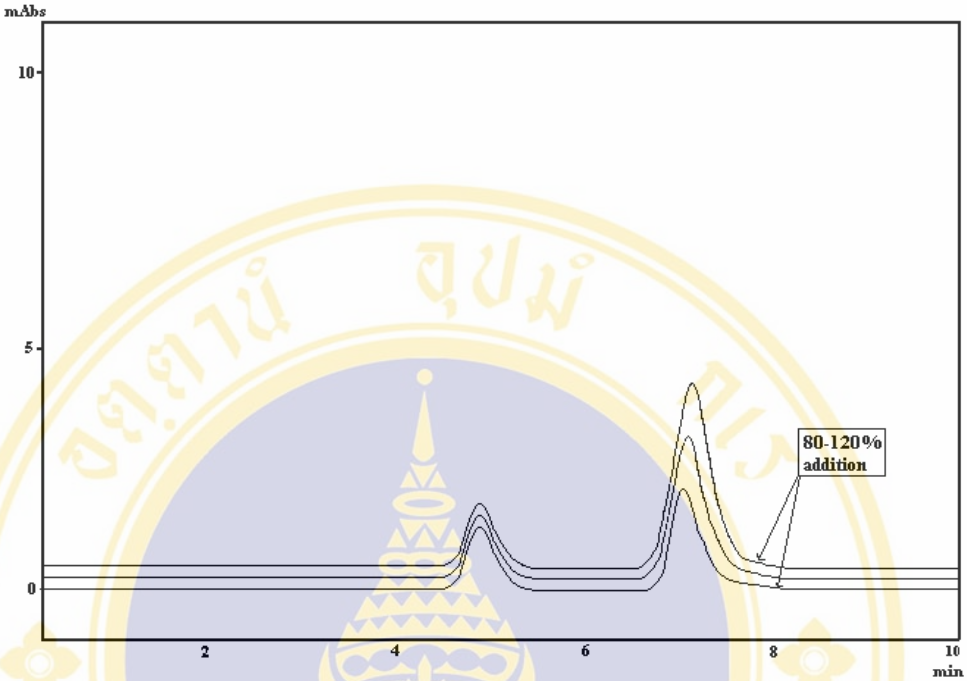

Figure 28. HPLC chromatograms of curcumin (3.2, 4.0 and 4.8 µg/ml) in mice brain. Condition: analytical column was Hypersil ODS C18 (5 µm, 150 mm L × 4.6 mm I.D.) column; mobile phase was a mixture of acetonitrile /citric acid pH 3 (80:20, v/v); detection by UV absorbance at 423 nm; flow rate 0.3 ml/min; injection volume was 20 µl.

2.4 Limit of detection and limit of quantitation

The limit of detection (LOD) and limit of quantitation (LOQ) are related to the noise of system and usually is defined as a peak. LOD and LOQ were expressed as concentrations in µg/ml which were calculated from the regression equation. The LOD was determined as described in experimental section 2.3.6. The results were shown in Tables 17-18. The chromatograms of LOD and LOQ were shown in Figure 29.

Table 17. The LOQ and LOD data

No. of injection (n = 3)	Peak area noise[a]	Peak area noise[b]	LOD Peak area ratio × 3	LOQ Peak area ratio × 10
1	5607	4418	2.364	7.880
2	5634	4435	2.361	7.871
3	5652	4455	2.365	7.883

[a] Peak area noise at the retention time of 4.98 minutes
[b] Peak area noise at the retention time of 7.21 minutes

Table 18. LOD and LOQ of curcumin assay

Parameters	Concentration (µg/ml) ± S.D. (n = 3)	% R.S.D.
LOD	1.58 ± 0.001	0.12
LOQ	6.46 ± 0.006	0.08

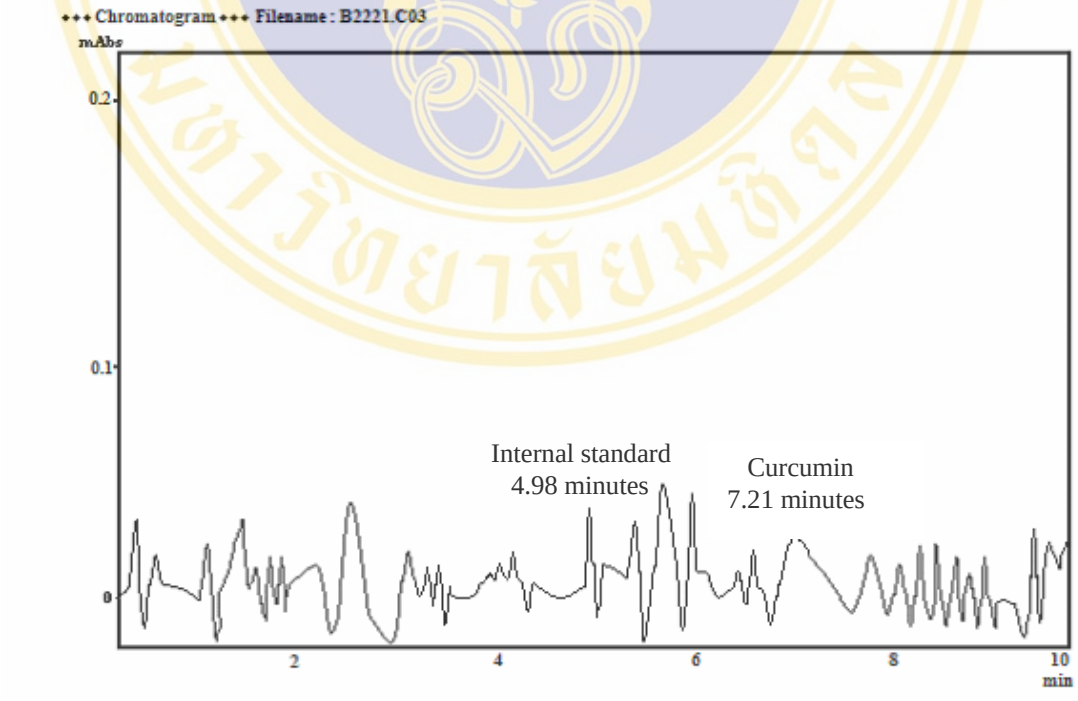

Figure 29. HPLC chromatograms of blank. Condition: analytical column was Hypersil ODS C18 (5 µm, 150 mm L × 4.6 mm I.D.) column; mobile phase was a mixture of acetonitrile /citric acid pH 3 (80:20, v/v); detection by UV absorbance at 423 nm; flow rate 0.3 ml/min; injection volume was 20 µl.

3. Determination of curcumin content and entrapment efficiency

The entrapment efficiency was determined as described in the experimental section 2.4.1 and 2.4.2. The results of entrapment efficiency were in Tables 19-21.

Table 19. The entrapment efficiency[a] of curcumin nanoparticles

No. of batch	Added curcumin (g)	Curcumin in filtrate (g) ± S.D.	Entrapped curcumin (g)	Curcumin entrapment (% w/w)
1	2.00	0.37 ± 0.01	1.63	81.50
2	2.00	0.44 ± 0.02	1.56	78.00
3	2.00	0.39 ± 0.01	1.61	80.50

[a]Average ± S.D. (n = 3)

Table 20. The content[a] of curcumin in nanoparticles

No. of batch	Added curcumin (g)	Nanoparticles (g)	Curcumin in filtrate (g) ± S.D.	Curcumin content (% w/w)
1	2.00	2.55	0.37 ± 0.01	63.92
2	2.00	2.55	0.44 ± 0.02	61.17
3	2.00	2.60	0.39 ± 0.01	61.92

[a]Average ± S.D. (n = 3)

Table 21. Entrapment efficiency and curcumin content in nanoparticles (n = 3)

Batch no.	Curcumin content (% w/w)	Curcumin entrapment (% w/w)
1	63.92	81.50
2	61.17	78.00
3	61.92	80.50
Average ± S.D.	62.33 ± 1.42	80.00 ± 1.80

C. Brain Accessibility

The mice were divided into 18 groups with 3-4 mice per group, 10 groups treated with polysorbated 80-coating curcumin-loaded nanoparticles (P80-CLNP) and 8 groups treated with curcumin solution (CS). The curcumin in P80-CLNP and CS were equivalent dose of curcumin at 150 mg/kg. The brains of mice treated with P80-CLNP were extracted and assayed for the amount of curcumin by HPLC at 0.5, 1, 2, 3, 4, 6, 8, 10, 12 and 15 hours after the injections. And the brains of mice treated with CS were extracted and assayed for the amount of curcumin by HPLC at 2, 3, 4, 6, 8, 10, 12 and 15 hours after the injections.

The validated HPLC method was applied for the determination of curcumin in mice brains. The assay chromatograms of curcumin extracted from mice brain were shown in Figure 30. The retention time of curcumin in the chromatographic system was 7.2 min and resolved from the peaks of brain components. The calibration curves of the peak-area versus the concentrations of curcumin was linear with r^2 = 0.9992. The amounts of curcumin in mice brain vs. time after subcutaneously injection of P80-CLNP and curcumin solution to mice at equal dose of curcumin (150 mg curcumin/kg) were tabulated in Table 22. The amount of curcumin in mice brain at various time were compared between mice treated with curcumin loaded nanoparticles (P80-CLNP) and mice treated with curcumin solution as shown in Figure 31.

Table 22. The amount of curcumin in mice brain after subcutaneous injections*

Time (h)	Curcumin ± S.D. (µg/ g of brain)	
	P80-CLNP	Curcumin solution
0.5	13.6510 ± 1.58	-
1	30.1150 ± 1.46	-
2	47.8250 ± 1.21	7.2560 ± 1.56
3	52.1240 ± 1.33	16.8840 ± 1.19
4	49.4510 ± 1.19	22.8640 ± 1.08
6	44.1130 ± 1.41	28.2780 ± 1.42
8	40.3290 ± 1.51	31.5660 ± 1.24
10	36.8500 ± 1.26	32.1470 ± 1.31
12	33.2568 ± 1.35	29.8560 ± 1.35
15	28.2212 ± 1.23	25.3320 ± 1.45

* Mice were injected subcutaneously with P80-CLNP or curcumin solution at equal dose of curcumin (150 mg curcumin/kg).

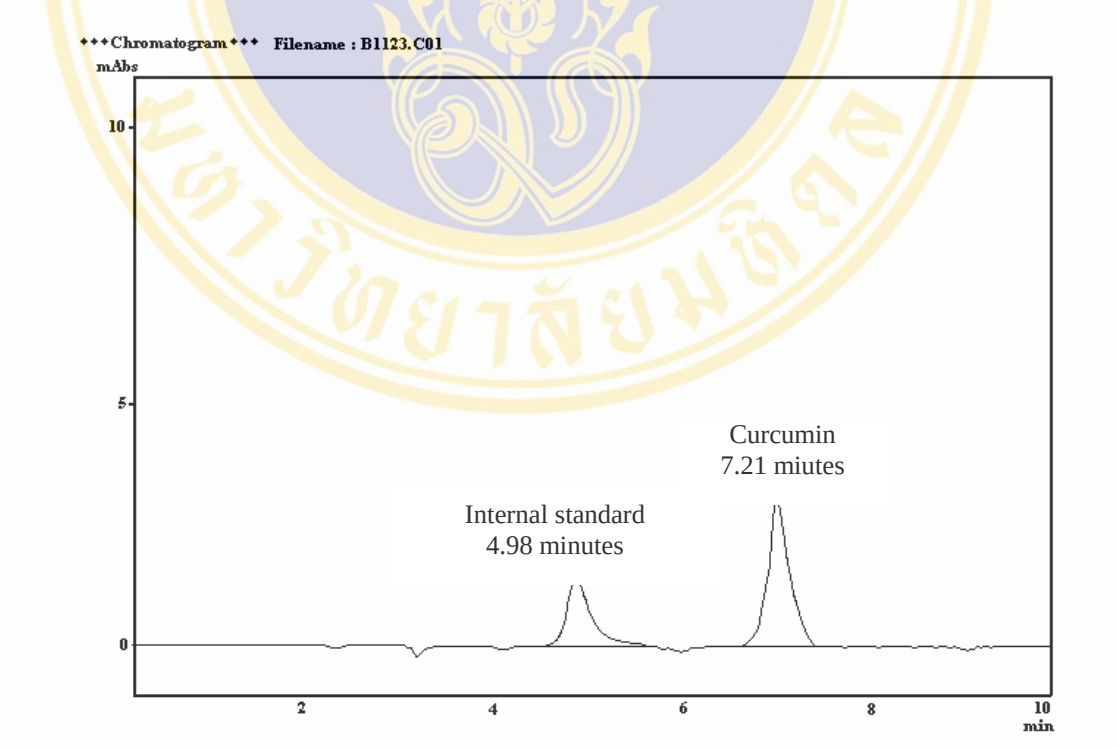

Figure 30. HPLC chromatograms of curcumin and internal standard in mice brain. Condition: analytical column was Hypersil ODS C18 (5 µm, 150 mm L × 4.6 mm I.D.) column; mobile phase was a mixture of acetonitrile and citric acid pH 3.0 (80:20, v/v); detection by UV absorbance at 423 nm; flow rate 0.3 ml/min; injection volume was 20 µl.

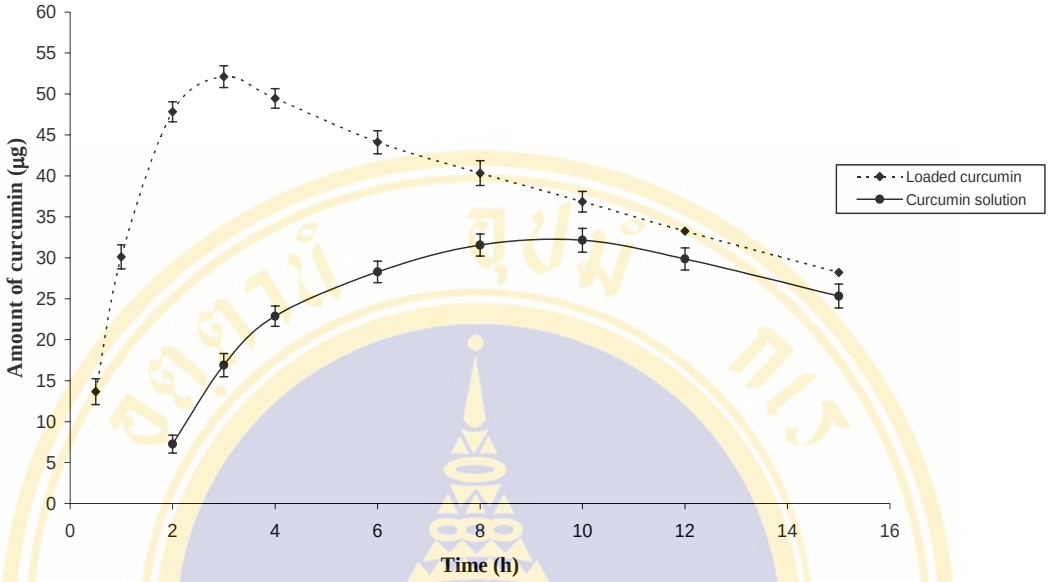

Figure 31. The amount of curcumin in mice brain at various time after subcutaneous injections of curcumin loaded nanoparticles (P80-CLNP) and curcumin solution at dose of 150 mg/kg.

CHAPTER V
DISCUSSION

In this study, incorporation of curcumin in the nanoparticles was the selected approach to enhance the brain accessibility and consequently improve the neuroprotective efficacy. Poly(methyl methacrylate) nanoparticles of curcumin coating with polysorbate 80 (P80-CLNP), were prepared; as it is well established that the nanoparticle-mediated transport to the brain depends on the overcoating of the particles with polysorbates, especially polysorbate 80 (9, 19, 29). According to literatures, several mechanisms of nanoparticle-mediated drugs across blood brain-barrier (BBB) had been proposed (225-227). Among them, the mechanism of endocytosis was supported by many experiments. It is very possible that polysorbate 80 on the surface of nanoparticles anchors apolipoprotein E (apo E), and plays an important role in the transport of the low density lipoprotein (LDL) into brain. After being bound with apo E at the surface, nanoparticles mimic LDL particles and interact with LDL receptors on brain micro-vessel endothelial cells (BMECs) (225). The interacted nanoparticles at the LDL receptor are then uptake by the endothelial cells via endocytosis. After endocytosis, the drug is released in these cells and diffused into the brain interior (10). The un-coated PMMA nanoparticles cannot adsorb apo E from blood plasma, the un-coated PMMA nanoparticles were thus unable to penetrate into the brain by LDL receptor. The preparation of unloaded nanoparticles (ULNP), curcumin loaded nanoparticles (CLNP) and P80-CLNP were carried out, the physicochemical properties and the brain delivery of the prepared curcumin nanoparticles were investigated as the followings.

A. Preparation of Nanoparticles

The core of nanoparticles was prepared by polymerization which poly(methylmethacrylate) is formed from methylmethacrylate monomers. The polymerization began with the reaction of two methylmethacrylate monomers, the carbon adjacent to ester functional group of one monomer reacting with the carbon of terminal alkene unit of the other monomer. The general chemical transformations that result in polymer can be divided into two types. These two types of polymerization were anionic polymerization and free radical polymerization.

The attempt to prepare the polymer in form of nanoparticles by anionic polymerization method was not successful because of very low yield. The anionic polymerization is the reaction of acid and an alkene, the hydronium ion is generated changed dramatically when using water as solvent. Solvation plays a major role in the generation of electrophiles from acids in aqueous solution. In water, it is the hydronium ion that donates a proton to the alkene. Therefore, its formation by protonation of methylmethacrylate takes place at carbon adjacent to ester group to produce the less stable primary carbocation (Scheme 1). As the carbocations which involve as intermediates in the addition of methylmethacrylates for the elongation step are less stable, the polymerization reaction was then rarely occurred.

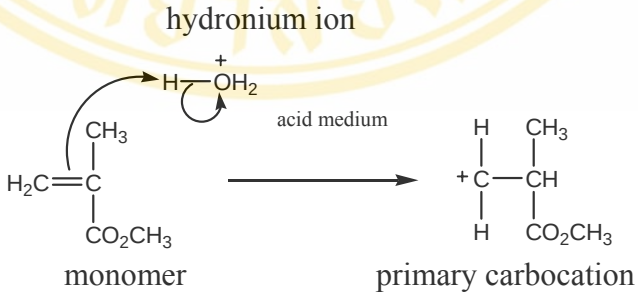

Scheme 1. The anionic polymerization between monomer (methylmethacrylate) and hydronium ion

Thus, the free radical polymerization method was used in this experiment to avoid this problem. The electrophilic attack by a carbocation is very similar to the attack by a carbon free radical on a double bond. The only significant difference is that radical intermediates rather than cations are formed. Bearing these facts in mind,

it should not be too surprising to find that the free radical formed by interaction of a methylmethacrylate with an initiator can attack another molecule of methylmethacrylate. The free radical polymerization of methylmethacrylate was presented in Scheme 2. The free radical polymerization was stable aggregates formed by the core of nanoparticles in non-polar matrix. The core of nanoparticles are generated by amphiphilic surfactants (poloxamer 407), a hydrophilic head group surrounding the water core and a hydrophobic tail that extends into the non-polar matrix. Micelles are the simplest structure: they are spherical objects formed by surfactant molecules separating lipophilic part and hydrophilic part. In this preparation, the monomer droplet (lipophilic part) was surrounded by micelle molecules and some monomers were dissolved in water with initiator (I_2) as shown in Figure 32. The ammonium peroxodisulfate (APS) in water was initiator that generated radical. The radical was interacted with some monomer which an initiator can attack another molecule of monomer in water change to oligomers radical. The oligomers radical were lipophilic molecules moved to inner part of micelles. They were reacted with monomers droplet in micelle become to polymer nanoparticles.

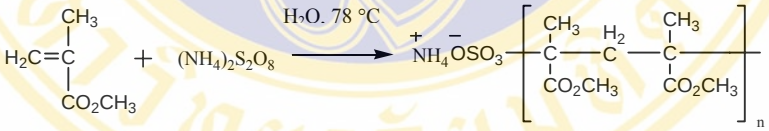

monomer initiator

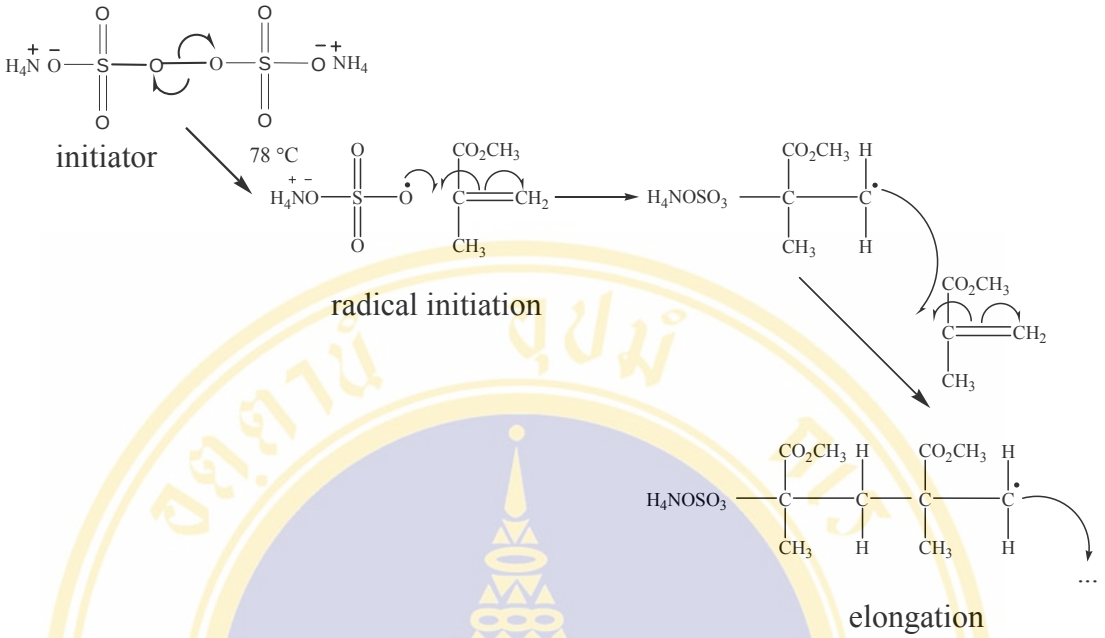

Scheme 2. The free radical polymerization between monomer (methylmethacrylate) and initiator (ammonium peroxodisulfate)

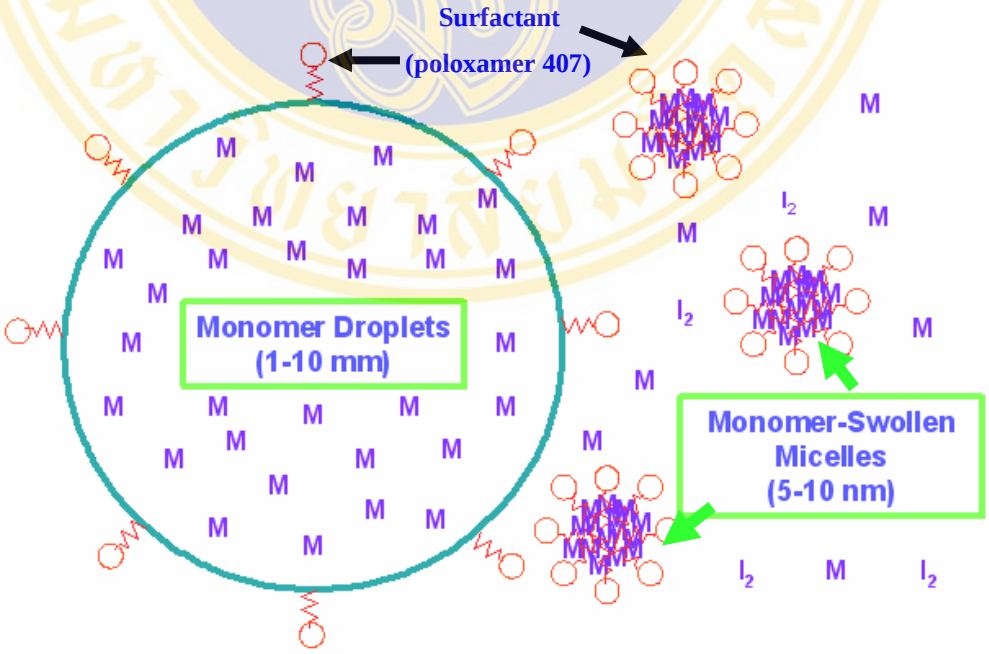

Figure 32. The formed of monomer droplet and monomer-swollen micelles in water. Abbreviation of M is monomer (methyl methacrylate) and I_2 is initiator (ammonium peroxodisulfate)

In general procedure, ammonium peroxodisulfate (APS) was used as an initiator. The initiator was soluble in water 78 °C to break the oxygen bond and the radical was formed to initiate polymerization. The reaction was run for 30 minutes at 78 °C to permit complete polymerization of the monomers. After 30 minutes polymerization, a milky white nanoparticle suspension was obtained. The suspension was filtered by sintered glass (10 μm pore size) to remove the particles with sizes larger than 10,000 nm. The nanoparticles in filtrate were ultracentrifuged and were lyophilized. The freeze-dried nanoparticles were the unloaded nanoparticles (ULNP).

After generation of the ULNP, the ULNP was loaded with curcumin to produce the curcumin loaded nanoparticles (CLNP). The curcumin was dissolved with the phosphate buffer saline containing 2% (v/v) ethanol. The ethanol was added to increase the solubility of curcumin. Curcumin was allowed to adsorb onto the nanoparticles surface for 4 hours. The obtained CLNP were lyophilized and stored at 4 ^{o}C until use. CLNP were coated with 1% polysorbate 80 before administration to yield P80-CLNP by mixing the 1% polysorbate 80 with the re-suspended freeze dried CLNP. The mixture was incubated with shaking at room temperature for 30 min. The obtained polysorbate 80-coated CLNP (P80-CLNP) was characterized.

B. Characterization of Nanoparticles

1. Size and surface charge

The unloaded-nanoparticles (ULNP), curcumin loaded-nanoparticles (CLNP) and polysorbate 80-coated CLNP (P80-CLNP) were characterized for size, shape and size distribution by photon correlation spectroscopy (PCS) and transmission electron microscopy (TEM). The surface charge expressed as Zeta potential was determined by electroacoustic measurement. The sizes and distribution of all nanoparticles were summarized in Table 20.

Table 23. Particle sizes, polydispersity and surface charges of prepared nanoparticles

PMMA nanoparticles	Mean diameter (nm)		Polydispersity index (PI)	Zeta potential (mV) (n = 3)
	PCS (n = 6)	TEM		
P80-CLNP	94 ± 8	86 ± 16	0.06 ± 0.04	-31.41 ± 0.27
CLNP	79 ± 9	68 ± 8	0.13 ± 0.07	-20.13 ± 0.78
ULNP	62 ± 8	53 ± 12	0.03 ± 0.04	-37.31 ± 0.36

The particle sizes of all nanoparticles (ULNP, CLNP and P80-CLNP) measured by PCS were 62 nm, 79 nm and 94 nm, respectively while measuring by TEM, the diameters were found to be 53 nm, 68 nm and 86 nm, respectively. The particles sizes measured by PCS were larger than those obtained from TEM. The differences in size of nanoparticles between two measuring methods: PCS and TEM, were in agreement with the notion explained by Finsy *et al.* since 1992 (223). It is because the contrast of the EM pictures allows only the visualization of the nanoparticle core; whereas the hydrodynamic radius of the particles is measured by PCS. The particle sizes of all nanoparticles measured by PCS were found to be about 1.1 times of those obtained by TEM.

According to the TEM images of the prepared nanoparticles (Figures 22-24), the observed shapes of ULNP and CLNP were spherical while the shape of P80-CLNP was pebble-like. The explanation of pebble-like shape of the nanoparticles was given by Fricke *et al*. since 1991 (224). It was because the P80-CLNP was surrounded by monolayers of the surfactant chains (polysorbate 80) in a thread-like manner. These chains tightened the nanoparticle cores resulting in a significant torsion shape or pebble-like shape.

The uniformity or dispersity homogeneity of the nanoparticles was determined by measuring the polydispersity index (*PI*). *PI* values closed to zero indicate a homogeneous dispersion while those greater than 0.3 indicate high heterogeneity. The *PI* values of the prepared nanoparticles, ULNP, CLNP and P80-CLNP, were 0.06, 0.13 and 0.03, respectively. The UNLP and P80-CLNP were surrounded by monolayer of surfactant chains, induces charge on surface of nanoparticles. The

surfactant (poloxamer 407 and polysorbate 80) contains lipophilic carbon chains, which accommodated in the lipid core protecting the PMMA molecules into aqueous phase, and extend hydrophilic chains (oxide groups) to aqueous phase. The hydrophilic chains can be induces negative charge. Negatively charged of hydrophilic chains are repulsed near the other negative charge of nanoparticles. This repulsive interaction was resulted in decrease size distribution of the nanoparticles. Thus, *PI* values of ULNP coating with poloxamer 407 and P80-CLNP coating with polysorbate 80 were less than CLNP as CLNP were surrounded with curcumin instead of surfactant.

The Zeta potentials of nanoparticles were determined by electroacoustic measurement as shown in Table 20. The nanoparticles with electrophoretic behavior of neutral Zeta potential values, between 15 mV and -15 mV, will aggregate and precipitate during storage. The nanoparticles with Zeta potential values above 15 mV and below -15 mV are well dispersed and stable. It is because the repulsion of the positive charges or negative charges impairs the aggregation of nanoparticles. The Zeta potentials of unloaded nanoparticles (ULNP), curcumin loaded nanoparticles (CLNP) and polysorbate 80 coated nanoparticles (P80-CLNP) were -37.13 mV, -20.13 mV and -31.41 mV, respectively. The negative zeta potentials of all nanoparticles confirmed the negative charge on the surface of nanoparticles. CLNP with Zeta potential of -20.13 ± 0.78 mV tend to be less stable than P80-CLNP. The P80-CLNP was surrounded by monolayer of surfactant chains (polysorbate 80) containing hydrophilic chains (oxide groups) extend into aqueous phase, which resulted in negative charges. After being coated with polysorbate 80 to yield P80-CLNP, the zeta potential of P80-CLNP increased from -20.13 ± 0.78 mV to -31.41 ± 0.27 mV. Hence, the roles of polysorbate 80 were not only to increase brain delivery but also to increase the stability.

The results demonstrate that permanently negatively charged poly(methylmethacrylate) nanoparticles can be prepared in the free radical polymerization method. Since their particles size was in the nanometer range, their size distribution depended with charge on surface of particles, the observed shape was related to surfactant coating and since their surface charge was depended oxide group

of surfactant, the prepared poly(methylmethacrylate) nanoparticles were useful as colloidal curcumin carrier.

2. Curcumin assay

HPLC was used to assay curcumin in nanoparticles and in the mice brain for determining the accessibility of curcumin to the brain. The system of acetonitrile: citric acid (pH 3.0) (80:20, v/v) was used as mobile phase. The retention times were found to be 7.21 minutes for curcumin and 4.98 minutes for 4-fluoro-4′-hydroxy-benzophenone, an internal standard. The peak of curcumin in this system completely resolved from the peak of the internal standard. The calibration curve was accomplished by plotting peak-area ratios between curcumin and internal standard versus the concentrations of curcumin, the regression line was linear with r^2 of 0.9992. Figures 25 showed typical chromatograms of the curcumin standard and internal standard. The analytical method was validated by the following parameters.

2.1 Accuracy

The accuracy of an analytical method is the closeness of the assay results obtained by the method to the true values, which accepted as a true value and the value found after several replicates. The accuracy is often expressed as percent recovery by the assay of known, added amounts of analyte. The percent recovery provides an indication of systematic error. The accepted percent recovery of the method is 98% to 102% of true value (222). It indicates that the method has good accuracy. The average percent recovery ± S.D. of the developed method was 99.97 ± 0.09. Thus, this method was accurate for the analysis of curcumin in nanoparticles and in mice brain.

2.2 Precision

The precision of an analytical method is the degree of agreement among individual test results when the procedure is applied repeatedly to multiple samplings of a homogeneous sample. The precision of an analytical method is usually express as the standard deviation or relative standard deviation. Precision may be a measure of either the degree of reproducibility or repeatability of the analytical method under

normal operating conditions. The precision of the method was expressed as the percentage of relative standard deviation (% R.S.D.) and the accepted value of R.S.D. is ≤ 2% (222). The % R.S.D. of injection precision (4.0 µg/ml) was 0.84% and the % R.S.D. of the assay of three different concentrations (2.0, 4.0 and 6.0 µg/ml) were 0.59%, 0.84% and 0.41%, respectively; which are in the accepted values, % RSD less than 2. Thus, the developed assay method can be used in the determination of curcumin in nanoparticles and in mice brain.

2.3 Linearity

The linearity of the method was determined by replicated injections (n = 3) of 20 µl of curcumin standards covering 1.0-10.0 µg/ml. Calibration data was calculated from ratios of peak area (between curcumin standard and internal standard) versus concentrations of curcumin standard solution in µg/ml (Table 8). The calibration curve of standard curcumin was linear with r^2 of 0.9992 and the regression equation was y = 1.1315x + 0.5724; where y is peak area ratio (between curcumin and internal standard) and x is the concentration of curcumin standard solutions in µg/ml.

The chromatograms of curcumin standards are shown in Figure 26. It is obviously that the correlation coefficient (r^2) was within the accepted criteria (r^2 greater than 0.990) (222). Thus, this calibration curve was suitable for the determination of curcumin in nanoparticles and in mice brain.

2.4 Limit of measurement

There are two categories within the level of measurement, the limit of detection (LOD) and the limit of quantitation (LOQ). LOD is the point at which a measured value is larger than the uncertainty associated with it; for example, the amount of samples exhibiting peak area ratio (between the retention time was 7.21 minutes and 4.98 minutes) three times the ratio of the baseline noises. A response to noise ratio of 3:1 is generally accepted as LOD.

The second category is referred to as the limit of quantitation (LOQ). Limit of quantitation is a parameter of qualitative assays for low levels of compounds in sample matrices, such as brain components. It is the lowest concentration of analyte in a sample that can be determined with acceptable precision and accuracy under the

stated experimental conditions. A common approach is to measure the magnitude of analytical background response by analyzing a number of blank samples and calculating the peak area ratio of noise (between 7.21 minutes and 4.98 minutes, the retention times of curcumin and internal standard). The peak area ratio of noises or responses multiply by a factor, usually 10, provides an estimate of the limit of quantitation. The limit of detection and limit of quantitation of this method were 1.58 μg/ml and 6.46 μg/ml, respectively. The LOD and LOQ are lower than the amount of curcumin in assayed solutions from mice brains and nanoparticles so the developed method was suitable for the determination of curcumin in nanoparticles and in mice brain.

3. Determination of curcumin content and entrapment efficiency

Variation of the ratio between curcumin and PMMA nanoparticles had been tried for the maximum entrapment. The ratio for loading nanoparticles with curcumin to get the highest entrapment of curcumin in the nanoparticles was found to be 4 mg curcumin/mg PMMA nanoparticles. The curcumin content and entrapment in PMMA nanoparticles (CLNP) were 62.33% ± 1.42 (w/w) and 80.00% ± 1.78 (w/w), respectively. The curcumin content and curcumin entrapment in nanoparticles were in satisfaction as they were greater than 50%, the accepted value (8-10, 14).

C. Brain Accessibility

In order to prove that nanoparticles improve the brain delivery, the accessibility of curcumin to the brain was determined. The mice were divided into 18 groups, 8 groups treated with polysorbated 80-coating curcumin-loaded nanoparticles (P80-CLNP) and 10 groups treated with curcumin solution (CS). The brains of mice treated with P80-CLNP and CS equivalent to curcumin 150 mg/kg were collected at various times for curcumin assay. The amounts of curcumin in mice brain were measured during 0.5-15 hours after subcutaneously injections. The typical chromatograms of the curcumin in mice brain showed that curcumin peak was not interfered by the brain matrix (Figure 30). The time that the amount of curcumin in the brain reached the maximum (52.12 μg) in the P80-CLNP treated mice was 3 hours

after injections whereas the maximum amount of curcumin in the brains of curcumin solution treated group was 32.14 μg at 10 hours after injections (Figure 31).

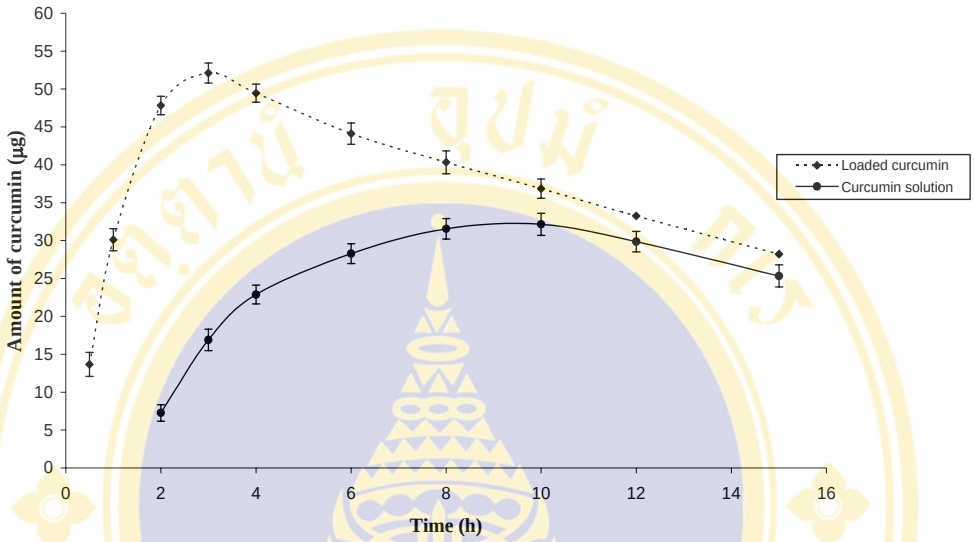

Figure 31. The amount of curcumin in mice brain at various time after subcutaneous injections of curcumin loaded nanoparticles (P80-CLNP) and curcumin solution at dose of 150 mg/kg.

The results at 2 hours showed that the amount of curcumin in the brains of curcumin nanoparticle treated group was 6.5 times greater than those treated with the curcumin solution. The overall results during 0.5-15 hours after injection showed that the polysorbate 80 curcumin loaded nanoparticles (P80-CLNP) increased the transportation of curcumin across the blood-brain barrier. The amount of curcumin in the brain of mice treated with curcumin nanoparticles (P80-CLNP) was significantly greater than those treated with curcumin solution ($p < 0.001$) at 0-10 hours. It is apparent that curcumin loaded nanoparticles improved the brain delivery of curcumin both in the increased amount of penetrated curcumin and the faster onset.

CHAPTER VI
CONCLUSION

Curcumin in form of nanoparticles was prepared in this study in order to improve the free radical scavenging ability and neuroprotective actions of curcumin. Incorporation of curcumin in the nanoparticles aims at the enhancement of brain accessability, which was consequently resulting in good neuroprotective actions. The nanoparticles of curcumin coating with polysorbate 80 were prepared and investigated for the physicochemical properties. The brain delivery of curcumin from the curcumin loaded nanoparticles was evaluated in mice to prove the capability of nanoparticles in the enhancement of brain delivery. The performed studies were summarized as the following.

1. Nanoparticles were synthesized by radical polymerization methods namely:

(i) Unloaded poly(methylmethacrylate) nanoparticles (ULNP),

(ii) Curcumin loaded nanoparticles (CLNP) and

(iii) Polysorbate 80 coated curcumin loaded nanoparticles (P80-CLNP).

2. The prepared nanoparticles were characterized on (i) size and size distribution, (ii) shape, (iii) surface charge and (iv) entrapment efficiency and curcumin content.

(i) The size of ULNP, CLNP and P80-CLNP were 62.0 nm, 79.0 nm and 94.0 nm, respectively when determined by the photon correlation spectroscopy (PCS). The sizes measured by the transmission electron microscope (TEM) which reflected the size of the solid core of the nanoparticles, were approximately 10 nm lesser. It was apparent that the sizes were below 100 nm; which was categorized as good nanoparticles. The *PI* values of the prepared nanoparticles, ULNP, CLNP and P80-CLNP, were 0.06, 0.13 and 0.03, respectively. The *PI* values of all nanoparticles were indicated homogeneous dispersion.

(ii) The shapes of ULNP and CLNP were found to be spherical while the shape of P80-CLNP was pebble-like due to the polysorbate 80 coating.

(iii) The surface charges of the prepared nanoparticles, ULNP, CLNP and P80-CLNP were negative, with zeta potential of –37.31 mV, -20.13 mV and -31.41 mV, respectively. The prepared nanoparticles were considered to be stable according to the zeta potential below -15 mV.

(iv) The curcumin content and entrapment efficiency of ULNP, CLNP and P80-CLNP were determined by the validated HPLC method. The percent of curcumin content and percent of curcumin entrapment in PMMA nanoparticles were 62.33% ± 1.42 (w/w) and 80.00% ± 1.78 (w/w), respectively. The curcumin content and curcumin entrapment in nanoparticles were in satisfaction as they were greater than 50%.

3. The amount of curcumin in the brain of mice treated with curcumin nanoparticles was significantly greater than those treated with curcumin solution ($p < 0.001$). The amount of curcumin in the brains of curcumin nanoparticle treated group was 6.5 times greater than those treated with the curcumin solution at 2 hours after injection. The time that the amount of curcumin in the brain reached the maximum (52.12 μg) in the P80-CLNP treated mice was 3 hours after injections whereas the maximum amount of curcumin in the brains of curcumin solution treated group was 32.14 μg at 10hours after injections

It is apparent that curcumin loaded nanoparticles improved the brain delivery of curcumin both in the increased amount of penetrated curcumin and the faster onset.

REFERENCES

1. Bigon E, Boarato E, Bruni A, *et al*. Pharmacological effects of phosphatidylserine liposomes: Regulation of glycolysis and energy level in brain. Br J Pharmacol 1979; 66: 167-74.
2. Toffano G, Leon A, Benvegnu D, *et al*. Effects of brain cortex phospholipids on catecholamine content. Pharmacol Res Commun 1976; 8: 581-90.
3. Tokes ZA, Todd JA, *et al*. Availability of liposome content to the nervous system: Liposomes and the blood-brain barrier. Brain Res 1980; 188: 282-6.
4. Vincenzo C, Felice L, Luigi S, *et al*. Synthesis and biological evaluation of GABA derivatives able to cross the blood–brain barrier in rats. Bioorganic & Medicinal Chemistry Letters 2003;13: 3765-9.
5. Mariana S, Tamas F, Pal R, *et al*. *In vitro* opioid activity profiles of 6-amino acid substituted derivatives of 14-o-methyloxymorphone. Eur J Pharmacol 2004; 483: 301– 8.
6. Felicia L, Abdeslam C, Marcelo A, *et al*. Effects of some antioxidative aporphine derivatives on striatal dopaminergic transmission and on MPTP-induced striatal dopamine depletion in B6CBA mice. Eur J Pharm Sci 2003; 18: 133–40.
7. Neuwelt EA (1989) Barnett PA. Blood-brain barrier disruption in the treatment of brain tumors: Animal studies. In Implications of the blood-brain barrier and its Manipulation.Newyork: Plenum, p.195-217.
8. Kreuter J, Alyautdin RN, Kharkevich DA, Ivanov AA. Passage of peptides through the blood–brain barrier with colloidal polymer particles (nanoparticles). Brain Res 1995; 674: 171–4.
9. Kreuter J. Nanoparticulate systems for brain delivery of drugs. Adv Drug Deliv Rev 2001; 47: 65–81.

10. Alyautdin RN, Petrov VE, Langer K, Berthold A, Kharkevich DA, Kreuter J. Delivery of loperamide across the blood–brain barrier with polysorbate 80-coated polybutylcyanoacrylate nanoparticles. Pharm Res 1997; 14: 325–28.

11. Alyautdin RN, Tezikov EB, Ramge P, Kharkevich DA, Begley DJ, Kreuter J. Significant entry of tubocurarine into the brain of rats by adsorption to polysorbate 80-coated polybutylcyanoacrylate nanoparticles: an *in situ* brain perfusion study. J Microencapsul 1998; 15: 67–74.

12. Friese A, Seiller E, Quack G, Lorenz B, Kreuter J. Increase of the duration of the anticonvulsive activity of a novel NMDA receptor antagonist using poly(butylcyanoacrylate) nanoparticles as a parenteral controlled release system. Eur J Pharm Biopharm 2000; 49: 103– 9.

13. Sopala M, Schweizer S, Schafer N, Nurnberg E, Kreuter J, Seiller E,Danysz W. Neuroprotective activity of a nanoparticulate formulation of the glycine B site antagonist MRZ 2/576 in transient focal ischaemia in rats. Arzneimittelforschung 2002; 52: 168–74.

14. Gulyaev AE, Gelperina SE, Skidan IN, Antropov AS, Kivman GY, Kreuter J, Significant transport of doxorubicin into the brain with polysorbate 80-coated nanoparticles. Pharm Res 1999; 16: 1564–9.

15. Gelperina SE, Khalansky AS, Skidan IN, Smirnova ZS, Bobruskin AI, Severin SE, Turowski B, Zanella FE, Kreuter J. Toxicological studies of doxorubicin bound to polysorbate 80-coated poly(butyl cyanoacrylate) nanoparticles in healthy rats and rats with intracranial glioblastoma. Toxicol Lett 2002; 126: 131–41.

16. Hoffmann F, Cinatl J, Kabic H, Cinatl J, Kreuter J, Stieneker F. Preparation, characterization and cytotoxicity of methylmethacrylate copolymer nanoparticles with a permanent positive surface charge. Int J Pharm 1997; 157: 189–98.

17. Langer K, Marburger C, Berthold A, Kreuter J, Stieneker F. Methylmethacrylate propylmethacrylate copolymer nanoparticles for drug delivery. Part I:

preparation and physicochemical characterization. Int J Pharm 1996; 137: 67-74.

18. Vauthier C, Dubernet C, Fattal E, Couvreur P. Poly(alkyl cyanoacrylates) as biodegradable materials for biomedical applications. Adv Drug Deliv Rev 2003; 55: 519–48.

19. Lee J, Cho E, Cho K. Incorporation and release behavior of hydrophobic drug in functionalized poly(D,L-lactide)-block–poly(ethylene oxide) micelles. J Control Release 2004; 94: 323-35.

20. Berkland C, Pack DW, Yekyoon KK. Controlling surface nano-structure using flow-limited field-injection electrostatic spraying (FFESS) of poly(D,L - lactide-co-glycolide). Biomaterials 2004; 25: 5649-58.

21. Matsumoto K, Hasegawa H, Matsuoka H. Synthesis of sodium-polystyrenesulfonate-grafted nanoparticles by core-cross-linking of block copolymer micelles. Tetrahedron 2004; 60: 7197-204.

22. Sullivan O, Birkinshaw C. *In vitro* degradation of insulin-loaded poly (n-butylcyanoacrylate) nanoparticles. Biomaterials 2004; 25: 4375-82.

23. Dong, Y, Feng S. Methoxy poly(ethylene glycol)-poly(lactide) (MPEG-PLA) nanoparticles for controlled delivery of anticancer drugs. Biomaterials 2004; 25: 2843-49.

24. Troster SD, Muller U, Kreuter J. Modification of the body distribution of poly(methylmethacrylate) nanoparticles in rats by coating with surfactants. Int J Pharm 1990; 61: 85-100.

25. Borchard G, Audus KL, Shi F, Kreuter J. Uptake of surfactant coated poly(methylmethacrylate) nanoparticles by bovine brain microvessel endothelial cell monolayers. Int J Pharm 1994; 110: 29-35.

26. Martin J, Todd D, Brian M, Li A, *et al*. Immunogenicity of bovine parainfluenza type 3 virus proteins encapsulated in nanoparticle vaccines, following intranasal administration to mice. Res Veter Sci 2003; 74 : 187–90.

27. Ahlin P, Kristl J, Kristl A, Vrecer F. Investigation of polymeric nanoparticles as carriers of enalaprilat for oral administration. Int J Pharm 2002; 239: 113–20.

28. Araujo L, Lobenberg R, Kreuter J. Influence of the surfactant concentration on the body distribution of nanoparticles. J Drug Target 1999; 6: 373–85.

29. Rieger J, Horn D. Organic nanoparticles in aqueous phase. Angew Chem Int Ed 2001; 40: 4330-61.

30. Unnikrishnan MK, Roa MN. Inhibition of nitrite induce oxidation of hemoglobin by curcuminoids. Pharmazie 1995; 50: 490-2.

31. Sreejayan S, Roa MNA. Curcuminoids as potent inhibitors of lipid peroxidation. J Pharm Pharmacol 1994; 46: 1013-6.

32. Masuda T, Isobe J, Jitoe A, *et al*. Antioxidative curcuminoids from rhizomes of *Curcuma xanthorrhiza*. Phytochemistry 1992; 31: 3645-7.

33. Arora RB, Basu N, Kapoor V, Jain AP. Anti-inflammatory studies on *Curcuma longa* (Turmeric). Indian J Med Res 1972; 59: 1289-95.

34. Ozaki K, Kawata Y, Amano S, Hanazawa S. Stimulatory effect of curcumin on osteoclast apoptosis. Biochem Pharmacol 2000; 59: 1577-81.

35. Vajragupta O, Boonchoong P, Watanabe H, *et al*. Manganese complexes of curcumin and its derivatives evaluation for the radical scavenging ability and neuroprotective activity. Free Radical Biology & Medicine, 2003; 35: 1632-44.

36. Eigner D, Scholz D. *Ferula asa-foetida* and *Curcuma longa* in traditional medical treatment and diet in Nepal. J Ethnopharmacol 1999; 67: 1-6.

37. Unnikrishann MK, Rao MNA. Curcumin inhibits nitrogen dioxide induced oxidation of hemoglobin. Mol Cell Biochem 1995; 146: 35-7.

38. Masuda T, Hidaka K, Shinlhara A, Maekawa T, Takeda Y, Yamaguchi H. Chemical studies on antioxidant mechanism of curcuminoid: analysis of radical reaction products from curcumin. J Agric Food Chem 1999; 47: 71-7.

39. Jovanovic SV, Boone CW, Steenken S, Trinoga M, Kaskey RB. How curcumin works preferentially with water-soluble antioxidants. J Am Chem Soc 2001; 123: 3064-8.

40. Jovanovic SV, Steenken S, Bone CW, Simic MG. H-atom transfer is a preferred antioxidant mechanism of curcumin. J Am Chem Soc 1999; 121: 9677-81.

41. Khopde SM, Priyadarsini KI, Venkatesan P, Rao MNA. Free radical scavenging ability and antioxidant eficiency of curcumin and its substituted analogue. Biophys Chem 1999; 80: 85-91.

42. Das KC and Das CK. Curcumin (diferuloylmethane), a singlet oxygen ($^1O_2$) quencher. Biochem Biophys Res Com 2002; 295: 62-6.

43. Ruby AJ, Kuttan G, Babu KD, Rajasekharan KN, Kuttan R. Anti-tumour and antioxidant activity of natural curcuminoids. Cancer Lett 1995; 94: 79-83.

44. Reese T, Karnovsky M. Fine structural localization of a blood–brain barrier to exogenous peroxidase. J. Cell Biol. 1967; 34: 207–17.

45. Huang X, Cuajungco M, Atwood C. Cu (II) potentiation of Alzheimer AB neurotoxicity. J. Biol. Chem. 1999; 274: 37111– 6.

46. Smith Q. A Review of Blood Brain Barrier Transport Techniques. Humana Press, Inc., Totowa, NJ, 2003.

47. Nag S. Morphology and Molecular Properties of Cellular Components of Normal Cerebral Vessels. Humana Press, Totowa, NJ, 2003.

48. Yan Q, Sage E. Transforming growth factor-beta 1 induces apoptotic death in cultured retinal endothelial cells but not in pericytes: association with decreased expression of p21 wafl/ cip1. J. Cell. Biochem. 1998; 70: 70–83.

49. Hirshi K, Armore PD, Control of angiogenesis by pericytes: molecular mechanisms and significance. EXS 1997; 79: 19–28.

50. Johanson C. Permeability and vascularity of the developing brain: cerebellum vs. cerebral cortex. Brain Res. 1980; 190: 31– 16.

51. Pardridge W. Molecular Biology of the Blood–Brain Barrier. Humana Press, Totowa, NJ, 2003.

52. Crone C, Olesen S. Electrical resistance of brain microvascular endothelium. Brain Res. 1982; 241: 49–55.

53. Krause D, Mischeck U, Galla H, Dermietzel R. Correlation of zonua occludens ZO-1 antigen and transendothelial resistance in porcine and rat cultured cerebral endothelial cells. Neurosci. Lett. 1991; 128: 301– 4.

54. Smith Q, Rapoport S. Cerebrovascular permeability coefficients to sodium, potassium and chloride. J. Neurochem. 1986; 46: 1732– 42.

55. Furuse M, Hirase T, Ito M. Occludin: a novel integral membrane protein localizing at tight junctions. J. Cell Biol. 1993; 123: 1777–88.

56. Wolburg H, Lippoldt A. Tight junctions of the blood–brain barrier: development, composition and regulation. Vasc. Pharmacol. 2002; 38: 323–37.

57. Wolburg H, Wolburg-Bucholz K, Kraus J, Rascher-Eggstein G, Liebner S, Hamm S, Duffner F. Localization of claudin-3 in tight junctions of the blood–brain barrier is selectively lost during experimental autoimmune encephalomyelitis and human glioblastoma multiforme. Acta Neuropathol. 2003; 105: 586– 92.

58. Martin-Padura I, Lostaglio S, Schneemann M. Junctional adhesion molecule, a novel member of the immunoglobulin superfamily that distributes at intercellular junctions and modulates monocyte transmigration. J. Cell Biol. 1998; 142: 117–27.

59. Morita K, Sasaki H, Furuse M, Tsukita S. Endothelial claudin: claudin-5/TMVCF constitutes tight junction strands in endothelial cells. J. Cell Biol. 1999; 147: 185– 94.

60. Mitic L, Anderson J. Molecular physiology and pathophysiology of tight junctions. Am. J. Physiol.: Gasterointest. Liver Physiol. 2000; 279: G250–G4.

61. Furuse M, Fujimoto K, Sato N, Hirase T. Overexpression of occludin, a tight junction integral membrane protein, induces the formation of intracellular multilamellar bodies bearing tight junction-like structures. J. Cell. Sci. 1996: 109: 429–35.

62. Mitic L, Anderson J. Molecular architecture of tight junctions. Annu. Rev. Physiol. 1998; 60: 121– 42.

63. Reichel A (2003), Begley D, Abbott N. in: S. Nag (Ed.), Methods in Molecular Medicine: The Blood–Brain Barrier: Biology and Research Protocols, Humana Press, Inc., Totowa, NJ, pp. 307– 325.

64. Ring A, Weiser J, Tuomanen E. Pneumococcal trafficking across the blood–brain barrier: molecular analysis of a novel bidirectional pathway. J. Clin. Invest. 1998; 102: 347– 60.

65. Pron B, Taha M, Rambaud C, Fournet J. Interaction of *Neisseria meningitidis* with the components of the blood–brain barrier correlates with an increased expression of PilC. J. Infect. Dis. 1997; 176: 1285–92.

66. Neuwelt E. Mechanisms of disease: the blood–brain barrier. Neurosurgery 2004; 54: 131– 41.

67. Huber J, Witt K, Hom S. Inflammatory pain alters blood–brain barrier permeablility and tight junctional protein expression. Am. J. Physiol. 2001; 280: H1241– H8.

68. Smith E (1989), in: E. Neuwelt (Ed.), Implications of the Blood Brain Barrier and its Manipulation, Plenum Press, New York, 85– 118.

69. Lee G, Dallas S, Hong M. Drug transporters in the central nervous system: brain barriers and brain parenchymal considerations. Pharmacol. Rev. 2001; 53: 569– 96.

70. Kabanov A, Batrakova E. New technologies for drug delivery across the blood–brain barrier. Curr. Pharm. Des. 2004;10: 1355– 63.

71. Kreuter J (1994), in: J.B.J. Swarbrick (Ed.), Encyclopedia of Pharma. Tech., Marcel Dekker, New York, pp. 165– 90.

72. Agnihotri SA, Mallikaujuana NN, Aminabhavi TM. Recent advances on chitosan-based micro and nanoparticles in drug delivery. J. Control. Release 2004; 100: 5– 28.

73. Aminabhavi TM, Soppimath KS, Kulkarni KR. Biodebradable polymeric nanoparticles as drug delivery devices. J. Control. Release 2001; 70: 1– 20.

74. Behan N, Birkinshaw C, Clarke N. Poly n-butyl cyanoacrylate nanoparticles: a mechanistic study of polymerization and particle formation. Biomaterials 2001; 22: 1335– 44.

75. Fessi H, Puisieux F, Devissaguet J. Nanocapsule formation by interfacial polymer deposition following solvent displacement. Int. J. Pharm. 1989; 55: R1–R4.

76. Gubha S, Mandal B. Dispersion polymerization of acrylamide. J. Colloid Interface Sci. 2004; 271: 55– 9.

77. Leroux J, Allemann E, Doelker E. New approach for the preparation of nanoparticles by an emulsification–diffusion method. Eur. J. Pharm. Biopharm. 1995; 41: 14– 8.

78. Li Y, Pei Y, Zhou Z. PEGylated polycyanoacrylate nanoparticles as tumor necrosis factor-alpha carriers. J. Control. Release 2001; 73: 287– 96.

79. Lobenberg R, Araujo L, Briesen H. Body distribution of azidothymidine bound to hexyl-cyanoacrylate nanoparticles after i.v. injection to rats. J. Control. Release 1998; 50: 21– 30.

80. Murakami H, Yoshino M, Mizobe M. Preparation of poly(d,l-lactide-coglycolide) latex for surface modifying material by a double coacervation method. Proc. Int. Symp. Control. Release Bioact. Mater. 1996; 23: 361– 2.

81. Niwa T, Takeuchi H, Hino T. Preparations of biodegradable nanospheres of water-soluble and insoluble drugs with d,l-lactide/glycolide copolymer by a novel spontaneous emulsification solvent diffusion method and the drug release behavior. J. Control. Release 25 1993; 16: 265-9.

82. Peracchia M, Vauthier C, Desmaele D. PEGylated nanoparticles from a novel MePEGcyanoacrylate hexadecylcyanoacrylate amyphiphilic copolymer. Pharm. Res. 1998; 15: 548–54.

83. Quintanar G, Ganem Q, Allemann E. Influence of the stabilizer coating layer on the purification and freeze drying of poly (d,l-lactic acid) nanoparticles prepared by the emulsification–diffusion technique. J. Microencapsul. 1998; 15: 107–19.

84. Scholes P, Coombes A, Illum L. The preparation of sub-500 nm poly(lactide-co-glycolide) microspheres for site-specific drug delivery. J. Control. Release 1993; 25: 145– 53.

85. Wehrle P, Magenheim P, Benita S. Influence of process parameters on the PLA nanoparticle size distribution evaluated by means of factorial design. J. Pharm. Biopharm. 1995; 41: 19–26.

86. Zambaux M, Bonneaux F, Gref R. Influence of experimental parameters on the characteristics of poly(lactic acid) nanoparticles prepared by double emulsion method. J. Control. Release 1998; 50: 31– 40.

87. Kreuter J. Nanoparticulate systems for brain delivery of drugs. Adv. Drug Deliv. Rev. 2001; 47: 65– 81.

88. Kreuter J, Alyautdin R, Kharkevich D. Passage of peptides through the blood–brain barrier with collodial polymer particles (nanoparticles). Brain Res. 1995; 674: 171– 4.

89. Schroeder U, Sommerfeld P, Sabel B. Efficacy of oral dalargin–loaded nanoparticle delivery across the blood–brain barrier. Peptides 1998; 19: 777–80.

90. Schroeder U, Sabel B, Schroeder H. Diffusion enhancement of drugs by loaded nanoparticles *in vitro*. Prog. Neuro-Psychopharmacol. Biol. Psychiatry 1999; 29: 941– 9.

91. Vauthier C, Dubernet C, Chauvierre C. Drug delivery to resistant tumors: the potential of poly (alkyl cyanoacrylate) nanoparticles. J. Control. Release 2003; 93: 151– 60.

92. Munk P, Aminabhavi TM. Introduction to Macromolecular Science. John Wiley & Sons, Inc., New York, 2002.

93. Lockman P, Mumper R, Khan M. Nanoparticle technology for drug delivery across the blood–brain barrier. Drug Dev. Ind. Pharm. 2002; 28: 1 –13.

94. Koziara J, Lockman P, Allen D. *In situ* blood–brain barrier transport of nanoparticles, Pharm. Res. 2003; 20: 1772– 8.

95. Yang C, Chang C, Tsai P. Nanoparticle-based *in vivo* investigation on blood–brain barrier permeability following ischemia and reperfusion. Anal. Chem. 2004; 76: 4465– 71.

96. Broaddus W, Prabhu C, Wu-Pong S. Strategies for the design and delivery of antisense oligonucleotides in central nervous system, Methods Enzymol. 2000; 314: 121– 35.

97. Yang S, Lu L, Cai Y. Body distribution in mice of intravenously injected campothecin solid lipid nanoparticles and targeting effect on brain. J. Control. Release 1999; 59: 299– 307.

98. Boussif O, Lezoualc F, Zanta M. A versatile vector for gene and oligonucleotide transgene into cells in culture and *in vivo*: polyethylenimine. Proc. Natl. Acad. Sci. U. S. A. 1995; 92: 7297– 303.

99. Jeong J, Kim S, Park T. A new antisense oligonucleotide delivery system based on self-assembled ODN–PEG hybrid conjugate micelles. J. Control. Release 2003; 93: 183– 91.

100. Kim J, Kim B, Maruyama A. A new nonviral DNA delivery vector: the terplex system. J. Control. Release 1998; 53: 175–82.

101. Meyer O, Kirpotin D, Hong K. Cationic liposomes coated with polyethylene glycol as carriers for oligonucleotides. J. Biol. Chem. 1998; 25: 15621– 7.

102. Vinogradov S, Batrakova E, Kabanov A. Poly(ethyleneglycol)-[polyethyleneimine NanoGel particles: novel drug delivery systems for antisense oligonucleotides. Colloids Surf., B Biointerfaces 1999; 16: 291–304.

103. Soppimath KS, Kulkarni AR, Aminabhavi TM. Chemically modified polyacrylamide-g-guar gum based cross-linked anionic microgels as pH-sensitive drug delivery systems: preparation and characterization. J. Control. Release 2001; 75: 331–45.

104. Lin YH, Chung CK, Chen CT. Preparation of nanoparticles composed of chitosan/ poly-A´-glutamic acid and evaluation of their permeability through Caco-2 cells. Biomacromolecules 2005; 6: 1104–12.

105. Furuse M, Fujita K, Hiiragi T. Claudin-1 and -2: novel integral membrane protein localizing at tight junctions. J. Cell Biol. 1998; 141: 1539–50.

106. Chavany C, Doan T, Couvreur P. Polyalkylcyanoacrylate nanoparticles as polymeric carriers for antisense oligonucleotides. Pharm. Res. 1992; 9 : 441–9.

107. Lin YH, Chung CK, Chen CT. Preparation of nanoparticles composed of chitosan/poly-r-glutamic acid and evaluation of their permeability through Caco-2 cells. Biomacromolecules 2005; 6: 1104–12.

108. Garcia-Garcia E, Andrieux K, Gil S. Collodial carriers and blood–brain barrier (BBB) translocation: a way to deliver drugs to the brain. Int. J. Pharm. 2005; 298: 274–92.

109. Lockman P, Oyewumi M, Koziara J. Brain uptake of thiamine-coated nanoparticles, J. Control. Release 2003; 93: 271–82.

110. Wang JX, Sun X, Zhang ZR. Enhanced brain targeting by synthesis of 3V,5V-diocyanoyl-5-fluoro-2V-deoxyuridine and incorporation into solid lipid nanoparticles. Eur. J. Pharm. Biopharm. 2002; 54: 285–90.

111. Lu W, Tan YZ, Hu KL, Jiang XG. Cationic albumin conjugated pegylated nanoparticle with its transcytosis ability and little toxicity against blood–brain barrier. Int. J. Pharm. 2005; 295: 247– 60.

112. Burton GW, Ingold KU. Extraordinary kinetic behavior of the α-tocopheroxyl (vitamin E) radical. J Org Chem 1995; 60: 5456-67.

113. Jacobsen EJ, BanDoornik FJ, Ayer DE, *et al*. 2-(Aminomethyl)chromans that inhibit iron-dependent lipid peroxidation and protect against central nervous system trauma and ischemia. J Med Chem 1992; 35: 4464-72.

114. Spinnewyn B, Cornet S, Auguet M, Chabrier PE. Synergistic protective effects of antioxidant and nitric oxide synthase inhibitor in transient focal ischemia. J Cereb Blood Flow Metab 1999; 19: 139-43.

115. Cross CE, Halliwell B, Borish ET. Oxygen radicals and human disease. Annal Inter Med 1987; 107: 526-45.

116. Okezie IA. Assessment of potential pro-oxidant and antioxidant actions. JOACS 1996; 1617-25.

117. Roberfroid M, Colderon PB. Definitions, properties and reactions of radicals. In: Roberfroid M, Colderon PB, editors. Free radicals and oxidation phenomena in bilogical systems. New York: University of Catholique de Louvain Brussels; 1995. P.11-32.

118. Romer W, Oettel M, Menzenbach B, *et al*. Novel estrogens and their radical scavenging effects, iron-chelating and total antioxidative activities: 17α-substitutes analogs of $\Delta^{9(11)}$-dehydro-17β-estradiol. Steroids 1997; 62: 688-94.

119. Halliwell B, Gutteridge JMC. Lipid peroxidation: a radical chain reaction. In: Halliwell B, Gutteridge JMC, editors. Free radicals in biology and medicine. 2nd ed. Oxford Clarendon: Oxford University; 1989. p.91-142.

120. Roberfroid M, Colderon PB. Biomolecular tagets for radicals and reactive oxygen species. In: Roberfroid M, Colderon PB, editors. Free radicals and oxidation phenomena in biological systems. New York: University of Catholique de Louvain Brussels; 1995. P.143-92.

121. Braughler JM, Duncan LA, Chase RI. The involvement of iron in lipid peroxidation. Gutteridge. J Biol Chem 1986; 261(22): 10282-9.

122. Minotti G, Aust SD. The role of iron in oxygen radical mediated lipid peroxidation. Chem Biol Int Interactions 1989; 71:1-19.

123. Esterbauer H, Gebicki J, Puhl H, *et al*. The role of lipid peroxidation and antioxidants in oxidative modification of LDL. Free Radic Biol Med 1992; 13:341-90.

124. Denisov ET, Khudyakov IV. Mechanisms of action and reactivities of the free radicals of inhibitors. Chem Rev 1987; 87: 1313-57.

125. Simonian NA, Coyle JT. Oxidative stress in neurodegenerative diseases. Ann Rev Pharmacol 1996; 23: 239-57.

126. Araujo CAC, Leon LL. Biological activities of Curcuma longa L. Men Inst Osealdo Crus 2001; 96: 723-8.

127. Srimal RC. Turmeric: a brief review of medicinal properties. Fitoterapia 1997; 6: 483-93.

128. Jayaprakasha GK, Rao LJM Sakariah KK. Improved HPLC method for the determination of curcumin, demethoxycurcumin and bisdemethoxycurcumin. J Agric Food Chem 2002, 50: 3668-72.

129. Roughley PJ, Whiting DA. Experiments in the biosynthesis of curcumin. J Chem Soc 1973; 20: 2379-88.

130. Sun YM, Zang HY, Chaen DZ, Liu CB. Theoretical elucidation on the antioxidant mechanism of curcumin: a DFT study. Org Lett 2002; 4: 2909-11.

131. Unnikrishnan MK, Rao MN. Inhibition of nitrite induce oxidation of hemoglobin by curcuminoids. Pharmazie 1995; 50: 490-2.

132. Reddy AC, Lokes BR. Studies on spice principles as antioxidants in the inhibition of lipid peroxidation of rat liver microsomes. Mol Cell Biochem 1992; 111: 117-24.

133. Reddy AC, Lokesh BR. Effect of dietary turmeric (*Curcuma longa*) on iron-induced lipid peroxidation in the rat liver. Food Chem Toxicol 1994; 32: 279-83.

134. Sreejayan S, Rao MNA. Curcuminoids as potent inhibitors of lipid peroxidation. J Pharm Pharmacol 1994; 46: 1013-6.

135. Sreejayan S, Rao MNA. Curcumin inhibits iron-dependent lipid peroxidation. Int J Pharmaceutics 1993; 100: 93-7.

136. Pratro BS, Rele S, Chintalwar GJ, Chattopadhyay S, Adhkari S, Mukherjee T. Protective activities of some phenolic 1,3-diketones against lipid peroxidation: possible involvement of the 1,3-diketones moiety. Chem Biol 2002; 3: 364-70.

137. Joe B, Lokesh BR. Role of capsaicin, curcumin and dietary n-3 fatty acids in lowering the generation of reactive oxygen species in rat peritoneal macrophages. Biochim Biophys Acta 1994; 1224: 255-63.

138. Ghoneim AI, Abdel-Naim AB, Khalifa A, El-Denshary ES. Protective effects of curcumin against ischemia/reperfusion insult in rat forebrain. Pharmacol Res 2002; 46: 273-9.

139. Oyama Y, Masuda T, Nakata M, *et al*. Protective actions of 5/-n-alkylated curcumins on living cells suffering from oxidative stress. Eur J Pharmacol 1998; 360: 65-71.

140. Kunchandy E, Roa MNA. Oxygen radical scavenging activity of curcumin. Int J Pharmaceutics 1990; 58: 237-40.

141. Tonnesen HH, Greenhill JV. Studies on curcumin and curcuminoids XXII: curcumin as a reduction agent and radical scavenger. Int J Pharm 1992; 87: 79-87.

142. Masuda T, Isobe J, Jitoe A, *et al*. Antioxidative curcuminoids from rhizomes of *Curcuma xanthorrhiza*. Phytochemistry 1992; 31: 3645-7.

143. Das KC and Das CK. Curcumin (diferuloylmethane), a singlet oxygen (1O2) quencher. Biochem Biophys Res Com 2002; 295: 62-6.

144. Ruby AJ, Kuttan G, Babu KD, Rajasekharan KN, Kuttan R. Anti-tumour and antioxidant activity of natural curcuminoids. Cancer Lett 1995; 94: 79-83.

145. Unnikrishann MK, Rao MNA. Curcumin inhibits nitrogen dioxide induced oxidation of hemoglobin. Mol Cell Biochem 1995; 146: 35-7.

146. Masuda T, Hidaka K, Shinlhara A, Maekawa T, Takeda Y, Yamaguchi H. Chemical studies on antioxidant mechanism of curcuminoid: analysis of radical reaction products from curcumin. J Agric Food Chem 1999; 47: 71-7.

147. Jovanovic SV, Boone CW, Steenken S, Trinoga M, Kaskey RB. How curcumin works preferentially with water-soluble antioxidants. J Am Chem Soc 2001; 123: 3064-8.

148. Jovanovic SV, Steenken S, Bone CW, Simic MG. H-atom transfer is a preferred antioxidant mechanism of curcumin. J Am Chem Soc 1999; 121: 9677-81.

149. Khopde SM, Priyadarsini KI, Venkatesan P, Rao MNA. Free radical scavenging ability and antioxidant eficiency of curcumin and its substituted analogue. Biophys Chem 1999; 80: 85-91.

150. Masuda T, Bando H, Maekawa T, Takeda Y, Yamaguchi H. A novel radical terminated compound produced in the antioxidant process of curcumin against oxidation of a fatty acid ester. Tetrahedron Let 2000; 41: 2157-60.

151. Masuda T, Maekawa T, Hidaka K, Bando H, Takeda Y, Yamaguchi H. Chemical studies on antioxidant mechanism of curcumin: analysis of oxidative coupling products from curcumin and linolate. J Agric Food Chem 2001; 49: 2539-47.

152. Masuda T, Toi Y, Bando H, Maekawa T, Takeda Y, Yamaguchi H. Structural identification of new curcumin dimers and their contribution to the antioxidant mechanism of curcumin. J Agric food Chem 2002; 50: 2524-30.

153. Mukophadhyay A, Basu N, Ghatak N, Gujral PK. Anti-inflammatory and irritant activities of curcumin analogues in rats. Agents and Actions 1982; 12: 508-15.

154. Arora RB, Basu N, Kapoor V, Jain AP. Anti-inflammatory studies on *Curcuma longa* (Turmeric). Indian J Med Res 1972; 59: 1289-95.

155. Ghatak N, Basu N. Sodium curcuminate as an effective anti-inflammatory agent. Indian J Exp Biol 1972; 10: 235-6.

156. Srimal RC, Dhawan BN. Pharmacology of diferuloylmethane (curcumin), a non-steroidal anti-inflammatory agent. J Pharm Pharmacol 1973; 25: 447-52.

157. Huang MT, Lysz T, Ferraro T, Abidi TF, Laskin JD, Conney AH. Inhibitory effects of curcumin on *in vitro* lipoxygenase and cyclooxygenase activities in mouse epidermis. Cancer Res 1991; 51: 813-19.

158. Ammon HPT, Anazodo MI, Safayhi H, Dhawan BN, Srimal RC. Curcumin: a potent inhibitor of Leukotriene B4 formation in rat peritoneal polymorphonuclear neutrophils (PMNL). Planta Med 1992; 58: 226.

159. Abe Y, Hashimoto S, Horie T. Curcumin inhibition of inflammatory cytokine production by human peripheral blood monocytes and alveolar macrophages. Pharmacol Res 1999; 39: 41-47.

160. Chuang SE, Chen AL, Lin JK, Kuo ML. Inhibition by curcumin of diethylnitrosamine-induced hepatic hyperplasia, inflammation, cellular gene products and cell-cycle-related proteins in rats. Fd Chem Toxicol 2000; 38: 991-5.

161. Ammon HPT, Wahl MA. Pharmacology of Curcuma longa. Planta Med 1991; 57: 1-7.

162. Deodhar SD, Sethi R, Srimal RC. Preliminary study on antirheumatic activity of curcumin (diferuloyl methane). Indian J Med Res 1980; 71: 632-4.

163. Satoskar RR, Shah SJ, Shenoy SG. Evaluation of anti-inflammatory property of curcumin (diferuloyl methane) in patients with postoperative inflammation. Int J Clin Pharmacol Ther Toxicol 1986; 24: 651-4.

164. Surh YJ. Molecular mechanisms of chemopreventive effects of selected dietary and medicinal phenolic substances. Mut Res 1999; 428: 305-27.

165. Soni KB, Rajan A, Kuttan R. Reversal of aflatoxin induced liver damage by turmeric and curcumin. Cancer Lett 1992; 66: 115-21.

166. Conney AH, Lou Y-R, Xie J-G, *et al*. Some perspectives on dietary inhibition of carcinogenesis; studies with curcumin and tea. Proc Soc Exp Biol Med 1997; 216: 234-45.

167. YP Lu, Chang RL, Huang MT, Conney AH. Inhibitory effects of topical application of low doses of curcumin on 12-*O*-tetradecanoylphorbol-13-acetate-induced increase in ornithine decarboxylase mRNA in mouse epidermis. Carcinogenesis 1993; 14: 293-7.

168. Huang M-T, Smart RC, Wong C-Q, Conney AH. Inhibitory effect of curcumin, chlorogenic acid, caffeic acid, and ferulic acid on tumor promotion in mouse skin by 12-*O*-tetradecanoylphorbol-13-acetate. Cancer Res 1988; 48: 5941-6.

169. Ishizaki C, Oguro T, Yoshida T, Wen CQ, Sueki H, Iijima M. Enhancing effect of ultraviolet A on ornithine decarboxylase induction and dermatitis evoked by 12-*O*-tetradecanoylphorbol-13-acetate and its inhibition by curcumin in mouse skin. Dematol 1996; 193: 311-7.

170. Huang M-T, Lusz T, Ferraro T, Abidi TF, Laskin JD, Conney AH. Inhibitory effects of curcumin on *in vitro* lipoxygenase and cyclooxygenase activities in mouse epidermis. Cancer Res 1991; 51: 813-9.

171. Rao CV, Rivenson A, Simi B, Reddy BS. Chemoprevention of colon carcinogenesis by dietary curcumin, a naturally occurring plant phenolic compound. Cancer Res 1995; 55: 259-66.

172. Shih CA, Lin JK. Inhibition of 8-hydroxyguanosine formation by curcumin in mouse fibroblast cells. Carcinogenesis 1993; 14: 709-12.

173. Liu JY, Lin SJ, Lin JK. Inhibitory effects of curcumin on protein kinase C activity induced by 12-*O*-tetradecanoylphorbol-13-acetate in NIH3T3 cells. Carcinogenesis 1993; 14: 857-61.

174. Kakar SS, Roy D. Curcumin inhibits TPA induced expression of c-fos, c-jun and c-myc proto-oncogenes messenger RNAs in mouse skin. Cancer Lett 1994; 87: 85-9.

175. Korutla L, Kumar R. Inhibitory effect of curcumin on epidermal growth factor receptor kinase activity in A431 cells. Biochim. Biophys. Acta 1994: 1224: 597-600.

176. Korutla L, Cheung JY, Mendelsohn J, Kumar R. Inhibition of ligand-induced activation of epidermal growth factor receptor tyrosine phosphorylation by curcumin. Carcinogenesis 1995; 16: 1741-5.

177. Reddy S, Aggarwal BB. Curcumin is a non-competitive and selective inhibitor of phosphorylase kinase. FEBS Lett 1994; 341: 19-22.

178. Huang TS, Lee SC, Lin JK. Suppression of c-Jun/AP-1 activation by an inhibitor of tumor promotion in mouse fibroblast cells. Proc Natl Acad Sci USA 1991; 88: 5292-6.

179. Chan MMY. Inhibition of tumor necrosis factor by curcumin, a phytochemical. Biochem. Pharmacol 1995; 49: 1551-6.

180. Singh S, Aggarwal BB. Activation of transcription factor NF-κ B is suppressed by curcumin. J Biol Chem 1995; 270: 24995-5000.

181. Iersel ML, Ploemen JP, Lo Bello M, Federici G, Bladeren PJ. Interactions of alpha, beta-unsaturated aldehydes and ketones with human glutathione S-transferase P1-1. Chem Biol Interact 1997 12; 108: 67-78.

182. Jee SH, Shen SC, Tseng CR, Chiu HC, Kuo ML. Curcumin induces a p53-dependent apoptosis in human basal cell carcinoma cells. J Invest Dermatol 1998; 111: 656-61.

183. Choudhuri T, Pal S, Agwarwal ML, Das T, Sa G. Curcumin induces apoptosis in human breast cancer cells through p53-dependent Bax induction. FEBS Lett 2002; 512: 334-40.

184. Ozaki K, Kawata Y, Amano S, Hanazawa S. Stimulatory effect of curcumin on osteoclast apoptosis. Biochem Pharmacol 2000; 59: 1577-81.

185. Kelloff GJ, Crowell JA, Hawk ET, *et al*. Strategy and planning for chemopreventive drug development: clinical development plans II. J Cell Biochem Suppl 1996; 26: 54-71.

186. Cheng AL, Hsu CH, Lin JK, *et al*. Phase I clinical trial of curcumin, a chemopreventive agent, in patients with high-risk or pre-malignant lesions. Anticancer Res 2001; 21: 2895-900.

187. Devasena T, Rajasekaran K, Menone V. Bis-1,7-(2-hydroxyphenyl)-hepta-1,6-diene-3,5-dione (a curcumin analog) amiliorates DMH-induced hepatic oxidative stress during colon carcinogenesis. Pharmacol Res 2002; 46: 39-45.

188. Shim JS, Kim DH, Jung HJ, *et al*. Hydrazinocurcumin, a novel synthetic curcumin derivative, is a potent inhibitor of endothelial cell proliferation. Bioorg Med Chem 2002; 10: 2987-92.

189. Adams BK, Cai J, Armstrong J, *et al*. EF24, a novel synthetic curcumin analog, induces apoptosis in cancer cells via a redox-dependent mechanism. Anti-cancer Drugs 2005; 16(3): 263-75.

190. Mazumder A, Wang S, Neamati N, *et al*. Antiretroviral agents as inhibitors of both human immunodeficiency virus type 1 integrase and protease. J Med Chem 1996; 39: 2472-81.

191. Mazumder A, Neamati N, Sunder S, *et al*. Curcumin analogs with altered potencies against HIV-1 integrase as probes for biochemical mechanisms of drug action. J Med Chem 1997; 40: 3057-3063.

192. Eigner D, Scholz D. *Ferula asa-foetida* and *Curcuma longa* in traditional medical treatment and diet in Nepal. J Ethnopharmacol 1999; 67: 1-6.

193. Negi PS, Jayaprakasha GK, Jagan Mohan Rao L, Sakariah KK. Antibacterial activity of turmeric oil: a byproduct from curcumin manufacture. J Agric Food Chem 1999; 47: 4297-300.

194. Bhavani Sankar TN, Murthy S. Effect of Turmeric (*Curcuma longa*) fractions on the growth of some intestinal and pathogenic bacteria *in vitro*. Indian J Exp Biol 1979; 17: 1363-6.

195. Park EJ, Jeon CH, Ko G, Kim J, Sohn DH. Protective effect of curcumin in rat liver injury induced by carbon tetrachloride. J Pharm Pharmacol 2000; 52: 437-40.

196. Lee SE, Campbell BC, Molyneux RJ, Hasegawa S, Lee HS. Inhibitory effects of naturally occurring compounds on aflatoxin B(1) biotransformation. Agric Food Chem 2001; 49: 5171-7.

197. Soni KB, Lahiri M, Chackradeo P, Bhide SV, Kuttan R. Protective effect of food additives on aflatoxin-induced mutagenicity and hepatocarcino genicity. Cancer Lett 1997; 115: 129-33.

198. Donatus IA, Sardjoko, Vermeulen NPE. Cytotoxic and cytoprotective activities of curcumin. Effects on paracetamol-induced cytotoxicity, lipid peroxidation and glutathione depletion in rat hepatocytes. Biochem Pharmacol 1990; 39: 1869-1875.

199. Reddy AC, Lokesh BR. Effect of curcumin and eugenol on iron-induced hepatic toxicity in rats. Toxicology 1996; 107: 39-45.

200. Mukhopadhyay MJ, Saha A, Mukherjee A. Studies on the anticlastogenic effect of turmeric and curcumin on cyclophosphamide and mitomycin C *in vivo*. Food Chem Toxicol 1998; 36: 73-6.

201. Singh A, Singh SP, Bamezai R. Postnatal modulation of hepatic biotransformation system enzymes via translactational exposure of F1 mouse pups to turmeric and curcumin. Cancer Lett 1995; 96: 87-93.

202. Thapliyal R, Deshpande SS, Maru GB. Effects of turmeric on the activities of benzo(a)pyrene-induced cytochrome P-450 isozymes. J Environ Pathol Toxicol Oncol 2001; 20: 59-63.

203. Oetari S, Sudibyo M, Commandeur JN, Samhoedi R, Vermeulen NP. Effects of curcumin on cytochrome P450 and glutathione S-transferase activities in rat liver. Biochem Pharmacol 1996; 51: 39-45.

204. Araújo CAC, Alegrio LV, Castro D, Lima MEF, Gomes-Cardoso L, Leon LL. Studies on the effectiveness of diarylheptanoids derivatives against *Leishmania amazonensis*. Mem Inst Oswaldo Cruz 1999; 94: 791-4.

205. Gomes Dde C, Alegrio LV, de Lima ME, Leon LL, Araujo CA. Synthetic derivatives of curcumin and their activity against *Leishmania amazonensis*. Arzneimittelforschung 2002; 52: 120-4.

206. Rasmussen HB, Christensen SB, Kvist LP, Karazmi A. A simple and efficient separation of the curcumins, the antiprotozoal constituents of *Curcuma longa*. Planta Med 2000; 66: 396-8.

207. Venkatesan N, Chandrakasan G. Modulation of cyclophosphamide-induced early lung injury by curcumin, an anti-inflammatory antioxidant. Mol Cell Biochem 1995; 142: 79-87.

208. Venkatesan N, Punithavathi V, Chandrakasan G. Curcumin protects bleomycin-induced lung injury in rats. Life Sci. 1997; 61: PL51- PL58.

209. Deters M, Siegers C, Hansel W, Schneider KP, Hennighausen G. Influence of curcumin on cyclosporin-induced reduction of biliary bilirubin and cholesterol excretion and on biliary excretion of cyclosporin and its metabolites. Planta Med. 2000; 66: 429-34.

210. Deters M, Siegers C, Muhl P, Hansel W. Choleretic effects of curcuminoids on an acute cyclosporin-induced cholestasis in the rat. Planta Med. 1999; 65: 610-3.

211. Brouet I, Ohshima H. Curcumin, an anti-tumour promoter and anti-inflammatory agent, inhibits induction of nitric oxide synthase in activated macrophages. Biochem Biophys Res Commun 1995; 206: 533-40.

212. Chan MY, Ho CT, Huang HI. Effects of three dietary phytochemicals from tea, rosemary and turmeric on inflammation-induced nitrite production. Cancer Lett 1995; 96: 23-9.

213. Chan MM, Huang HI, Fenton MR, Fong D. *In vivo* inhibition of nitric oxide synthase gene expression by curcumin, a cancer preventive natural product with anti-inflammatory properties. Biochem. Pharmacol. 1998; 55: 1955-62.

214. Onoda M, Inano H. Effect of curcumin on the production of nitric oxide by cultured rat mammary gland. Nitric Oxide 2000; 4: 505-15.

215. Ravindranath V, Chandrasekhara N. Absorption and tissue distribution of curcumin in rats. Toxicology 1980; 16: 259-65.

216. Ravindranath V, Chandrasekhara N. *In vitro* studies on the intestinal absorption of curcumin in rats. Toxicology 1981; 20: 251-7.

217. Ravindranath V, Chandrasekhara N. Metabolism of curcumin-studies with [^{3}H] curcumin. Toxicology 1982; 22: 337-44.

218. Vajragupta O, Toasaksiri S, Boonyarat C, Wongkrajang Y, Peungvicha P, Watanabe H, Boonchoong P. Chroman amide and nicotinyl amide derivatives: inhibition of lipid peroxidation and protection against head trauma. Free Radic Res 2000; 32: 145-55.

219. Snyder LR, *et al*. Practical HPLC Method Development. 2nd edition; Wiley: New York 1997.

220. http://www.shu.ac.uk/

221. Jenke DR. Chromatographic method validation: a review of current pratices and procedures. II. Guideline for primary validation parameters. J Liq Crom & Rel Technol 1996; 19 : 737-57.

222. Validation of analytical methods by FDA laboratories. Pharmaceutical technology. March 1986.

223. Finsy R., De Jaeger N, Sneyers R, Gelade E. Particle sizing by Photon correlation spectroscopy. Part III: Mono and bimodal distribution and data analysis. Part Part Syst Charact 1992; 9: 125–37.

224. Fricke S, Huttenrauch R . Einflux der Wasserstrukturauf das Zeta-potential suspendierter Partikel. Eur. J. Pharm. Biopharm 1991; 37: 55–9.

225. Kreuter J. Nanoparticulate systems for brain delivery of drugs. Adv Drug Deliv Rev 2001; 47: 65–81.

226. Kreuter J, Alyautdin RN, Kharkevich DA, Ivanov AA. Passage of peptides through the blood–brain barrier with colloidal polymer particles (nanoparticles). Brain Res 1995; 674: 171–4.

227. Gulyaev AE, Gelperina SE, Skidan IN, Antropov AS, Kivman GY, Kreuter J. Significant transport of doxorubicin into the brain with polysobate 80-coated nanoparticles. Pharm Res 1999; 16: 1564–9.

APPENDIX

MATERIAL SAFETY DATA SHEET

1. CHEMICAL PRODUCT AND COMPANY IDENTIFICATION

Product Name: MMA Monomer, Lightly Inhibited

Synonyms: Methyl Methacrylate; methylester of methacrylic acid; MMA

Chemical family: Ester

Molecular formula: $C_5H_8O_2$

Molecular weight: 100.13

2. HAZARDS IDENTIFICATION

EMERGENCY OVERVIEW

APPEARANCE AND ODOR:

Color: colorless

Appearance: liquid

Odor: pungent

STATEMENTS OF HAZARD:

WARNING! FLAMMABLE LIQUID AND VAPOR

CAUSES EYE IRRITATION

MAY CAUSE ALLERGIC SKIN REACTION

POLYMERIZATION MAY OCCUR FROM EXCESSIVE HEAT OR CONTAMINATION

POTENTIAL HEALTH EFFECTS

EFFECTS OF OVEREXPOSURE:

Direct contact with this material can cause moderate eye irritation. Repeated or prolonged dermal contact may cause allergic skin reactions. Overexposure to vapor may cause respiratory tract irritation and central nervous system depression.

3. PHYSICAL AND CHEMICAL PROPERTIES

Color:	colorless
Appearance:	liquid
Odor:	pungent
Boiling point:	101 °C 214 °F
Melting point:	-48 °C -54 °F
Vapor pressure:	44mm Hg at 26 °C
Specific gravity:	0.94 at 26 °C
Vapor density:	3.6
pH:	Not applicable
Evaporation rate:	3.1
Solubility in water:	1.6g/100 g at 20 °C
Volatile organic content:	940 gm/L
Flash point:	10 °C 50 °F closed cup

4. STABILITY AND REACTIVITY

Stability:	Stable
Conditions to avoid:	Reactive monomer, avoid storage above 4.4 °C (40 °F) heat and ignition sources.
Polymerization:	May occur
Conditions to avoid:	Heat and oxidizing agents will initiate polymerization.
Materials to avoid:	Oxidizing agents, reducing agents and mineral acids

Table A. Analytical data of curcumin entrapment and content in nanoparticles

Batch No.	Retention time		Peak area	
	Curcumin	Internal standard[a]	Curcumin	Internal standard[a]
1	7.261	4.925	62294	17256
	7.247	4.963	62529	17321
	7.255	4.954	62759	17289
2	7.266	4.992	96648	17414
	7.272	4.977	95770	17287
	7.235	4.945	96499	17356
3	7.217	4.952	85924	17254
	7.229	4.912	86931	17456
	7.241	4.936	87119	17529

[a] Internal standard was 4-fluoro-4′-hydroxy-benzophenone at 2.0 μg/ml

Table A. Peak area ratios[a] of curcumin entrapment and content in nanoparticles (cont.)

Batch no.	Peak area ratio ± S.D. *	% R.S.D.
1	3.62 ± 0.01	0.31
2	4.98 ± 0.01	0.12
3	5.55 ± 0.01	0.18

[a]Average ± S.D. (n = 3)

Table B. Analytical data of curcumin in mice brain after injected subcutaneously with P80-CLNP and curcumin solution (CS) at equivalent dose of curcumin (150 mg curcumin/kg)

Time (h)	Peak area (P80-CLNP)		Peak area (CS)	
	Curcumin	Internal standard[a]	Curcumin	Internal standard[a]
0.5	59225	17368	-	-
	59600	17581	-	-
	59011	17459	-	-
	59050	17266	-	-
1	135805	17256	-	-
	137394	17458	-	-
	138858	17644	-	-
	137104	17399	-	-
2	172077	17364	36758	17421
	171795	17318	36866	17555
	171908	17382	36532	17232
	170371	17244	-	-
3	181949	17312	70273	17266
	183454	17389	70652	17445
	183799	17488	70118	17399
	184541	17492	-	-
4	185139	17499	98058	17448
	186674	17644	96634	17318
	182558	17255	97339	17382
	186204	17583	-	-
6	156098	17325	122026	17583
	156972	17345	122829	17547
	157212	17468	121668	17456
	157931	17587	-	-
8	153056	17236	135369	17422
	154698	17421	135649	17458
	154343	17381	135559	17469
	153957	17357	-	-

Time (h)	Peak area (P80-CLNP)		Peak area (CS)	
	Curcumin	Internal standard[a]	Curcumin	Internal standard[a]
10	165919	17651	131828	17255
	163531	17584	132663	17387
	166310	17324	133064	17394
	169478	17472	-	-
12	159063	17422	118722	17357
	159051	17459	120165	17568
	158798	17355	120642	17612
	159668	17412	-	-
15	119135	17266	96970	17472
	120440	17455	96637	17412
	120485	17361	96180	17361
	121325	17482	-	-

[a] Internal standard was 4-fluoro-4′-hydroxy-benzophenone at 2.0 μg/ml

Table B. Peak area ratio of curcumin in mice brain after injected subcutaneously with P80-CLNP and curcumin solution (CS) at equivalent dose of curcumin (150 mg curcumin/kg) (cont.)

Time (h)	Peak area ratio ± S.D.[a] (P80-CLNP)	Peak area ratio ± S.D.[b] (CS)
0.5	3.40 ± 0.02	-
1	7.87 ± 0.01	-
2	9.90 ± 0.02	2.11 ± 0.01
3	10.53 ± 0.02	4.05 ± 0.02
4	10.58 ± 0.01	5.60 ± 0.02
6	9.01 ± 0.02	6.97 ± 0.03
8	8.88 ± 0.01	7.77 ± 0.01
10	9.50 ± 0.01	7.64 ± 0.01
12	9.14 ± 0.03	6.84 ± 0.01
15	6.92 ± 0.02	5.55 ± 0.01

[a]Average ± S.D. (n = 4)

[b]Average ± S.D. (n = 3)

Table B. The amount of curcumin in mice brain after injected subcutaneously with P80-CLNP and curcumin solution (CS) at equivalent dose of curcumin (150 mg curcumin/kg) (cont.)

Time (h)	P80-CLNP		Curcumin solution	
	Amount of curcumin ± S.D.[a] (µg)	Weight of brain ± S.D.[a] (g)	Amount of curcumin ± S.D.[b] (µg)	Weight of brain ± S.D.[b] (g)
0.5	2.4990 ± 0.02	0.1831 ± 0.01	-	-
1	6.4517 ± 0.01	0.2141 ± 0.02	-	-
2	8.2436 ± 0.01	0.1723 ± 0.01	1.3589 ± 0.02	0.1877 ± 0.01
3	8.8004 ± 0.02	0.2257 ± 0.01	3.0734 ± 0.01	0.1821 ± 0.01
4	8.8468 ± 0.01	0.1789 ± 0.02	4.4433 ± 0.02	0.1945 ± 0.01
6	7.4570 ± 0.02	0.1691 ± 0.02	5.6541 ± 0.02	0.2001 ± 0.01
8	7.3399 ± 0.01	0.1821 ± 0.02	6.3582 ± 0.01	0.2015 ± 0.02
10	7.8901 ± 0.02	0.2140 ± 0.03	6.2462 ± 0.02	0.1944 ± 0.02
12	7.5719 ± 0.02	0.2276 ± 0.03	5.5421 ± 0.01	0.1856 ± 0.03
15	5.6099 ± 0.02	0.1988 ± 0.02	4.3962 ± 0.01	0.1736 ± 0.03

[a]Average ± S.D. (n = 4)

[b]Average ± S.D. (n = 3)

BIOGRAPHY

NAME Mr. Umnart Sudyajai

DATE OF BIRTH November 01, 1980

PLACE OF BIRTH Bangkok, Thailand

INSTITUTION ATTENDED Mahidol University, 1998-2002:
Bachelor of Science (Chemistry)
Mahidol University, 2003-2006:
Master of Science (Pharmaceutical Chemistry and Phytochemistry)

RESEARCH GRANT Faculty of Graduate studies, Mahidol University

POSITION & OFFICE Student
Department of Pharmaceutical Chemistry,
Faculty of Pharmacy
Mahidol University
Bangkok, Thailand
Tel. 0-2644-8677-91 ext. 1410